Applying the MDCT to Image Compression

Rikus Muller

Dissertation presented for the degree of Doctor of Science at Stellenbosch University.

Promotors: Prof. B.M. Herbst and Dr. K.M. Hunter

March 2009

Declaration

By submitting this dissertation electronically, I declare that the entirety of the work contained therein is my own, original work, that I am the owner of the copyright thereof (unless to the extent explicitly otherwise stated) and that I have not previously in its entirety or in part submitted it for obtaining any qualification.

Signature: ..... Date: .....

Rikus Muller

Abstract

The replacement of the standard discrete cosine transform (DCT) of JPEG with the windowed modified DCT (MDCT) is investigated to determine whether improvements in numerical quality can be achieved. To this end, we employ an existing algorithm for optimal quantisation, for which we also propose improvements. This involves the modelling and prediction of quantisation tables to initialise the algorithm, a strategy that is also thoroughly tested. Furthermore, the effects of various window functions on the coding results are investigated, and we find that improved quality can indeed be achieved by modifying JPEG in this fashion.

Opsomming

Die vervanging van JPEG se standaard diskrete kosinus transform (DCT) met die gevensterde gemodifiseerde DCT (MDCT) word ondersoek om vas te stel of verbeteringe in numeriese kwaliteit verkry kan word. Vir hierdie doel maak ons gebruik van 'n bestaande algoritme vir optimale kwantisering, waarvoor ons ook verbeteringe aanbeveel. Hierdie verbeteringe behels die modellering en voorspelling van aanvanklike kwantiseringstabelle vir die algoritme, 'n strategie wat ook deeglik getoets word. Ons ondersoek ook die uitwerking van verskeie vensterfunksies op die koderingsresultate, en vind dat verbeterde kwaliteit inderdaad verkry kan word deur JPEG op hierdie manier te modifiseer.

Contents

Chapter 1

Introduction

1.1 Motivation

In classical lossy image compression techniques where transform coding is used, the transform is applied to non-overlapping sub-blocks of the image. This is in particular the case with the lossy modes of JPEG, where a 2D discrete cosine transform (DCT) is applied to non-overlapping 8×8 sub-blocks.

Yet it is standard practice to use windowed overlap-and-add transforms, specifically the windowed modified DCT (MDCT), in audio compression techniques. The reason for doing so is to mitigate undesirable edge effects, namely the contamination of frequency components caused by the resulting discontinuities at the boundaries of transform blocks.

While modern transform coding based image compression algorithms (such as JPEG2000) have eliminated this problem by applying wavelet transforms to entire images, one is still faced with the question: What if we were to do the same in image compression as is done in audio compression, replacing the standard DCT with a windowed MDCT?

No investigation into this has been published thus far, therefore the aim of this research is to thoroughly conduct such an investigation; to give answers to such questions as: Are there improvements to be gained by modifying JPEG to use a windowed MDCT, and how would we meaningfully/optimally quantise the resulting frequency components? We

will refer to this modification as MJPEG. Furthermore, when using overlap-and-add the transform blocks at image boundaries do not have enough neighbouring blocks to overlap with during reconstruction; we propose an implementation of MJPEG that efficiently addresses this issue.

For optimal quantisation we adapt and apply an algorithm, proposed by Fung and Parker [1] and designed for JPEG, to MJPEG. This algorithm is an improvement on the one by Wu and Gersho [2] in order to reduce running time. No improvements to the algorithm by Fung and Parker have since been proposed, with an alternative to the one by Wu and Gersho instead devised by Ratnakar and Livny [3, 4]. This alternative is known as RD-Opt. The algorithm by Fung and Parker can, however, still be improved upon to further reduce running time. A secondary aspect of this dissertation is therefore the proposal of such improvements. Moreover, the usage of a genetic algorithm to reduce running time even further is also considered.

Finally, we compare results obtained using MJPEG with optimal quantisation with those obtained using JPEG with optimal quantisation. These results are generated for four grayscale images (three of dimensions 256×256 and one of dimensions 512×512) over a wide range of compression ratios. With many window functions to choose from when using an MDCT, the effects on coding performance are also investigated for several window functions.

1.2 Quality Measurement

In this dissertation we only work with grayscale images, which are $m \times n$ matrices of non-negative integers representing pixels. Since lossy compression gives approximations to the original images, we would like to measure the quality of such approximations. There are two distinct approaches to doing this: gauging the perceptual (subjective) quality, and calculating the numerical (objective) quality. For this dissertation the second approach is chosen.

The *mean-squared-error* (MSE) forms the basis for the tradditional objective quality mea-

sures. Given an original image I and its approximation $\widehat{I}$, both of dimensions $m \times n$, the MSE is defined as

$$\text{MSE} = \frac{1}{mn} \sum_{x=1}^{m} \sum_{y=1}^{n} [I(x,y) - \widehat{I}(x,y)]^2. \tag{1.1}$$

From this, other tradditional measures such as the *root-mean-square* (RMS) and the *peak-signal-to-noise-ratio* (PSNR) can be calculated. The RMS is merely

$$\text{RMS} = \sqrt{\text{MSE}}, \tag{1.2}$$

while the PSNR, measured in decibels (dB), is defined as

$$\text{PSNR} = 10 \log_{10} \left(\frac{peak^2}{\text{MSE}} \right), \tag{1.3}$$

where *peak* is the largest value a pixel can assume. For images of 8-bit precision, this value is 255, which gives us

$$\text{PSNR} = 10 \log_{10} \left(\frac{255^2}{\text{MSE}} \right). \tag{1.4}$$

The PSNR will be the quality measure used throughout this dissertation, and, since all test images used here are of 8-bit precision, (1.4) will be the formula used to calculate it.

From the two approaches to quality measurement mentioned above, two distinct paradigms for optimal quantisation emerge: Quantising such that perceptual quality is optimised (known as perceptual coding) versus quantising such that numerical quality is optimised. With our choice of quality measure being the PSNR, our approach to optimal quantisation is within the second paradigm.

1.3 Overview

Since we intend to investigate the replacement of a component (the DCT) of JPEG's lossy modes of compression, it is appropriate to dedicate a chapter to some of the basics of JPEG. This discussion takes place in Chapter 2, and focusses specifically on JPEG's sequential mode. We also briefly discuss JPEG's weaknesses and ways to improve upon it, such as using wavelet transforms.

In Chapter 3 window functions and the overlap-and-add technique are introduced by explaining the reasons for their usage in audio compression. This culminates in a detailed discussion of the MDCT.

Chapter 4 explains how JPEG can be modified to use a windowed MDCT. We encounter the problem pertaining to transform blocks at image boundaries mentioned earlier, and discuss various strategies that address this issue. The last of these is the one that we propose, and we describe a Matlab implementation of MJPEG that utilises it. The need for optimal quantisation arises as a natural consequence at the end of this chapter when we attempt to meaningfully compare JPEG and MJPEG.

The next two chapters are then devoted to the two paradigms for optimal quantisation mentioned earlier. Chapter 5 gives an overview of the basics of perceptual coding, primarily those of perceptual image coding. In Chapter 6 the problem of quantising so as to optimise numerical quality is formalised, and algorithms that attempt to solve this problem are discussed. In particular, the algorithms designed for JPEG by Wu and Gersho [2] and Fung and Parker [1] are described, as well as our proposed improvements to the latter. The basics of genetic algorithms are also described, since an attempt will be made to further reduce running time with their usage. The chapter ends with a description of a C++ implementation of the discussed algorithms.

Our proposed improvements to the algorithm by Fung and Parker involves the construction of initial quantisation tables for the algorithm. Chapter 7 therefore gives a detailed account of the approach taken to model and predict these initial tables. Our constructed models are then thoroughly tested on three images for a particular instance of MJPEG, and the incorporation of a genetic algorithm is also put to the test.

Lastly, in Chapter 8 we compare MJPEG to JPEG, when optimal quantisation is used. As mentioned earlier, the effects of window functions are also investigated, specifically to see if a "best" window can be found. This is followed by a discussion of the conclusions to be drawn from our results, and an outline of possible future research.

Chapter 2

JPEG

JPEG possesses three lossy modes, with the sequential mode being the most popular. For this reason, our modification of JPEG is specifically applied to this mode, to which we limit this chapter's discussion. For details of JPEG's other modes, we refer the reader to [5].

2.1 Transform Coding

Lossy JPEG is an example of a *transform coding* technique and our discussion is therefore within this framework. Figure 2.1 below gives a classic diagrammatic depiction of this approach to lossy compression. During the encoding stage, shown in Figure 2.1(a), a mathematical transformation, known as the *forward transform*, is applied to an input signal, yielding an alternate form of it that can be manipulated for compression. The forward transform is invertible; applying its *inverse transform* immediately afterward will give us the original signal back.

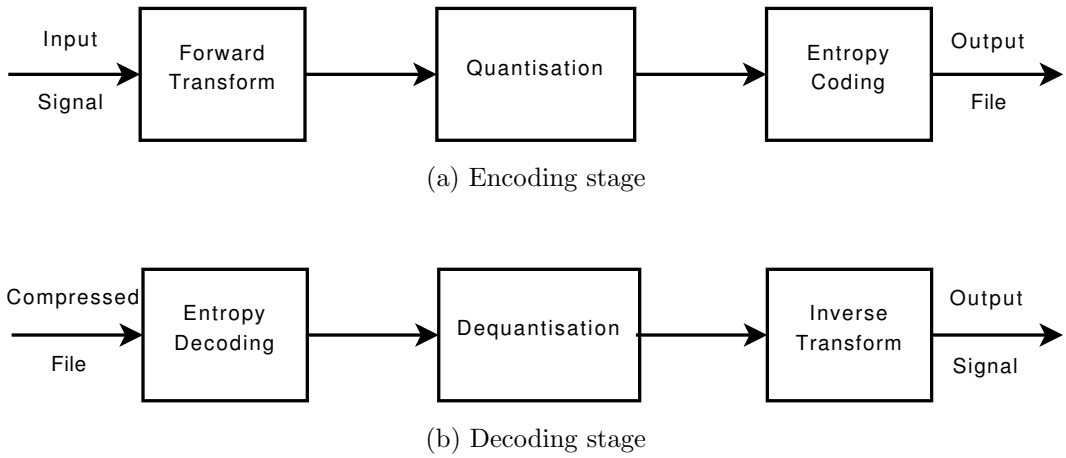

(a) Encoding stage

(b) Decoding stage

Figure 2.1: Lossy compression using transform coding

The alternate form of the signal is then manipulated toward greater compressibility by means of the next stage: *quantisation*. This stage is where information-loss takes place. The more information we throw away here, *i.e.* the more severely we quantise, the more compression we can achieve. This is known as the quality versus compression trade-off.

In the final stage lossless data compression is applied to the quantised data, a process conventionally referred to as *entropy coding*. Various entropy coding algorithms exist; those employed in image compression are typically Huffman coding or Arithmetic coding. During this stage the resulting compressed data is written to an output file.

Figure 2.1(b) also shows the decoding stage. Here we undo the actions performed by the encoder, only in the reverse order. In the absence of quantisation the output signal from the decoder will be identical to the input signal to the encoder, and this is how lossless compression can be achieved.

2.2 Discrete Cosine Transform

In the case of JPEG, the forward transform used is the 2D *discrete cosine transform* (DCT). Given an image to be compressed, a "level shift" is first performed by subtracting 128 from each pixel value. The image is then partitioned into contiguous 8×8 sub-blocks,

with the 2D DCT applied to each, in the order left-to-right, top-to-bottom. For such an 8×8 block, say A, the forward 2D DCT is defined as

$$F(k,l) = \frac{C(k)}{2}\frac{C(l)}{2}\sum_{i=1}^{8}\sum_{j=1}^{8} A(i,j)\cos\left[\frac{(2i-1)(k-1)\pi}{16}\right]\cos\left[\frac{(2j-1)(l-1)\pi}{16}\right], \quad (2.1)$$
$$k = 1,\ldots,8, \quad l = 1,\ldots,8,$$

where

$$C(n) = \begin{cases} \frac{1}{\sqrt{2}}, & n = 1, \\ 1, & \text{otherwise.} \end{cases}$$

The DCT is a mapping into the frequency domain — each block A of 64 numbers in the spatial domain is associated with a unique block F, consisting of 64 numbers in the frequency domain. Therefore the numbers $F(k,l)$ are called the *frequency components* of A.

Notice that the DCT "rewrites" a matrix A as a linear combination of 64 linearly independent matrices, known as the *DCT basis functions* — discretely sampled cosine functions of various frequencies. Each entry $F(k,l)$ records the contribution made by its corresponding basis function to the linear combination. As a result, we also refer to the entries $F(k,l)$ as the *DCT coefficients* of A. In particular, the first coefficient $F(1,1)$ is called the *DC coefficient*, since it corresponds to the basis function of frequency 0, while the others are called *AC coefficients*.

Consider, for example, the first 8×8 block of pixels from the 256×256 Lena image (shown

in Appendix A) which, after level shifting, gives us

$$A = \begin{bmatrix} 9 & 8 & 5 & 8 & 10 & 6 & 6 & 4 \\ 9 & 8 & 5 & 8 & 10 & 6 & 6 & 4 \\ 10 & 5 & 6 & 6 & 8 & 4 & 2 & 2 \\ 5 & 5 & 5 & 2 & 6 & 5 & 0 & -3 \\ 1 & 5 & 2 & 2 & 5 & 3 & 4 & 0 \\ 3 & 5 & 2 & -6 & 4 & 3 & 2 & 2 \\ 3 & 2 & 2 & 2 & 4 & 3 & 0 & 2 \\ 3 & 4 & 2 & 2 & 3 & 3 & 2 & 0 \end{bmatrix}.$$

Applying (2.1) to block A, we find that its DCT is, rounded to four decimals,

$$F = \begin{bmatrix} 31.7500 & 7.1983 & -3.1311 & 7.2608 & 0.2500 & -4.2844 & -1.6796 & 3.0593 \\ 14.8539 & 3.1651 & -2.3714 & 1.2428 & 3.6567 & 2.0431 & -1.6362 & -0.0087 \\ 5.6554 & -1.0094 & 0.5732 & -0.7337 & 2.9630 & 1.6565 & -1.1161 & -1.8256 \\ -1.0214 & -3.7645 & 2.6375 & 0.0421 & -1.9652 & -2.6852 & -1.7208 & 1.0916 \\ -1.2500 & 0.3573 & -2.6692 & 0.0515 & -2.2500 & 1.0094 & -1.8710 & -1.2653 \\ -1.5480 & 1.9691 & -1.1503 & 0.3755 & 1.3049 & -0.1028 & 3.1041 & 0.0033 \\ -0.7189 & 0.8567 & 2.8839 & 0.6720 & -0.6861 & -1.0352 & 0.9268 & 1.8997 \\ 1.1394 & -0.9480 & -1.1851 & -1.8109 & 2.5863 & 2.1821 & -0.9581 & -1.1044 \end{bmatrix}.$$

If we were to assign a label to each DCT basis function, say $B_{k,l}$ ($k = 1, \ldots, 8,\ l = 1, \ldots 8$), then in terms of the above discussion, matrix A can be written as the following linear combination

$$A = (31.75)B_{1,1} + (7.1983)B_{1,2} + \ldots + (-1.1044)B_{8,8}.$$

In other words, by summing the linear combination, A is reconstructed. This is precisely what the inverse DCT (IDCT) does, which is defined as

$$A(i,j) = \sum_{k=1}^{8} \frac{C(k)}{2} \sum_{l=1}^{8} \frac{C(l)}{2} F(k,l) \cos\left[\frac{(2i-1)(k-1)\pi}{16}\right] \cos\left[\frac{(2j-1)(l-1)\pi}{16}\right], \quad (2.2)$$
$$i = 1, \ldots, 8, \quad j = 1, \ldots, 8.$$

2.3 Quantisation

In JPEG, quantisation is done by dividing each DCT coefficient by a corresponding 8-bit positive integer stored in a *quantisation table* (QT) and rounding off. Each integer is allowed to assume a value between 1 and 255, since we cannot divide by 0. The standard QT used for grayscale images and the so-called luminance component of colour images is listed in Table 2.1 below.

16	11	10	16	24	40	51	61
12	12	14	19	26	58	60	55
14	13	16	24	40	57	69	56
14	17	22	29	51	87	80	62
18	22	37	56	68	109	103	77
24	35	55	64	81	104	113	92
49	64	78	87	103	121	120	101
72	92	95	98	112	100	103	99

Table 2.1: The standard JPEG luminance quantisation table

For instance, the quantised version of the block F of frequency components in our example above will be

$$F_q = \begin{array}{|cccccccc|}\hline 2 & 1 & 0 & 0 & 0 & 0 & 0 & 0 \\ 1 & 0 & 0 & 0 & 0 & 0 & 0 & 0 \\ 0 & 0 & 0 & 0 & 0 & 0 & 0 & 0 \\ 0 & 0 & 0 & 0 & 0 & 0 & 0 & 0 \\ 0 & 0 & 0 & 0 & 0 & 0 & 0 & 0 \\ 0 & 0 & 0 & 0 & 0 & 0 & 0 & 0 \\ 0 & 0 & 0 & 0 & 0 & 0 & 0 & 0 \\ 0 & 0 & 0 & 0 & 0 & 0 & 0 & 0 \\ \hline \end{array}.$$

Similarly, we dequantise by multiplying quantised coefficients by their corresponding QT

entries. Thus, in the case of our example, we will have

$$F_{dq} = \begin{array}{|cccccccc|}\hline 32 & 11 & 0 & 0 & 0 & 0 & 0 & 0 \\ 12 & 0 & 0 & 0 & 0 & 0 & 0 & 0 \\ 0 & 0 & 0 & 0 & 0 & 0 & 0 & 0 \\ 0 & 0 & 0 & 0 & 0 & 0 & 0 & 0 \\ 0 & 0 & 0 & 0 & 0 & 0 & 0 & 0 \\ 0 & 0 & 0 & 0 & 0 & 0 & 0 & 0 \\ 0 & 0 & 0 & 0 & 0 & 0 & 0 & 0 \\ 0 & 0 & 0 & 0 & 0 & 0 & 0 & 0 \\ \hline \end{array}$$

which serves as an approximation to our original F. We see that DCT coefficients that are quantised to zero cannot be recovered, and the number that meet this fate is determined by the severity of the quantisation.

The resulting quality versus compression trade-off can be adjusted by multiplying the standard QT by a scale factor, say α. Many applications obtain α by means of a quality parameter, say $qual$, that ranges between 1 and 100, according to the formula

$$\alpha = \begin{cases} \frac{50}{qual}, & 1 \leq qual \leq 50, \\ 2 - \frac{qual}{50}, & 50 < qual \leq 100. \end{cases} \tag{2.3}$$

After multiplying Table 2.1 by α, we round off the entries in the new table and clip their values between 1 and 255. Notice that the standard QT corresponds to a quality parameter of $qual = 50$, and that larger values of $qual$ lead to less severe quantisation, and vice versa. Returning to our example DCT coefficient block F, let us quantise it with the QT obtained with $qual = 60$, namely

$$Q = \begin{array}{|cccccccc|}\hline 13 & 9 & 8 & 13 & 19 & 32 & 41 & 49 \\ 10 & 10 & 11 & 15 & 21 & 46 & 48 & 44 \\ 11 & 10 & 13 & 19 & 32 & 46 & 55 & 45 \\ 11 & 14 & 18 & 23 & 41 & 70 & 64 & 50 \\ 14 & 18 & 30 & 45 & 54 & 87 & 82 & 62 \\ 19 & 28 & 44 & 51 & 65 & 83 & 90 & 74 \\ 39 & 51 & 62 & 70 & 82 & 97 & 96 & 81 \\ 58 & 74 & 76 & 78 & 90 & 80 & 82 & 79 \\ \hline \end{array}.$$

This gives us

$$F_q = \begin{array}{|cccccccc|}\hline 2 & 1 & 0 & 1 & 0 & 0 & 0 & 0 \\ 1 & 0 & 0 & 0 & 0 & 0 & 0 & 0 \\ 1 & 0 & 0 & 0 & 0 & 0 & 0 & 0 \\ 0 & 0 & 0 & 0 & 0 & 0 & 0 & 0 \\ 0 & 0 & 0 & 0 & 0 & 0 & 0 & 0 \\ 0 & 0 & 0 & 0 & 0 & 0 & 0 & 0 \\ 0 & 0 & 0 & 0 & 0 & 0 & 0 & 0 \\ 0 & 0 & 0 & 0 & 0 & 0 & 0 & 0 \\ \hline \end{array}$$

where fewer coefficients have indeed been quantised to zero. As a result, its dequantised counterpart

$$F_{dq} = \begin{array}{|cccccccc|}\hline 26 & 9 & 0 & 13 & 0 & 0 & 0 & 0 \\ 10 & 0 & 0 & 0 & 0 & 0 & 0 & 0 \\ 11 & 0 & 0 & 0 & 0 & 0 & 0 & 0 \\ 0 & 0 & 0 & 0 & 0 & 0 & 0 & 0 \\ 0 & 0 & 0 & 0 & 0 & 0 & 0 & 0 \\ 0 & 0 & 0 & 0 & 0 & 0 & 0 & 0 \\ 0 & 0 & 0 & 0 & 0 & 0 & 0 & 0 \\ 0 & 0 & 0 & 0 & 0 & 0 & 0 & 0 \\ \hline \end{array}$$

is hopefully a better approximation to the original F.

2.4 Huffman Coding

JPEG supports two entropy coding techniques: Huffman coding and Arithmetic coding. Here we discuss the use of Huffman coding, specifically with the predetermined Huffman tables published in the JPEG standard, since this approach is the easiest to implement and hence the one most often used. For the more general case of Huffman coding as well as the use of Arithmetic coding, the reader is referred to [5].

Huffman coding works by replacing a sequence of symbols with codewords of variable length that are stored in a *Huffman table*. JPEG uses 2 Huffman tables for the luminance component of an image (and 2 for the chrominance components, for a total of 4 tables); one for the coding of DC coefficients and one for the coding of AC coefficients.

As we can see from the quantised coefficients F_q in the previous section's example, those corresponding to higher frequencies tend to be zero — therefore the sequence in which coefficients are encoded is chosen as depicted in Figure 2.2 below. This reordering of coefficients is termed the *zigzag sequence*.

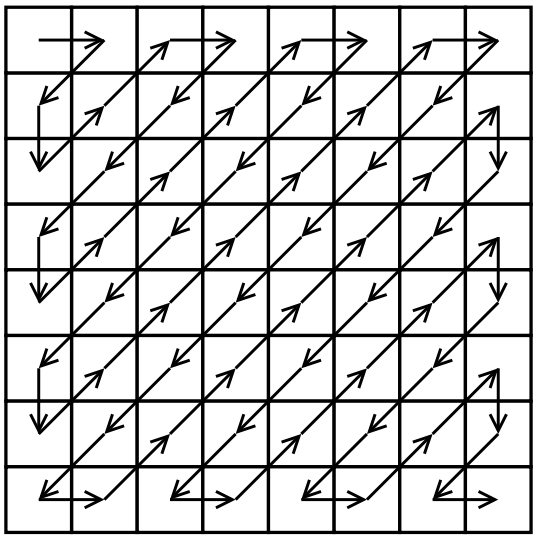

Figure 2.2: The zigzag sequence used by JPEG

The benefit of this can be seen from the zigzag reordering, say $\mathbf{z}$, of our second example F_q, namely

$$\mathbf{z} = \boxed{2}\boxed{1}\boxed{1}\boxed{1}\boxed{0}\boxed{0}\boxed{1}\boxed{0}\boxed{0}\cdots\boxed{0}\boxed{0}.$$

We see that this zigzag reordering has resulted in runs of zeroes; in particular we have a large run of terminating zeroes formed by the higher frequency quantised coefficients. This is exploited by combining the Huffman coding of AC coefficients with *runlength coding*. We now illustrate the procedure by encoding **z** above. Since our focus is on JPEG's sequential mode, the coding is performed via a single pass through the data.

DC coefficients are differentially coded: In order to exploit any correlation between them, the difference between the current DC coefficient and the one from the previous 8×8 block is encoded. In our example we have the very first DC coefficient, whose predecessor is conventionally chosen as 0, thus the difference to encode is 2.

When encoding a number, an alternative digital representation of integers is used here, in the form of the pair (**category**, **value**). A number's **category** is the least number of bits required to encode it in 1's complement, while **value** is the actual encoding (in 1's complement). Table 2.2 lists the categories for integers relevant to lossy JPEG.

Category	**Number**
0	0
1	-1, 1
2	-3, -2, 2, 3
3	-7, ..., -4, 4, ..., 7
4	-15, ..., -8, 8, ..., 15
5	-31, ..., -16, 16, ..., 31
6	-63, ..., -32, 32, ..., 63
7	-127, ..., -64, 64, ..., 127
8	-255, ..., -128, 128, ..., 255
9	-511, ..., -256, 256, ..., 511
10	-1023, ..., -512, 512, ..., 1023
11	-2047, ..., -1024, 1024, ..., 2047

Table 2.2: Categories associated with integers where encoding them in 1's complement

The codewords in the DC Huffman table are assigned to these categories and can be found in [5, Table K.3, p.509]. We see that the difference of 2 in our example belongs to category 2, with Huffman code 011, and its representation in 1's complement is 10; therefore our first few bits of compressed data are

0	1	1	1	0

.

The runlength/Huffman coding of AC coefficients is done by grouping each non-zero coefficient with a number indicating how many zeroes preceded it, forming a new symbol (**runlength**, **number**). In the case of our example, the symbols (0, 1), (0, 1), (0, 1) and (2, 1) are formed.

For encoding, the quantity **number** is once again represented as (**category**, **value**) (meaning that the information to be conveyed is now of the form (**runlength**, **category**, **value**)), and Huffman codes are assigned to the pairs (**runlength**, **category**). These codewords constitute the AC Huffman table, shown in [5, Table K.5, p.510]. In our example, the first symbol was (0, 1) and, according to Table 2.2, its non-zero coefficient 1 belongs to category 1. Hence, we look up the Huffman code for the pair (**runlength**, **category**) = (0, 1), which is 00. With the 1's complement encoding of 1 simply being 1, the resulting bit string to add to the output will be 001, and our compressed data stream is now

0	1	1	1	0	0	0	1

.

Similarly, after encoding the next two non-zero coefficients, we have

0	1	1	1	0	0	0	1	0	0	1	0	0	1

as data stream. The last non-zero coefficient, also a 1, is preceded by a run of two zeroes, so we look up the Huffman code for the pair (2, 1), which is 11100, and add 111001 to our example data stream, yielding

0	1	1	1	0	0	0	1	0	0	1	0	0	1	1	1	1	0	0	1

.

Finally, the run of zeroes terminating the zigzag sequence is grouped together to form the special symbol *end-of-block* (EOB). This symbol has the Huffman code 1010, and subsequently, the complete encoding of **z** is

0	1	1	1	0	0	0	1	0	0	1	0	0	1	1	1	1	0	0	1	1	0	1	0

.

One more special symbol exists, namely zero-run-length (ZRL), which denotes a run of 16 zeroes. Due to practical restrictions on the size of Huffman tables, the quantity **runlength** in the pair (**runlength**, **category**) ranges between 0 and 15. In other words, it can only indicate a (preceding) run of zeroes of length up to 15. Anything longer is broken up into as many runs of length 16 as necessary, with each encoded by ZRL. Any remaining zeroes still preceding the non-zero coefficient, *i.e.* forming a run of length less than 16, are grouped with the coefficient to form the usual pairing.

2.5 Matlab Implementation

Matlab provides us with a convenient environment in which to access images and manipulate them. For instance, we can easily calculate the PSNR of an encoding with the use of matrix subtraction and the built-in `sum` function. Rather than repeatedly opening output files (created by a pre-existing implementation of JPEG) in Matlab to do so, it is much more efficient to just perform the encodings in Matlab as well.

In Appendix B.1.1 implementations of the sequential JPEG encoding and decoding stages, `my_jpeg.m` and `my_jpeg_dec.m`, respectively, are listed. The function `my_jpeg` accepts as input an $m \times n$ image and a QT to quantise it with, and outputs the resulting $m \times n$ matrix, say Y, of quantised DCT coefficients. We can, for example, generate a rescaled standard JPEG QT with the function `jpeg_qt.m`, which is an implementation of the approach using a quality parameter mentioned in Section 2.3.

Notice that no output file is generated — we do not need one in order to determine what its size will be. Since the Huffman codes are known, their lengths (in bits) are also known. Thus, when parsing through the quantised coefficients the way we normally would when

entropy coding, we simply add the lengths of the codewords that would have been output. This task is performed by the functions `dct2bytes.m` and `d2b.m`, where `dct2bytes` is the front-end to which Y is presented and `d2b` performs the actual calculations. The reason for this is the fact that our implementation of MJPEG will result in frequency blocks of three different dimensions, as will be seen in Section 4.2.3. In such cases, when presented with a matrix Y of quantised coefficients, `dct2bytes` will repeatedly make use of `d2b`. To distinguish between these two cases, `dct2bytes` makes use of an option parameter specified by the user. A value of 0 indicates that Y consists of DCT coefficients, while any other value will indicate MDCT coefficients.

Our file size calculations also take into account the small amount of overhead required by a JPEG file in practice. The QT and Huffman tables used need to be specified, as do the dimensions of the encoded image. Additionally, certain *marker* bytes enforce the format of the data stream, and the application program responsible for the encoding may also insert a comment early in the file. By using predetermined Huffman tables, this overhead will remain fixed for a particular application program[1]. The Linux application Gimp, for instance, creates Sequential mode JPEG files with 354 bytes of overhead under this restriction. When accounting for overhead, `dct2bytes` uses this number.

Finally, the function `my_jpeg_dec` takes as input a matrix of quantised DCT coefficients, along with the QT used to generate it, and outputs the corresponding reconstructed $m \times n$ image. The PSNR of the approximation can then be obtained by inputting the original image and its approximant to the function `decibels.m`.

2.6 Improving upon JPEG

A drawback to partitioning a signal into transform blocks is that it causes discontinuities at the boundaries of those blocks, something we discuss in detail in the next chapter. One way to overcome this problem is to use discrete wavelet transforms instead of the more tradditional transforms.

[1]Different Huffman tables require different amounts of overhead to be specified.

2.6.1 Wavelet Image Compression

A discrete wavelet transform (DWT), of which the definition and mathematical aspects are outside the scope of this dissertation, is applied to a signal in its entirety. It is an example of a filter bank [6]: Given a 1D input signal, say $\mathbf{x}$, the output consists of a concatenation of a low-pass filtering and high-pass filtering of $\mathbf{x}$. These filterings are each down-sampled by a factor of 2 before concatenation, so that the output is of the same length as the input. An illustration of this is shown in Figure 2.3, with $\mathbf{L_1}$ denoting the low-frequency subband and $\mathbf{H_1}$ the high-frequency subband. We call this a (1-level) *wavelet decomposition* of $\mathbf{x}$.

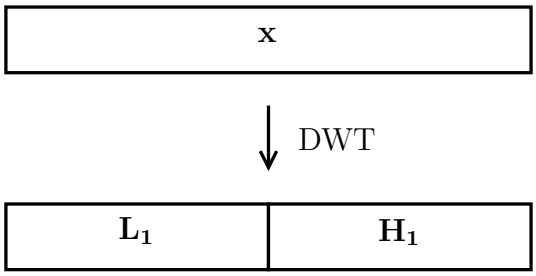

Figure 2.3: A 1-level wavelet decomposition of the signal $\mathbf{x}$

Further levels of decomposition are always applied to the lowest frequency subband; for example, a 3-level decomposition would proceed as shown in Figure 2.4 below.

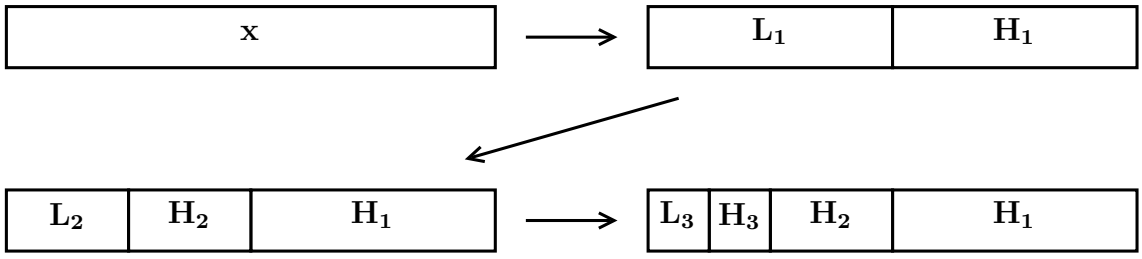

Figure 2.4: A 3-level wavelet decomposition of the signal $\mathbf{x}$, illustrating the repeated application of the DWT to the lowest frequency subband

In general, subbands $\mathbf{H_1}, \ldots, \mathbf{H_n}$ represent high-frequency detail extracted from the signal at successively lower levels of resolution, and $\mathbf{L_n}$ represents the remaining low-frequency

detail. For this reason, such a multi-level decomposition of a signal is also called a *multi-resolution analysis* (MRA). Furthermore, the numbers in $\mathbf{L_n}$ and $\mathbf{H_1}, \ldots, \mathbf{H_n}$ are called *wavelet coefficients*.

In a wavelet image compression technique the first level of decomposition is done by applying a wavelet transform to the image's rows, followed by the transform applied to the columns of the resulting output. This is illustrated in Figure 2.5 below, where we have labelled the image as I.

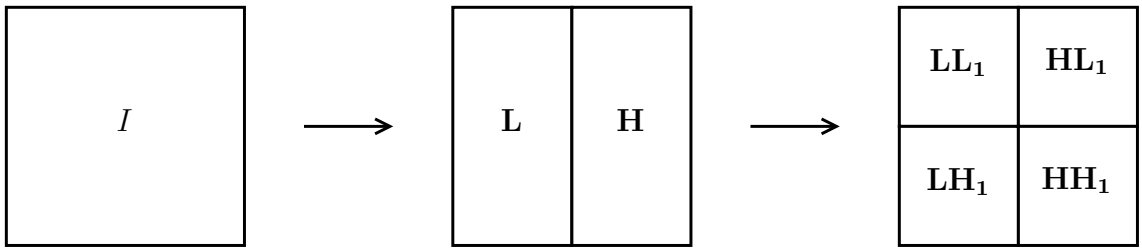

Figure 2.5: A 1-level wavelet decomposition of an image

Once again, subsequent levels of decomposition are applied to the lowest frequency subband. The second level, for instance, is shown in Figure 2.6. In the case of JPEG2000, arguably the most well-known wavelet image compression technique, the maximum number of decomposition levels supported is 32 [6].

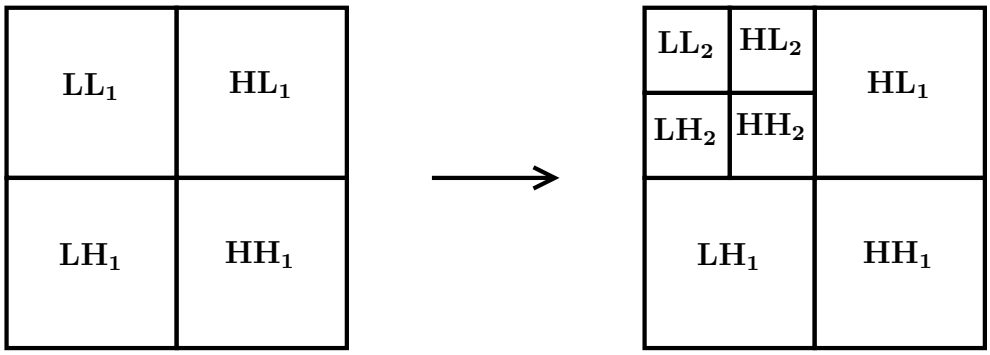

Figure 2.6: The second level of wavelet decomposition of an image, obtained from the first level

An MRA gives us a hierarchy of wavelet coefficients: coefficients in lower frequency subbands are more significant than ones in higher frequency subbands. By encoding coeffi-

cients in the order of higher significance to lower significance, most significant bit to least significant bit (known as *bit-plane coding*), increasingly better approximations to the original image are embedded in the output file. Furthermore, by completing the encoding, lossless compression is achieved[2]. Lossy compression results by terminating the encoding when a target file size is reached. This is in contrast to JPEG, where lossless compression requires its own mode of operation.

Embedded coding gives us the very desirable property of scalability. For example, internet users with different connection speeds will all be able to view the same sequence of encoded images in real-time, but at quality levels proportional to their connection speeds. This is done by transmitting only the first n, say, bytes of each encoding to users with slower connections, while transmitting the entire encodings to those users with fast enough connections.

A certain level of embedded coding can also be achieved with JPEG, by selecting either its progressive mode or its hierarchical mode. In progressive mode, successive approximation (bit-plane coding), spectral selection (where DCT coefficients are grouped into subbands), or a mixture of both can be selected. In hierarchical mode, versions of the input image at various resolutions are obtained via repeated down-sampling. The differences between these approximations, termed *differential images*, are then encoded either sequentially or progressively, depending on the user's choice.

With so many options to choose from, most users just end up choosing JPEG's sequential mode. A further benefit of wavelet image compression techniques is therefore the fact that all their features are unified under a single coding architecture.

Lastly, each wavelet image compression technique has its own approach to encoding wavelet coefficients, and it is here that such techniques can differ significantly. This is however outside the scope of this dissertation, and we refer the reader to the EBCOT algorithm employed by JPEG2000 [6] and Shapiro's EZW algorithm [7] as examples of such differences.

[2]Provided that an integer-to-integer DWT is used.

2.6.2 Using a Modified Transform

An alternative approach to dealing with the problem of discontinuities mentioned at the beginning of this section is to somehow modify the more tradditional transform in question. As stated in Chapter 1, we investigate the use of the windowed MDCT as an alternative to the DCT. This approach replaces one component of JPEG with another, meaning that its modes of operation are left more or less unchanged. As such, the other disadvantages JPEG has compared to wavelet image compression techniques remain present. We therefore strongly emphasise that this research cannot compete with such techniques, particularly not JPEG2000, and is not intended to do so.

In the next chapter, the basis for our approach, namely the MDCT, as well as the reasoning leading up to it, is discussed in detail.

Chapter 3

The Modified Discrete Cosine Transform (MDCT)

The compression of digital audio provides an ideal background for explaining the use of the MDCT. Much of this chapter's discussion will take a cue from the excellent textbook on the subject by Bosi and Goldberg [8].

3.1 Digital Audio

A digital audio signal is a 1D array of 16-bit numbers, each representing an audio sample. These samples are obtained by a method known as analogue-to-digital conversion [9], so called because actual audio is a continuous function of time, and thus an analogue signal.

Due to this continuous nature of audio, digital audio is not played back discretely, but instead used to reconstruct an analogue signal via digital-to-analogue conversion [9]. One might immediately be concerned that this reconstructed signal will merely be an approximation to the original signal that was sampled, *i.e.* that the information between samples will not be accurately recovered. Fortunately, the sampling theorem tells us that we can perfectly reconstruct the original signal, provided that the signal satisfies a certain requirement, and the sampling rate is high enough.

Before proceeding any further, we first define the *Fourier transform* (FT) of a function or analogue signal, say $f(t)$. The FT is the means by which the frequency content of such signals can be calculated, and is defined as

$$F(\omega) = \int_{-\infty}^{\infty} f(t) e^{-2\pi i \omega t} dt. \tag{3.1}$$

Returning now to the sampling theorem, it states that an analogue signal containing frequency content only up to a finite upper frequency, say $F_{\max}$, will be perfectly reconstructed from discrete samples if the sampling rate, say F_{s}, satisfies $F_{\mathrm{s}} \geq 2F_{\max}$. We call such a signal *band-limited*. When the sampling rate does not meet this condition, *aliasing* can occur — contributions made to the original signal by frequencies higher than $F_{\max}$ are mistaken for lower frequency contributions in the reconstructed signal.

To ensure that a signal is band-limited, it can be low-pass filtered to cut off all frequency content above $F_{\max}$. With regards to audio signals, they are limited to 22 kHz, because most human beings cannot hear beyond it. A sampling rate of 44.1 kHz is then used, both for good measure and historical reasons [9], thereby satisfying the sampling theorem's condition.

3.2 Window Functions

Let us now consider an attempt to apply lossy compression to a digital audio signal, using transform coding in particular. The forward transform shown in Figure 2.1(a) might now be a 1D time to frequency transform, such as a 1D DCT. As a result, the signal will again be partitioned into non-overlapping transform blocks. As stated in Section 2.6, this partitioning causes discontinuities at the edges of those blocks, and we now proceed to analyse this problem.

Let $f(t)$ denote the original bandlimited signal from which the digital audio signal to be encoded was obtained, as depicted in Figure 3.1(a). Furthermore, let $[0,\ T]$ refer to the time interval corresponding to the duration of some transform block $\mathbf{x}$.

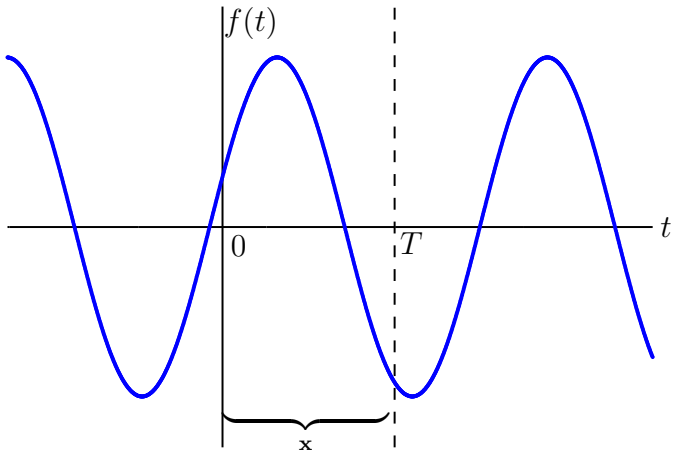

(a) Original audio signal

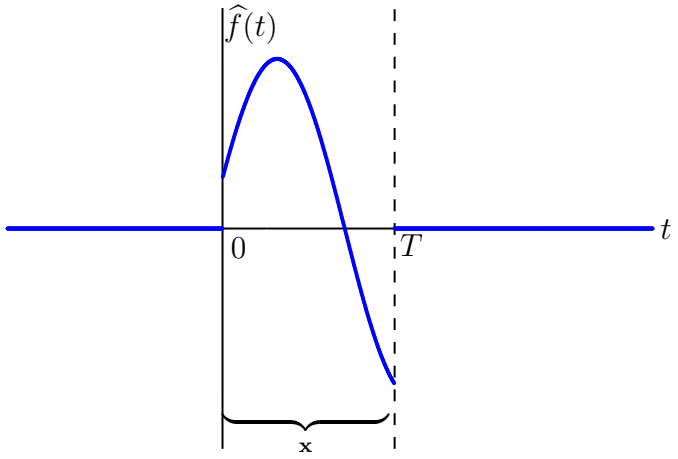

(b) Time-limited counterpart

Figure 3.1: Time-limiting resulting from the partitioning of a signal into transform blocks

Notice that by only working with block **x**, its samples could just as well have been obtained by sampling the *time-limited* counterpart of $f(t)$, namely $\widehat{f}(t)$, shown in Figure 3.1(b), rather than $f(t)$. However, $\widehat{f}(t)$ possesses sharp discontinuities at $t = 0$ and $t = T$; we

can therefore expect its frequency content to be quite different from that of $f(t)$.

3.2.1 The Rectangular Window

We can investigate the change from $f(t)$'s to $\widehat{f}(t)$'s frequency content by considering $\widehat{f}(t)$ to have been obtained by multiplying $f(t)$ with the function

$$w_{\text{rect}}(t) = \begin{cases} 1, & t \in [0,\ T], \\ 0, & \text{otherwise.} \end{cases} \tag{3.2}$$

called the *rectangular window*. This process is known as *windowing*.

By utilising the convolution theorem, we can understand the effect multiplication by w_{rect} had on the frequency content of $f(t)$: the theorem states that the FT of the product of two functions is equal to the convolution of the respective functions' FTs. Therefore, by convolving the frequency content of w_{rect} with that of $f(t)$, the frequency content of $\widehat{f}(t)$ is obtained. From (3.1) we find that the FT of the rectangular window is

$$\begin{aligned} W_{\text{rect}}(\omega) &= \int_{-\infty}^{\infty} w_{\text{rect}}(t) e^{-2\pi i\omega t} dt = \int_0^T e^{-2\pi i\omega t} dt \\ &= e^{-\pi i\omega T} \frac{\sin(\pi\omega T)}{\pi\omega}, \end{aligned} \tag{3.3}$$

and in Figure 3.2 this FT is shown, plotted for the case $T = 1$ over the interval $\omega \in [0,\ 5]$. Notice that, since the function values of (3.3) are complex, the modulus is taken before plotting.

We see from Figure 3.2 that the rectangular window is not band-limited. Even though its frequency content does eventually become negligible, allowing us to consider it essentially band-limited beyond a certain point, this does not happen "soon" enough. We say that W_{rect} has a slow *drop-off*.

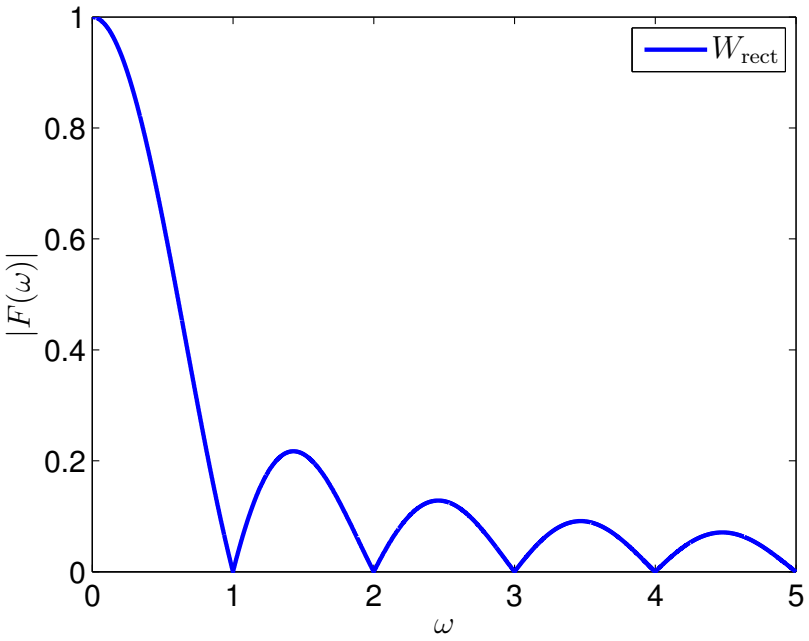

Figure 3.2: Modulus of the rectangular window's FT, illustrating its slow drop-off in energy

The implication of this is that, while the original signal $f(t)$ was sufficiently band-limited for the sampling rate that gave rise to the samples in block $\mathbf{x}$, $\widehat{f}(t)$ may not be. One could say that insisting on only working with the samples in block $\mathbf{x}$ is equivalent to sampling $\widehat{f}(t)$ with the original (but now inadequate) sampling rate. In the end, calculating the DCT of block $\mathbf{x}$ may result in coefficients contaminated with aliasing.

3.2.2 The Sine Window

As we just saw, the rectangular window caused the time-limited signal $\widehat{f}(t)$ to start and stop abruptly. Had the signal done so gradually, there might not have been a problem. One should therefore choose window functions that will force signals specifically to behave this way. Any "bell-shaped" function will do this, and a first attempt is the *sine window*,

given by the formula

$$w_{\sin}(t) = \begin{cases} \sin\left(\frac{\pi t}{T}\right), & t \in [0,\ T], \\ 0, & \text{otherwise.} \end{cases} \tag{3.4}$$

We of course do not actually window before sampling in practice; the equivalent is to pointwise multiply the samples in a transform block by a sampled version of the window function. For a transform block (or discretely sampled signal) consisting of N samples, the sine window is defined as

$$\mathbf{w}_{\sin}(i) = \sin\left(\frac{\pi(i-0.5)}{N}\right), \quad i = 1, \ldots, N. \tag{3.5}$$

In Figure 3.3, a sine window of length 32 shown.

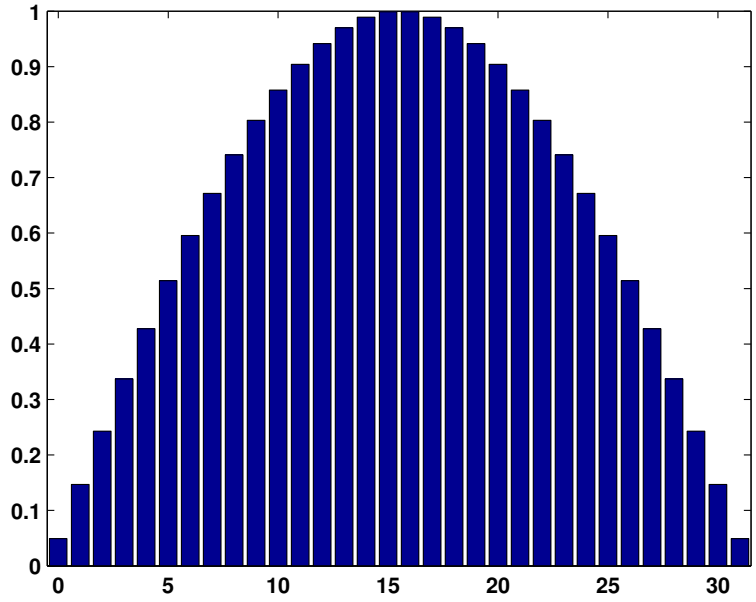

Figure 3.3: A bar-chart depiction of a sine window of length 32

To see how the effect of this window compares to that of w_{rect}, we calculate the FT of (3.4):

$$\begin{aligned} W_{\sin}(\omega) &= \int_{-\infty}^{\infty} w_{\sin}(t) e^{-2\pi i\omega t} dt = \int_0^T \sin\left(\frac{\pi t}{T}\right) e^{-2\pi i\omega t} dt \\ &= e^{-\pi i\omega T} \frac{2T\cos(\pi\omega T)}{\pi(1-(2\omega T)^2)}. \end{aligned} \tag{3.6}$$

In Figure 3.4 this transform is depicted, along with that of the rectangular window, obtained in the previous subsection.

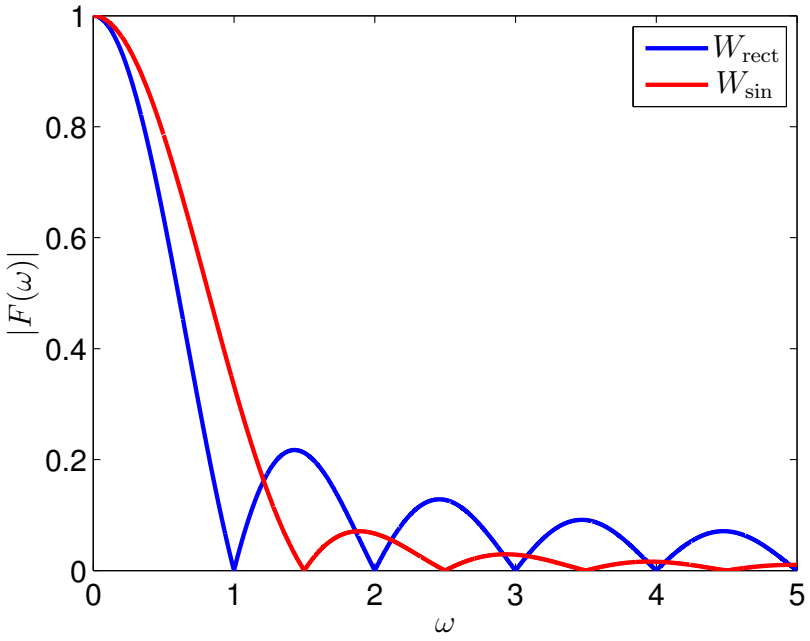

Figure 3.4: FTs of the rectangular and sine windows

From this figure we observe that the sine window's frequency content tends to zero much faster than that of the rectangular window; any aliasing caused by this window will thus be significantly less. The so-called main lobe of W_{sin} is, however, wider than the one belonging to W_{rect}. This width is a measure of how accurately we can identify the amplitudes of specific frequencies, known as *frequency resolution*: the wider the main lobe, the poorer the window function's frequency resolution will be.

3.2.3 The Hanning Window

From (3.4) we see that the sine window happens to have discontinuities in its first derivative at its end points — an example of a window function which addresses this is the

Hanning window:

$$w_{\text{Han}}(t) = \begin{cases} 0.5\left(1-\cos\left(\dfrac{2\pi t}{T}\right)\right), & t \in [0,\ T], \\ 0, & \text{otherwise.} \end{cases} \tag{3.7}$$

Its corresponding definition for discretely sampled signals is given by

$$\mathbf{w}_{\text{Han}}(i) = 0.5\left(1-\cos\left(\frac{2\pi(i-0.5)}{N}\right)\right), \quad i = 1,\ldots,N \tag{3.8}$$

and, once again, a graphical depiction of one of length 32 is shown in Figure 3.5.

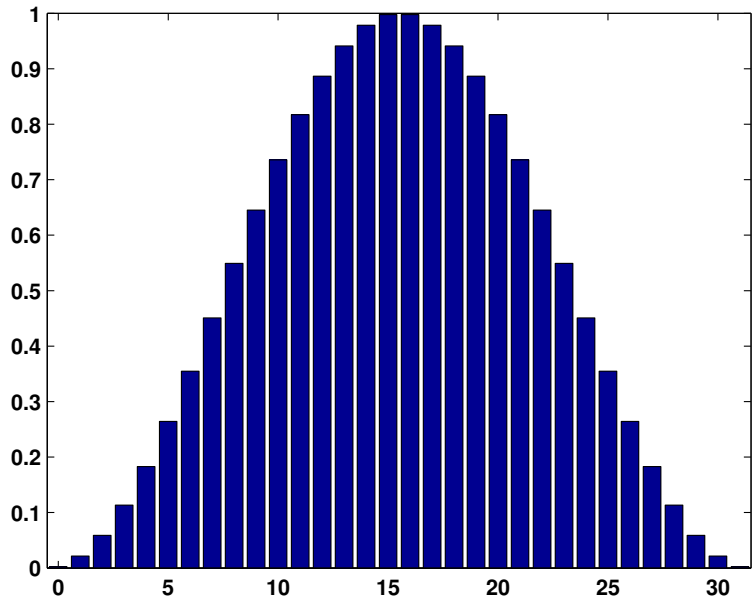

Figure 3.5: A bar-chart depiction of a Hanning window of length 32

To see if this window is an improvement on w_{sin}, we again calculate the FT, this time of (3.7), to find

$$\begin{aligned} W_{\text{Han}}(\omega) &= \int_{-\infty}^{\infty} w_{\text{Han}}(t)e^{-2\pi i\omega t}dt = \int_0^T 0.5\left(1-\cos\left(\frac{2\pi t}{T}\right)\right)e^{-2\pi i\omega t}dt \\ &= e^{-\pi i\omega T}\frac{sin(\pi\omega T)}{2\pi\omega(1-(\omega T)^2)}. \end{aligned} \tag{3.9}$$

Figure 3.6 shows the Fourier transforms of all three window functions considered thus far, with W_{Han} indeed having an even faster drop-off in energy.

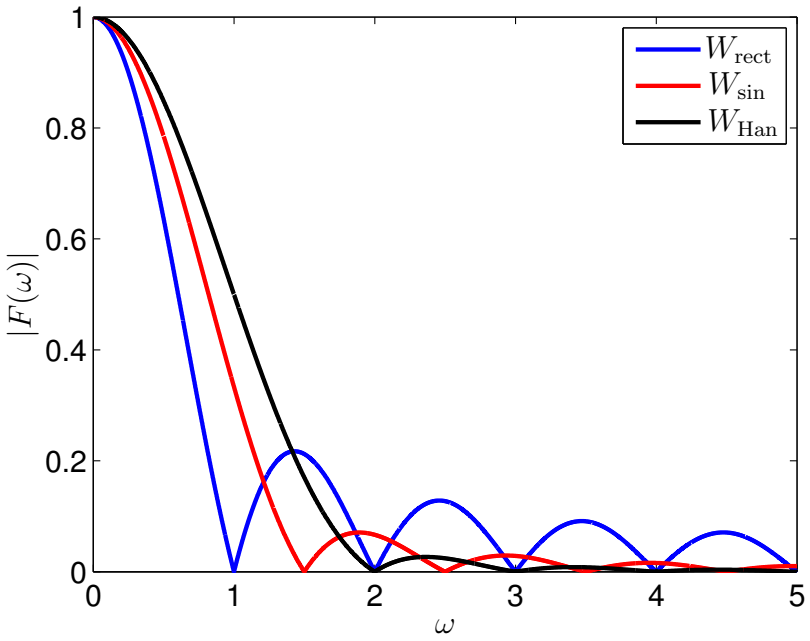

Figure 3.6: FTs of the rectangular, sine and Hanning windows

The width of its main lobe is, however, even larger than that of W_{sin}. This means that one is now faced with a trade-off when selecting a window function: We have to strike a balance between main lobe width and side lobe energy, or, equivalently, between frequency resolution and aliasing.

3.2.4 The Kaiser-Bessel Window

A window function that enables us to manipulate the abovementioned trade-off is the Kaiser-Bessel window. For discretely sampled signals it is defined as

$$\mathbf{w}_{\text{KB}}(i) = \frac{I_0\left(\pi\alpha\sqrt{1-\left(\frac{i-1-0.5(N-1)}{0.5(N-1)}\right)^2}\right)}{I_0(\pi\alpha)}, \quad i = 1,\ldots,N, \quad \alpha \geq 0, \tag{3.10}$$

where I_0 is the 0th order modified Bessel function. The parameter α is the means by which this manipulation is done: The larger α becomes, the narrower the window's bell shape becomes and the faster its side lobe energy drops off, but the poorer its frequency

resolution is. On the other hand, the smaller α becomes, the more $\mathbf{w}_{\mathrm{KB}}$ starts to resemble the rectangular window. In particular, when $\alpha = 0$, $\mathbf{w}_{\mathrm{rect}}$ is obtained.

Many other window functions exist, but the two typically used in audio compression techniques are the sine window and a version of the Kaiser-Bessel window known as the Kaiser-Bessel Derived (KBD) window[1]. For example, MPEG AAC makes use of the sine window and the KBD window with $\alpha = 4$ and $\alpha = 6$ [8].

3.3 Overlap-and-add

Utilising a bell-shaped window function unfortunately causes an unwanted side effect: After windowing and calculating the time-to-frequency transform, we intend to quantise the resulting transform coefficients. During the decoding process, after dequantising and inverting the transform, we have to divide (pointwise) by the window function to obtain an approximation to the original audio samples. In the absence of quantisation this poses no problem — perfect inversion will take place. However, dividing dequantised transform coefficients, now containing a quantisation error, will exacerbate that error when dividing by numbers close to zero. In other words, at the edges of our transform blocks, where the window function approaches zero, we end up inflating quantisation errors. We need to remove division by the window function and find another way of recovering the signal samples.

Let

$$\mathbf{x} = [x_1, x_2, \ldots, x_N]$$

denote the signal samples in a typical transform block, and

$$\mathbf{w} = [w_1, w_2, \ldots, w_N]$$

denote the entries in the chosen window function, where N is an even number. Thus,

[1] We obtain the KBD window by applying the normalisation formula (3.12) listed in the next section to $\mathbf{w}_{\mathrm{KB}}$.

after windowing, the input to the forward transform is

$$\mathbf{w} * \mathbf{x} = [w_1 x_1, w_2 x_2, \ldots, w_N x_N],$$

where the symbol "$*$" denotes the illustrated pointwise multiplication. In the absence of quantisation, the output of the inverse transform is again simply $\mathbf{w} * \mathbf{x}$, after which we would have liked to divide by $\mathbf{w}$, as mentioned above. Notice that in the above equation each $w_i x_i$ is a fraction of the corresponding x_i, and if we had an appropriate accompanying fraction of x_i, we could add them together to recover x_i.

Overlapping the transform blocks, thus using each sample x_i twice, gives us this second fraction, as seen in Figure 3.7. Conventionally, in overlap-and-add, windowing is also applied to the output of the inverse transform, thereby achieving encoding/decoding symmetry. A window used during encoding is referred to as an *analysis* window, while one used during decoding is called a *synthesis* window, since they are allowed to differ. Here we will only consider the case of identical analysis and synthesis windows, therefore the fractions requiring counterparts are now

$$w_i^2 x_i, \quad i = 1, \ldots, N.$$

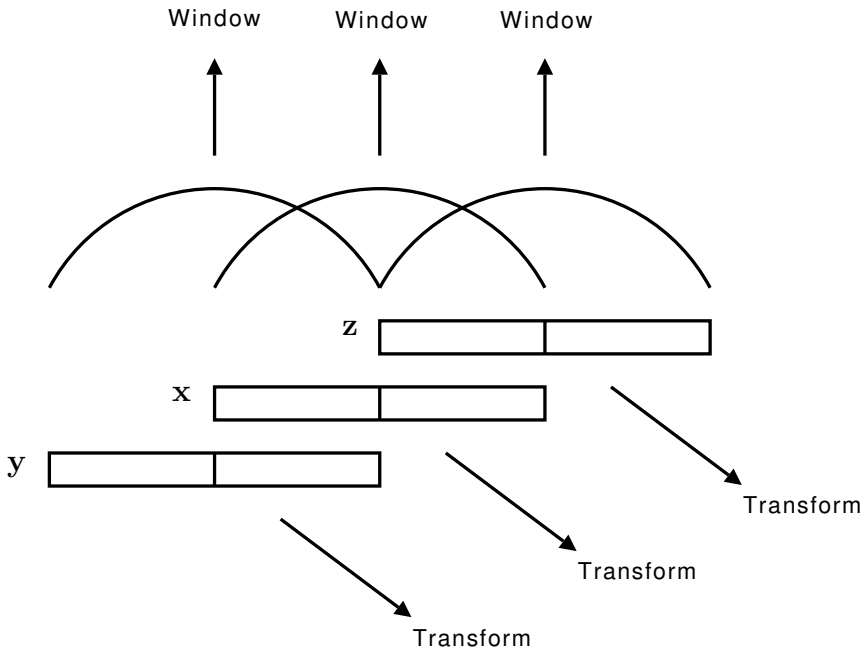

Figure 3.7: A graphical depiction of windowed overlap-and-add, with 50% overlap

Figure 3.7 depicts the specific case of 50% overlap, to which we limit our discussion. The transform block preceding block $\mathbf{x}$, denoted by $\mathbf{y}$, consists of the $\frac{N}{2}$ samples preceding block $\mathbf{x}$ followed by the first $\frac{N}{2}$ samples of block $\mathbf{x}$. Similarly, the last $\frac{N}{2}$ samples of $\mathbf{x}$ followed by the $\frac{N}{2}$ samples succeeding it form the subsequent block, denoted here by $\mathbf{z}$. Attempting to recover a particular x_i, we now overlap the appropriate portion of block $\mathbf{x}$ with the appropriate neighbouring block and add the twice windowed samples together. In the case of the first half of $\mathbf{x}$ we have

$$\begin{aligned} w_i^2 x_i + w_{\frac{N}{2}+i}^2 y_{\frac{N}{2}+i} &= w_i^2 x_i + w_{\frac{N}{2}+i}^2 x_i \\ &= x_i \left(w_i^2 + w_{\frac{N}{2}+i}^2 \right). \end{aligned}$$

Imposing the restriction

$$w_i^2 + w_{\frac{N}{2}+i}^2 = 1 \tag{3.11}$$

on the window function, we ensure that x_i is recovered, or, in terms of our previous discussion, that appropriate fractions of x_i are added together. This is known as a *perfect reconstruction* requirement. We also arrive at (3.11) when attempting to recover a sample from the second half of $\mathbf{x}$.

Given any window function, say $\mathbf{v}$, of length $\frac{N}{2}+1$, one of length N can easily be constructed that satisfies restriction (3.11), using the formula

$$\mathbf{w}(i) = \begin{cases} \dfrac{1}{s}\sqrt{\displaystyle\sum_{k=1}^{i} \mathbf{v}(k)}\ , & i = 1, \ldots, \frac{N}{2}, \\ \dfrac{1}{s}\sqrt{\displaystyle\sum_{k=i-\frac{N}{2}+1}^{\frac{N}{2}+1} \mathbf{v}(k)}\ , & i = \frac{N}{2}+1, \ldots, N, \end{cases} \tag{3.12}$$

where $s = \sqrt{\displaystyle\sum_{k=1}^{\frac{N}{2}+1} \mathbf{v}(k)}$. We call such a window a *normalized* window. Notice that the sine window already satisfies our restriction, due to the trigonometric identity

$$\sin^2 x + \cos^2 x = 1.$$

A more general derivation of the perfect reconstruction requirement can be found in [8], which takes into consideration more general analysis and synthesis windows as well as

more general overlap lengths. We conclude this section by summarising the encoding and decoding procedures resulting from the above discussion.

1. Form transform blocks using 50% overlap as suggested by Figure 3.7.
2. Apply a normalized window function to the blocks.
3. Apply a time to frequency mapping to these blocks, resulting in frequency components.
4. Quantise the frequency components.
5. Entropy code the quantised data.

Algorithm 3.1: Encoding procedure of a basic audio coding technique

1. Decompress entropy coded data, yielding quantised frequency components.
2. Dequantise the frequency components.
3. Apply the inverse transform.
4. Once again, apply the normalized window function.
5. Overlap the resulting data blocks as suggested by Figure 3.7 and add up corresponding entries.

Algorithm 3.2: Decoding procedure of a basic audio coding technique

3.4 The MDCT

We are faced with one more problem. Recall that in the case of JPEG an 8×8 block of pixels is mapped to an 8×8 block of frequency components, meaning that the amount of data to be entropy coded (output of the DCT) is the same as the original amount of data (input to the DCT). This desirable property is referred to as *critical sampling*.

In the case of overlap-and-add (with 50% overlap) described in the previous section, we have twice as many transform blocks (of the same size) as we would have had without overlapping. In the process, the amount of data to be compressed has thus doubled, and critical sampling is lost.

The *modified discrete cosine transform* (MDCT), invented by Princen and Bradley [10], overcomes this problem: whereas a standard DCT would map N samples of data to N new values, the MDCT maps an N-sample block, say $\mathbf{x}$, to a block consisting of $\frac{N}{2}$ new values, say $\mathbf{X}$, as illustrated in Figure 3.8.

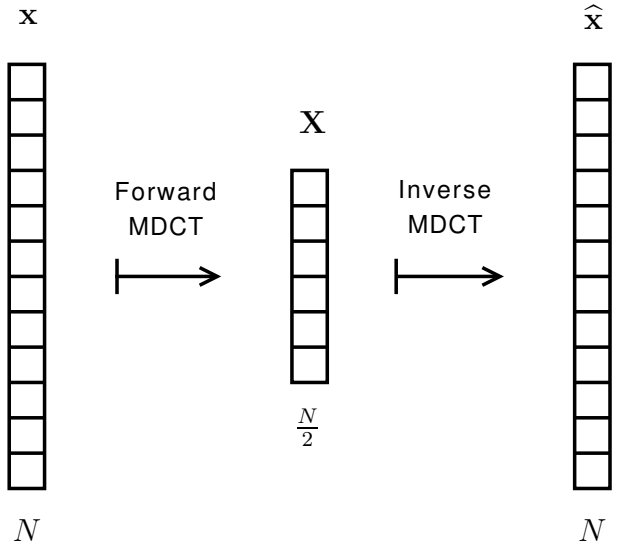

Figure 3.8: A graphical depiction of the forward and inverse MDCT

Given such an input block

$$\mathbf{x} = [x_1, x_2, \ldots, x_N]$$

its MDCT $\mathbf{X}$ is defined as

$$\mathbf{X}(j) = \sum_{i=1}^{N} \mathbf{x}(i) \cos\left(\frac{2\pi}{N}\left(i + \frac{N}{4} - \frac{1}{2}\right)\left(j - \frac{1}{2}\right)\right), \quad j = 1, \ldots, \frac{N}{2}, \tag{3.13}$$

where we omit the use of windowing for the time being.

The "inverse" transform (IMDCT) then maps $\mathbf{X}$ to a block once again consisting of N

values, say $\widehat{\mathbf{x}}$, as defined by

$$\widehat{\mathbf{x}}(i) = \frac{2}{N}\sum_{j=1}^{\frac{N}{2}} \mathbf{X}(j)\cos\left(\frac{2\pi}{N}\left(i+\frac{N}{4}-\frac{1}{2}\right)\left(j-\frac{1}{2}\right)\right), \quad i=1,\ldots,N. \tag{3.14}$$

We use the term inverse in quotations above, because, by itself, the MDCT is not invertible: $\widehat{\mathbf{x}}$ will not be equal to $\mathbf{x}$. Instead, it contains a "scrambled" version of the data originally contained in $\mathbf{x}$ — various samples of $\mathbf{x}$ will be added/subtracted forming the new samples of $\widehat{\mathbf{x}}$. Used in conjunction with overlap-and-add, though, perfect inversion will take place. We illustrate this for the specific case of transform blocks of length 16, because our modification of JPEG makes use of them, as will be seen in the next chapter. For the general derivation of perfect inversion the reader is referred to [10] and [8].

Let $\mathbf{x}$ be such a block consisting of 16 samples,

$$\mathbf{x} = \boxed{a_1 \mid a_2 \mid a_3 \mid a_4 \mid b_1 \mid b_2 \mid b_3 \mid b_4 \mid c_1 \mid c_2 \mid c_3 \mid c_4 \mid d_1 \mid d_2 \mid d_3 \mid d_4} \tag{3.15}$$

or

$$\mathbf{x} = \boxed{\mathbf{a} \mid \mathbf{b} \mid \mathbf{c} \mid \mathbf{d}}$$

for short. Then it is shown in [11] (for the general case of N divisible by 4) that

$$\widehat{\mathbf{x}} = \mathrm{IMDCT}(\mathrm{MDCT}(\mathbf{x})) = \frac{1}{2}\boxed{\mathbf{a}-\mathbf{b}_r \mid \mathbf{b}-\mathbf{a}_r \mid \mathbf{c}+\mathbf{d}_r \mid \mathbf{d}+\mathbf{c}_r}, \tag{3.16}$$

where the subscript r denotes the reversal of a vector, *e.g.*

$$\mathbf{a}_r = \boxed{a_4 \mid a_3 \mid a_2 \mid a_1},$$

and "+" and " − " refer to the usual addition and subtraction of vectors, respectively. For example, the first four entries of $\widehat{\mathbf{x}}$ will be

$$\boxed{\tfrac{1}{2}(a_1-b_4) \mid \tfrac{1}{2}(a_2-b_3) \mid \tfrac{1}{2}(a_3-b_2) \mid \tfrac{1}{2}(a_4-b_1)}.$$

We call this phenomenon *time-domain aliasing*, since it is analogous to the frequency domain aliasing that we explained earlier. Using 50% overlap, let $\mathbf{z}$ be the transform block succeeding block $\mathbf{x}$, of the form

$$\mathbf{z} = \boxed{c_1 \mid c_2 \mid c_3 \mid c_4 \mid d_1 \mid d_2 \mid d_3 \mid d_4 \mid e_1 \mid e_2 \mid e_3 \mid e_4 \mid f_1 \mid f_2 \mid f_3 \mid f_4} \tag{3.17}$$

or

$$\mathbf{z} = \boxed{\mathbf{c}\,|\,\mathbf{d}\,|\,\mathbf{e}\,|\,\mathbf{f}}$$

for short. Now we have that

$$\widehat{\mathbf{z}} = \text{IMDCT}(\text{MDCT}(\mathbf{z})) = \frac{1}{2}\boxed{\mathbf{c}-\mathbf{d}_r\,|\,\mathbf{d}-\mathbf{c}_r\,|\,\mathbf{e}+\mathbf{f}_r\,|\,\mathbf{f}+\mathbf{e}_r}\,.$$

Overlapping the appropriate portions of $\widehat{\mathbf{x}}$ and $\widehat{\mathbf{z}}$ and adding up gives us

$$\frac{1}{2}(\mathbf{c}+\mathbf{d}_r)+\frac{1}{2}(\mathbf{c}-\mathbf{d}_r)=\mathbf{c}$$

and

$$\frac{1}{2}(\mathbf{d}+\mathbf{c}_r)+\frac{1}{2}(\mathbf{d}-\mathbf{c}_r)=\mathbf{d}.$$

Similarly, we recover portions **a** and **b** by considering the transform block preceding block **x**.

Overlapping and adding has thus resulted in the cancellation of the contaminating signal portions, with perfect inversion indeed taking place. Consequently, the MDCT is an example of a *time domain aliasing cancellation* (TDAC) transform.

We, of course, intend to apply windowing as well, so it remains to show that overlap-and-add will also simultaneously remove windowing and time domain aliasing. Once again, let data block **x** be defined as in (3.15) and let the window function **w** be given by

$$\begin{aligned}\mathbf{w} &= \boxed{u_1\,|\,u_2\,|\,u_3\,|\,u_4\,|\,v_1\,|\,v_2\,|\,v_3\,|\,v_4\,|\,v_4\,|\,v_3\,|\,v_2\,|\,v_1\,|\,u_4\,|\,u_3\,|\,u_2\,|\,u_1}\\ &= \boxed{\mathbf{u}\,|\,\mathbf{v}\,|\,\mathbf{v}_r\,|\,\mathbf{u}_r}\,, \qquad (3.18)\end{aligned}$$

where we now also require the window function to be symmetric. Therefore, restriction (3.11) can now be written as

$$\mathbf{u}_r^2+\mathbf{v}^2=\boxed{1\,|\,1\,|\,1\,|\,1}$$

as well as

$$\mathbf{v}_r^2+\mathbf{u}^2=\boxed{1\,|\,1\,|\,1\,|\,1}\,,$$

where the exponent 2 denotes the pointwise multiplication of a vector with itself. Here the input to the MDCT will be

$$\mathbf{w} * \mathbf{x} = \boxed{\mathbf{u} * \mathbf{a} \mid \mathbf{v} * \mathbf{b} \mid \mathbf{v}_r * \mathbf{c} \mid \mathbf{u}_r * \mathbf{d}},$$

and, using (3.16), the output of the IMDCT will be

$$\begin{aligned} \widehat{\mathbf{x}} &= \text{IMDCT}(\text{MDCT}(\mathbf{w} * \mathbf{x})) \\ &= \frac{1}{2}\boxed{\mathbf{u} * \mathbf{a} - \mathbf{v}_r * \mathbf{b}_r \mid \mathbf{v} * \mathbf{b} - \mathbf{u}_r * \mathbf{a}_r \mid \mathbf{v}_r * \mathbf{c} + \mathbf{u} * \mathbf{d}_r \mid \mathbf{u}_r * \mathbf{d} + \mathbf{v} * \mathbf{c}_r}. \end{aligned}$$

Upon decoding, we once again window, yielding

$$\mathbf{w} * \widehat{\mathbf{x}} = \frac{1}{2}\boxed{\mathbf{u}^2 * \mathbf{a} - \mathbf{u} * \mathbf{v}_r * \mathbf{b}_r \mid \mathbf{v}^2 * \mathbf{b} - \mathbf{v} * \mathbf{u}_r * \mathbf{a}_r \mid \mathbf{v}_r^2 * \mathbf{c} + \mathbf{v}_r * \mathbf{u} * \mathbf{d}_r \mid \mathbf{u}_r^2 * \mathbf{d} + \mathbf{u}_r * \mathbf{v} * \mathbf{c}_r}.$$

With the subsequent transform block, $\mathbf{z}$, once again as defined by (3.17), its decoded (and windowed) version will be

$$\mathbf{w} * \widehat{\mathbf{z}} = \frac{1}{2}\boxed{\mathbf{u}^2 * \mathbf{c} - \mathbf{u} * \mathbf{v}_r * \mathbf{d}_r \mid \mathbf{v}^2 * \mathbf{d} - \mathbf{v} * \mathbf{u}_r * \mathbf{c}_r \mid \mathbf{v}_r^2 * \mathbf{e} + \mathbf{v}_r * \mathbf{u} * \mathbf{f}_r \mid \mathbf{u}_r^2 * \mathbf{f} + \mathbf{u}_r * \mathbf{v} * \mathbf{e}_r}.$$

This time overlapping and adding gives us

$$\begin{aligned} &\frac{1}{2}(\mathbf{v}_r^2 * \mathbf{c} + \mathbf{v}_r * \mathbf{u} * \mathbf{d}_r) + \frac{1}{2}(\mathbf{u}^2 * \mathbf{c} - \mathbf{u} * \mathbf{v}_r * \mathbf{d}_r) \\ &\quad = \frac{1}{2}\mathbf{c} * (\mathbf{v}_r^2 + \mathbf{u}^2) + \frac{1}{2}\mathbf{d}_r(\mathbf{v}_r * \mathbf{u} - \mathbf{v}_r * \mathbf{u}) \\ &\quad\quad = \frac{1}{2}\mathbf{c} * \boxed{1 \mid 1 \mid 1 \mid 1} = \frac{1}{2}\mathbf{c} \end{aligned}$$

and

$$\begin{aligned} &\frac{1}{2}(\mathbf{u}_r^2 * \mathbf{d} + \mathbf{u}_r * \mathbf{v} * \mathbf{c}_r) + \frac{1}{2}(\mathbf{v}^2 * \mathbf{d} - \mathbf{v} * \mathbf{u}_r * \mathbf{c}_r) \\ &\quad = \frac{1}{2}\mathbf{d} * (\mathbf{u}_r^2 + \mathbf{v}^2) + \frac{1}{2}\mathbf{c}_r(\mathbf{u}_r * \mathbf{v} - \mathbf{u}_r * \mathbf{v}) \\ &\quad\quad = \frac{1}{2}\mathbf{d} * \boxed{1 \mid 1 \mid 1 \mid 1} = \frac{1}{2}\mathbf{d}. \end{aligned}$$

By now slightly modifying the formula for the IMDCT for the case of windowing — multiplying by 2 — the desired reconstruction is obtained. Once again, portions $\mathbf{a}$ and $\mathbf{b}$ of $\mathbf{x}$ are similarly recovered by considering the transform block preceding block $\mathbf{x}$.

The formulas for the windowed MDCT and IMDCT are now

$$\mathbf{X}(j) = \sum_{i=1}^{N} \mathbf{w}(i)\mathbf{x}(i) \cos\left(\frac{2\pi}{N}\left(i + \frac{N}{4} - \frac{1}{2}\right)\left(j - \frac{1}{2}\right)\right), \quad j = 1, \ldots, \frac{N}{2} \tag{3.19}$$

and

$$\widehat{\mathbf{x}}(i) = \frac{4}{N}\mathbf{w}(i) \sum_{j=1}^{\frac{N}{2}} \mathbf{X}(j) \cos\left(\frac{2\pi}{N}\left(i + \frac{N}{4} - \frac{1}{2}\right)\left(j - \frac{1}{2}\right)\right), \quad i = 1, \ldots, N, \tag{3.20}$$

respectively, while they remain (3.13) and (3.14) in the absence of windowing.

Lastly, by now using the windowed MDCT in steps 2 and 3 in Algorithm 3.1 (listed in the previous section), a rough layout of a basic audio coding scheme is formed.

3.5 Final Note

While our example in the previous section made use of 16-sample transform blocks, those used in audio coding are actually much larger. Using MPEG AAC again as an example, it can switch between blocks of sizes 256 and 2048, depending on changes in signal conditions.

Also, the means by which audio coding techniques perform quantisation and entropy coding are again outside the scope of this dissertation. Detailed accounts of the approaches used by several such techniques can be found in [8].

Most importantly, the previous discussions on overlap-and-add actually made an implicit assumption about the sampled audio signal being worked with: it is bi-infinite. That is to say, any transform block $\mathbf{x}$ will always have a preceding as well as succeeding block to overlap with. In practice, this is of course not the case; a digital audio signal will have a beginning and an end. Thus we find that its first transform block will have nothing to overlap with to the "left", and its last transform block nothing to the "right".

In the case of audio coding, where we have a 1D signal, this problem is such a non-issue (its solution so trivial) that literature on the subject might not even mention it. However, the problem becomes much more significant for image compression, where the signal is 2-dimensional, as we will see in the next chapter. Section 4.2, in particular, focuses on various strategies for solving this problem, in the 1D as well as the 2D case.

Chapter 4

Modifying JPEG

In Chapter 3 we motivated using the windowed MDCT in audio coding. The aim of this research is to investigate if any improvements in quality can be achieved by doing the same for image compression. As stated in Chapter 1, we specifically modify JPEG by replacing the standard DCT with the windowed MDCT, and refer to the modification as MJPEG.

4.1 Modifications

We would like to retain JPEG's existing well-defined structure; among others, quantising 8×8 blocks of frequency components. By extending the 1D case of 16-sample transform blocks illustrated in Section 3.4 to two dimensions, this is achieved: Given a 16×16 block of pixels, we first apply (3.19) to its rows and then to the columns of the resulting 16×8 matrix, thereby implementing a 2D windowed MDCT. This transform therefore maps 16×16 transform blocks to 8×8 blocks of frequency components. By similarly using (3.20), the 2D inverse transform will map back to 16×16 blocks. This concept is illustrated in Figure 4.1.

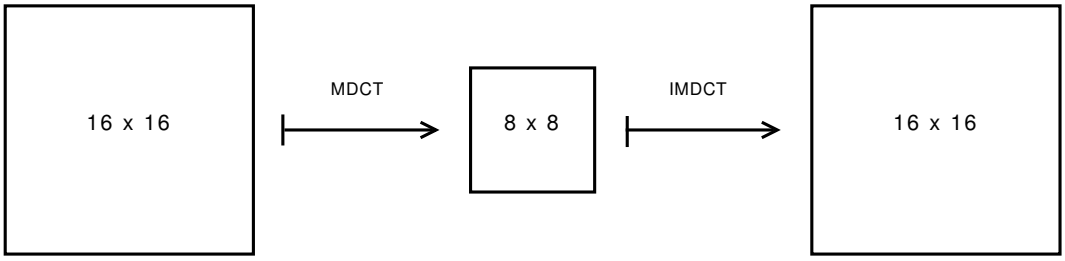

Figure 4.1: Extending the 1D MDCT to two dimensions in order to obtain 8×8 transform blocks

By doing this, overlap-adding is also extended to two dimensions, as demonstrated in Figure 4.2. Notice that each 2D transform block will have eight neighbouring blocks to overlap with.

Alternatively, one could first apply (3.19) to each row of an entire image, the same way we would to an audio signal, using 1D transform blocks of length 16. The same is then done to the columns of the resulting output. In the end, the same matrix, say Y, consisting of 8×8 blocks of frequency components is obtained. To decode, the reverse process is applied — first each column of Y is inversely transformed using (3.20) and overlap-added, then each row of the resulting output. Even though both of these implementations yield the same results, only the latter is compatible with the strategy to be proposed in Section 4.2.3, and is therefore the implementation we chose.

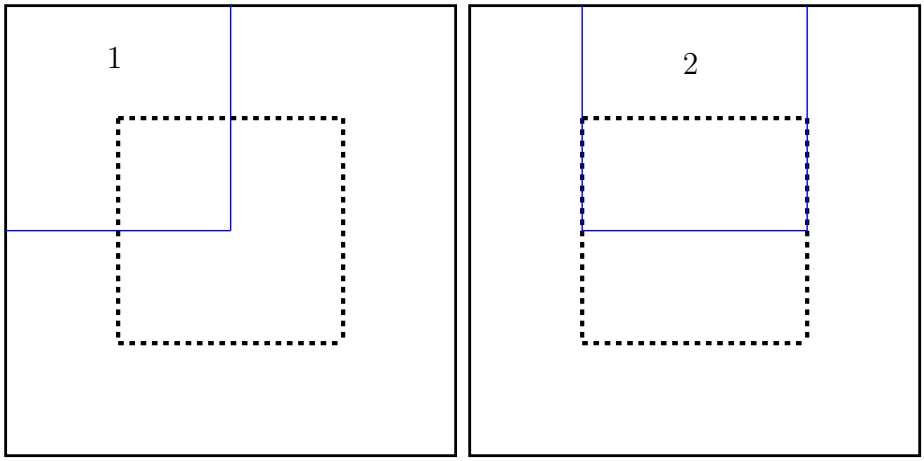

(a) 1st overlapping block (b) 2nd overlapping block

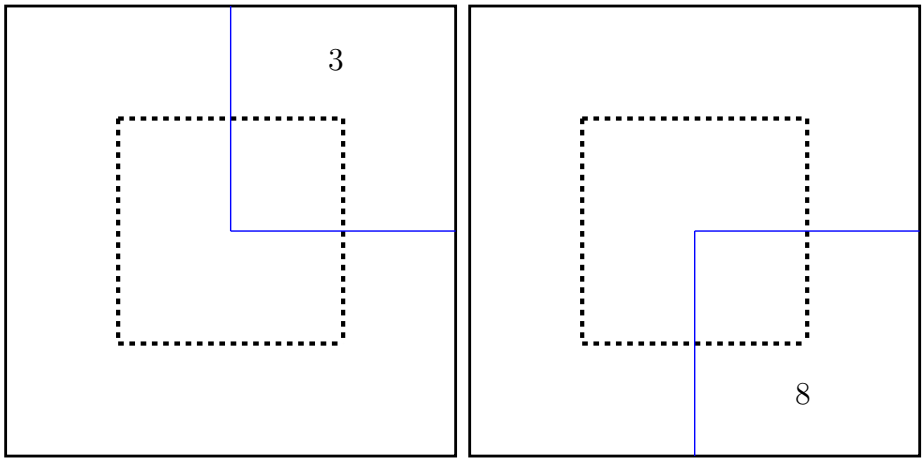

(c) 3rd overlapping block (d) 8th overlapping block

Figure 4.2: The extension of overlap-adding to two dimensions, resulting in 8 overlapping neighbouring blocks for each transform block

By retaining 8×8 blocks of frequency components, the overall operation of JPEG is retained by MJPEG. We can once again use an 8×8 quantisation table, form a zigzag sequence of length 64 from the quantised coefficients, and use the existing Huffman tables to encode it[1].

Lastly, we would also like any given QT to quantise both DCT and MDCT coefficients with

[1]From (3.19) one can see that no zero-frequency (DC) coefficient is generated by the MDCT. Fortunately, the first coefficient that is generated does still correspond to a low frequency. MJPEG therefore continues to differentially code these coefficients.

more or less the same severity. However, due to the differences between the respective defining equations, MDCT coefficients in an 8×8 block are roughly four times larger than DCT coefficients in an 8×8 block. Our implementation of MJPEG therefore divides such MDCT coefficients by four before quantisation and multiplies them by four after dequantisation.

4.2 What About the Image Boundary?

In Section 3.5 the problem concerning the first and last block of an audio signal was touched upon. As shown in Figure 4.3, for the simple case of two blocks, neither the first half of the first block nor the second half of the last block have any samples to overlap with. In image compression the entire image boundary will suffer from this problem.

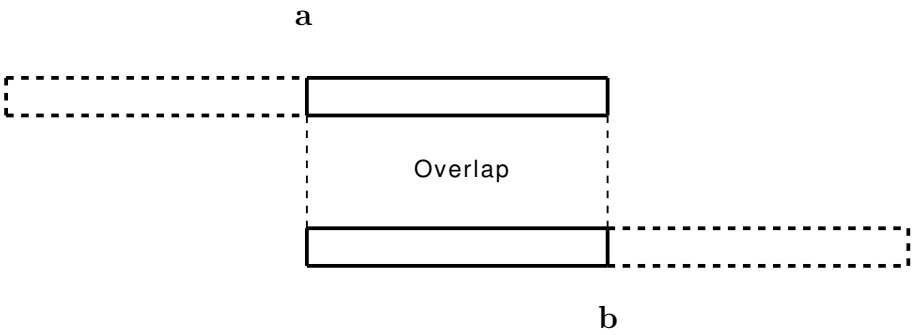

Figure 4.3: A simplified signal consisting of only two overlapping transform blocks, denoted by **a** and **b**

In this section, several strategies for solving this problem is discussed.

4.2.1 Padding

One way of addressing the problem shown in Figure 4.3, called *padding*, is by creating extra samples at the beginning and end of the signal — thereby creating two additional blocks to overlap with. As an example, let the signal in question consist of 24 samples, so that each transform block, labelled **a** and **b**, respectively, consists of 16 samples. This

signal is depicted in Figure 4.4 below.

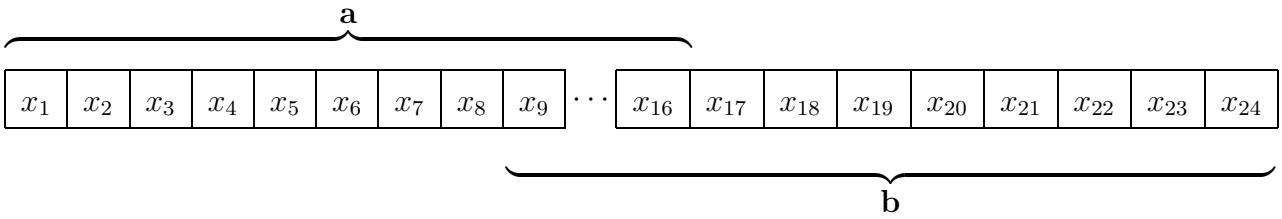

Figure 4.4: A 24-sample signal, with overlapping transform blocks **a** and **b** consisting of 16 samples each

Since the first 8 samples of **a** require overlap, the first auxilliary block, say $\widetilde{\mathbf{a}}$, will contain those samples as its second half, leaving us with 8 samples to create for its first half. These 8 samples may be chosen arbitrarily; however, in order to maximise continuity within the new block, they are chosen as shown in Figure 4.5: Samples x_1 to x_8 are replicated and reversed, forming the padded data.

x_8	x_7	x_6	x_5	x_4	x_3	x_2	x_1	x_1	x_2	x_3	x_4	x_5	x_6	x_7	x_8

Figure 4.5: Auxilliary block $\widetilde{\mathbf{a}}$ formed by padding

Clearly these samples will now be recovered during decoding; the additional samples, whether properly decoded or not, can then be discarded. In a similar fashion, an auxilliary block, say $\widetilde{\mathbf{b}}$, is formed by padding 8 samples at the end of the signal in Figure 4.4.

Notice that, since each of the four transform blocks above ($\widetilde{\mathbf{a}}$, **a**, **b**, and $\widetilde{\mathbf{b}}$) consist of 16 samples, they yield $4 \times 8 = 32$ frequency components during encoding, 8 more than the 24 samples started with. Padding therefore results in one extra transform block's worth of data to store. For audio coding, this is a minuscule amount of overhead, considering that a typical audio file consists of thousands of transform blocks. The amount is also fixed — it does not increase with the duration of the audio signal, becoming ever more negligible as the length of the signal increases.

This solution is immediately applicable to the 2D image compression case as well. Figure 4.6 illustrates the situation that results from this when utilising 2D transform blocks to

implement the 2D MDCT. The entire image is surrounded by padded data consisting of replicated pixels.

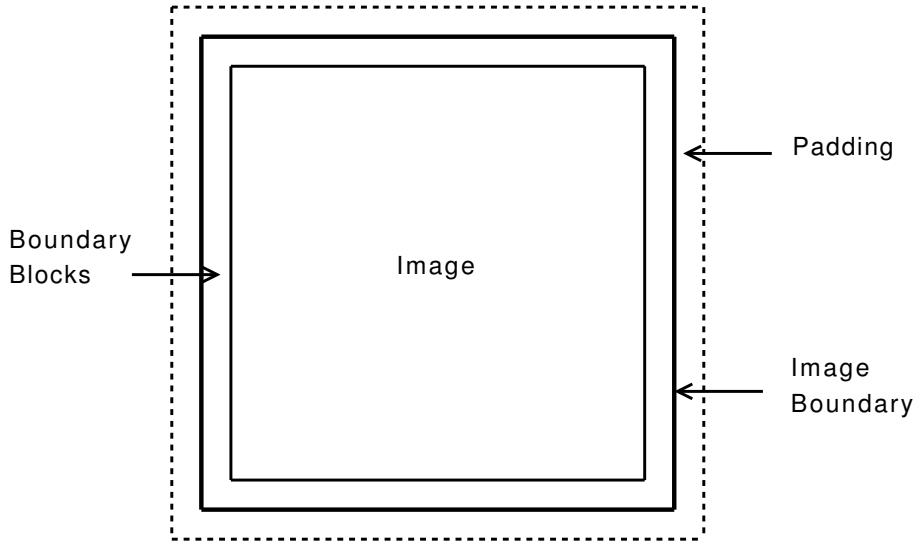

Figure 4.6: Padding applied to an image, resulting in a significant loss in critical sampling

When using our chosen implementation of the 2D MDCT, only the padding to the left and right of each image row would consist of replicated pixels. The padding above and below the columns of the output resulting from applying (3.19) to the rows will be made up of replicated 1D frequency components. Either way, the amount of padded data is the same.

The loss in critical sampling is no longer negligible, regardless of the size of the image. As the size of the image increases, so does the amount of padded data (it does decrease percentage-wise, relative to the total amount of data to be compressed). This additional amount, while not drastically large, is still large enough to sabotage competitiveness with JPEG, which is our main priority.

4.2.2 Wrap-around

Utilising the concept of periodic boundaries, we can devise a solution to the boundary problem that will maintain critical sampling — we will refer to it as *wrap-around*. Instead

of two, only one auxilliary transform block is formed by considering the first $\frac{N}{2}$ samples of a signal as succeeding the last $\frac{N}{2}$ samples, where N is the length of a transform block. When applied to the signal in Figure 4.4, this results in the signal shown in Figure 4.7 below.

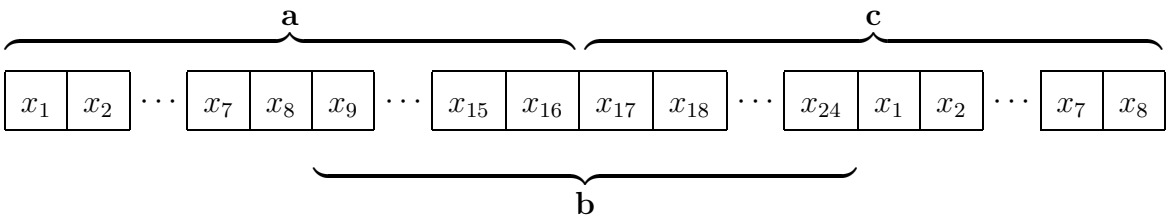

Figure 4.7: Periodic extension of the signal in Figure 4.4

Here **c** denotes the new block formed by letting the first 8 samples (x_1 to x_8) continue after the final 8 (x_{17} to x_{24}). Encoding can then be applied to blocks **a**, **b**, and **c**, in that order, resulting in 24 frequency components to store. With regards to decoding, samples x_1 to x_8 can now be recovered by overlapping and adding the first half and second half of the respective inverse transforms of blocks **a** and **c**'s frequency components. Similarly, samples x_{17} to x_{24} are recovered by overlapping and adding the second half of the inverse transform of **b**'s frequency components and the first half of the inverse transform of **c**'s frequency components.

Once again, we can readily apply the solution to the 2D case of image compression. Figure 4.8 illustrates the wrap-around concept in two dimensions, if one were to use 2D transform blocks. It shows, for instance, that all four corners of an image would overlap, via wrap-around, with each other. On the other hand, using 1D MDCTs, horizontal wrap-around will take place in the spatial domain, while vertical wrap-around will take place in the 1D frequency domain.

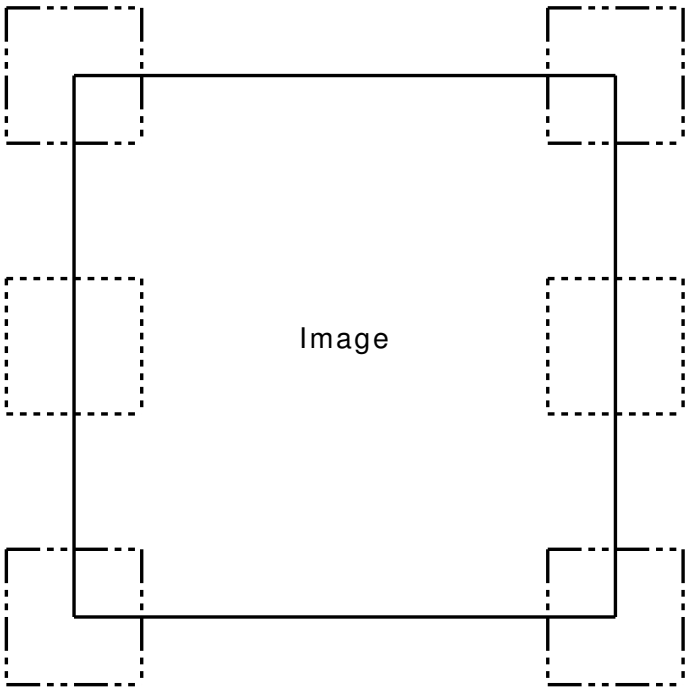

Figure 4.8: Wrap-around extended to two dimensions, illustrating the overlapping of boundary blocks

Regardless of how we choose to implement the 2D MDCT, the wrap-around technique causes a problem, as can be seen in Figure 4.7, when examining block **c**. Roughly speaking, the concatenated samples sequences $[x_{17}, \ldots, x_{24}]$ and $[x_1, \ldots, x_8]$ have nothing to do with each other. More precisely, the transition from the one to the other causes a sharp discontinuity in block **c**, and thus on the signal boundary. The same will also be true of an image — sharp discontinuities will be formed across the entire image boundary. This, of course, poses no problem in the absence of quantisation; however, in the presence of even mild quantisation the problem is severe, forming noticeable lines parallel to each boundary line of the reconstructed image. An example of this can be seen in Figure 4.9: an MJPEG encoding (with the sine window) of the 256×256 Lena image, where wrap-around in the spatial (pixel) domain was used. Quantisation was done using JPEG's standard QT, listed in Table 2.1.

Figure 4.9(a) shows the reconstructed image in its entirety, while Figure 4.9(b) shows an enlarged portion of it, pointing out the vertical lines that have been formed close to the

right boundary line.

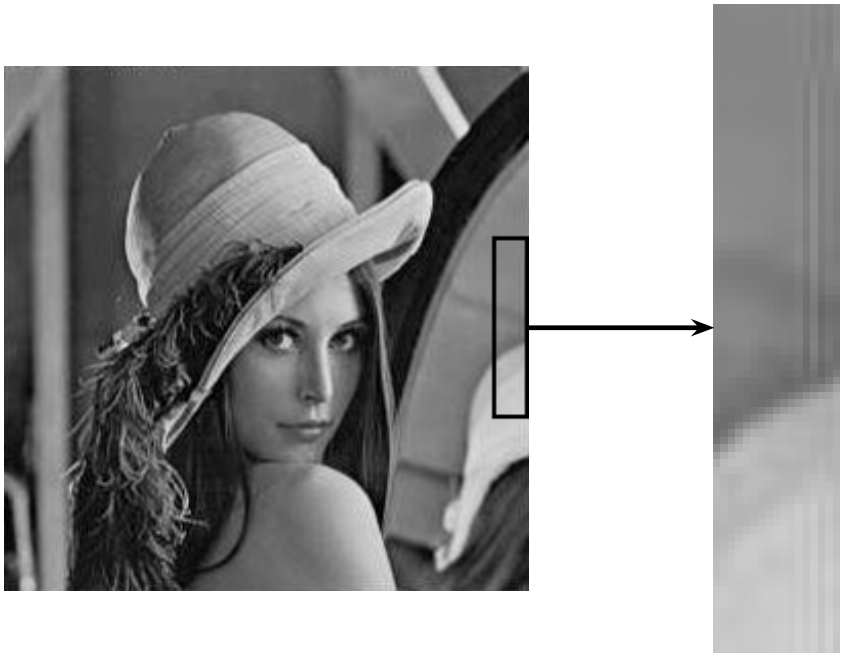

(a) Reconstructed Image (b) Right Boundary Region

Figure 4.9: Reconstruction of an MJPEG encoding of Lena, where the wrap-around technique is ultilised

We can neutralise these discontinuities by relaxing the quantisation of the frequency coefficients in the boundary blocks, but this will also decrease their compressibility. As was the case with padding, we are left with more data to store than we would prefer, and competitiveness with JPEG is again compromised.

4.2.3 Hybrid Coefficients

To encode an image's boundary more efficiently, we need to revisit the inner workings of the MDCT. Let us again consider our 24-sample signal, reproduced in Figure 4.10 below.

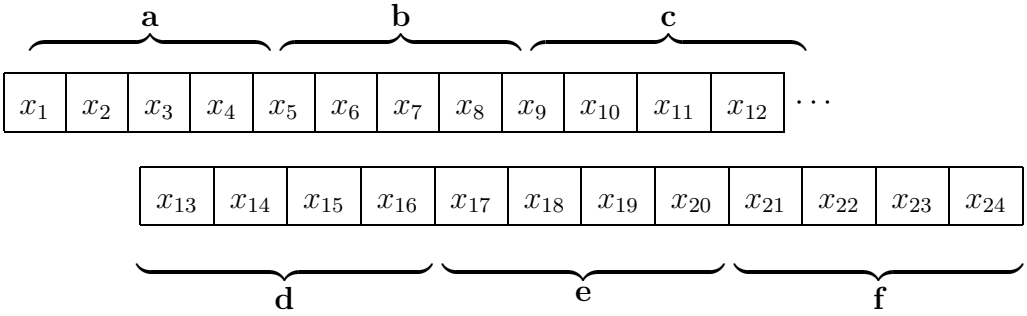

Figure 4.10: Reproduction of the 24-sample signal in Figure 4.4, with 4-sample portions labelled **a** to **f**

Using the notation introduced in Section 3.4, portions of the signal are labelled $\mathbf{a}, \mathbf{b}, \ldots, \mathbf{f}$, such that the first transform block consists of portions **a** to **d**, and the second consists of portions **c** to **f**. Upon encoding (windowing and performing the MDCT), each transform block yields 8 frequency components to be (quantised and) stored, say

X_1	X_2	X_3	X_4	X_5	X_6	X_7	X_8

and

X_9	X_{10}	X_{11}	X_{12}	X_{13}	X_{14}	X_{15}	X_{16}

for a total of 16 numbers to store. We thus have space for 8 more numbers. Recall from Section 3.4 that decoding the above frequency blocks (applying the IMDCT, windowing, and overlap-adding) yields

$\mathbf{u}^2 * \mathbf{a} - \mathbf{u} * \mathbf{v}_r * \mathbf{b}_r$	$\mathbf{v}^2 * \mathbf{b} - \mathbf{v} * \mathbf{u}_r * \mathbf{a}_r$	**c**	**d**	$\mathbf{v}_r^2 * \mathbf{e} + \mathbf{u} * \mathbf{v}_r * \mathbf{f}_r$	$\mathbf{v} * \mathbf{u}_r * \mathbf{e} + \mathbf{u}_r^2 * \mathbf{f}$

$\underbrace{\qquad\qquad}_{\alpha}$ $\underbrace{\qquad\qquad}_{\beta}$

where we have used the same notation for the portions of the window function **w** as in (3.18), as well additional labels $\boldsymbol{\alpha}$ and $\boldsymbol{\beta}$. If we were to store portion **a** (of Figure 4.10), consisting of 4 samples, not only would it be trivially recovered, but we would also be able to recover portion **b** from either portion $\boldsymbol{\alpha}$ or $\boldsymbol{\beta}$. For instance, upon obtaining **a** and $\boldsymbol{\beta}$, portion **a** can be reversed, multiplied by portions **v** and $\mathbf{u}_r$ (both of which are known), and the result added to $\boldsymbol{\beta}$, giving us

$$\mathbf{v}^2 * \mathbf{b} - \mathbf{v} * \mathbf{u}_r * \mathbf{a}_r + \mathbf{v} * \mathbf{u}_r * \mathbf{a}_r = \mathbf{v}^2 * \mathbf{b}.$$

Finally, dividing by $\mathbf{v}^2$ results in portion **b**. Similarly, storing portion **f** (a further 4 samples) allows us to recover portion **e**.

In summary, the 24 numbers we now have to store are

x_1	x_2	x_3	x_4	X_1	$\cdots$	X_{16}	x_{21}	x_{22}	x_{23}	x_{24}

.

We apply this strategy to an $m \times n$ image as follows.

1. The 1D MDCT incorporating the above approach is first applied to the rows of the image, resulting in a matrix consisting of an $m \times (n-8)$ interior of 1D frequency coefficients, and left and right outer strips of original pixel values, each of size $m \times 4$. Such a matrix is depicted in Figure 4.11.

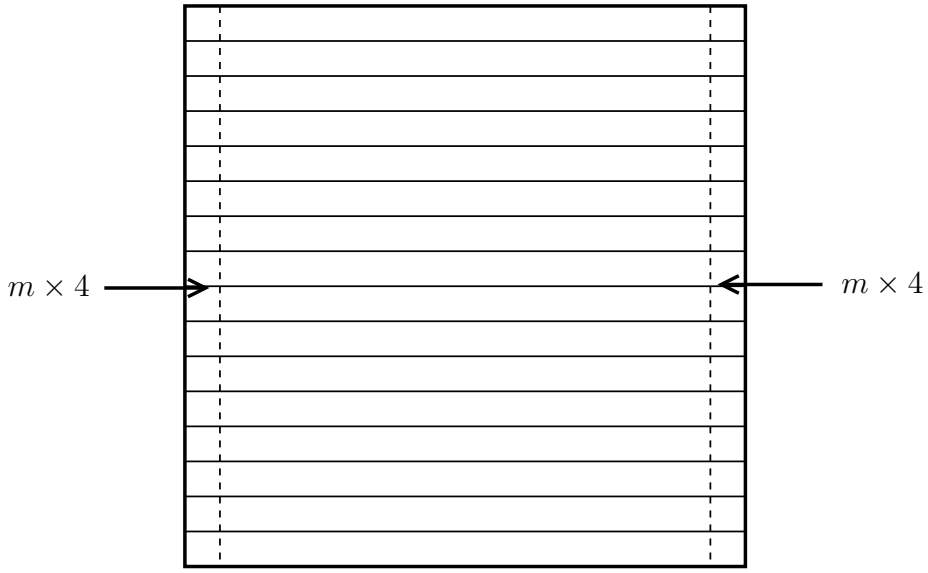

Figure 4.11: First stage output of our proposed MJPEG implementation

2. Since we want the interior to be composed of 8×8 frequency blocks, we next apply the 1D MDCT (incorporating the above approach) to the $n-8$ interior columns of this matrix. This gives us the matrix shown in Figure 4.12 below, now also with a top and bottom strip, each containing 1D frequency coefficients generated in the previous step. Both strips have dimensions $4 \times (n-8)$. Notice that the 8×8 interior

blocks are the same frequency blocks that would have been obtained using any of the previous strategies. Hence, normal quantisation can again be applied to them.

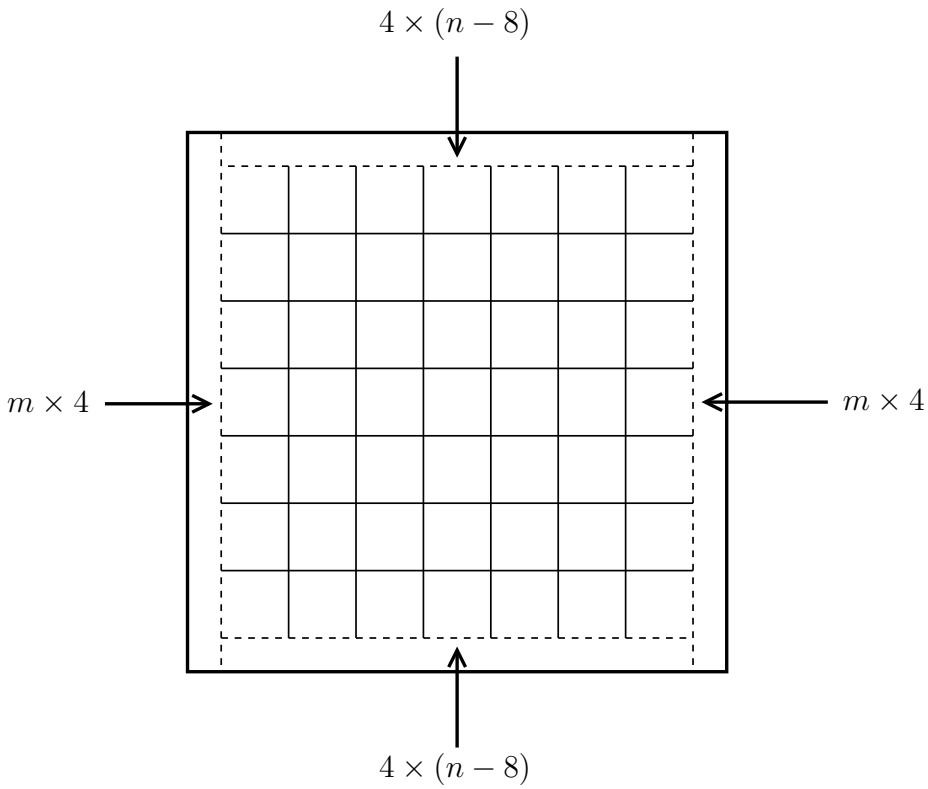

Figure 4.12: Second stage output of our proposed MJPEG implementation, containing outer strips of hybrid coefficients

In order to efficiently encode the image, we also have to apply lossy compression to the outer strips of Figure 4.12. This means that we would like them to also be in the form of 2D frequency components. Since the top and bottom strips contain 4 rows of 1D (horizontal) frequency components, with each row consisting of blocks of length 8, applying a standard 1D DCT to each column results in 4×8 blocks of 2D coefficients. Notice that these are *hybrid* MDCT/DCT coefficients. To the left and right strips, composed of original pixel values, we can apply a standard 2D DCT. For convenience, they are partitioned into (non-overlapping) 4×4 blocks, to which the 2D DCT is applied.

Each pair of strips now requires its own quantisation table: for the top and bottom strips we need a 4×8 table, while the left and right strips need a 4×4 table. Since our choice

of quality measure is the PSNR, we can disregard the physical interpretation of frequency coefficients, and derive the additional QTs from the primary 8×8 QT. This is done by repeatedly downsampling (by averaging adjacent entries) the primary table. For example, the standard JPEG QT shown in Table 2.1 can be successively downsampled as follows. First, vertical downsampling provides us with the 4×8 QT shown in Table 4.1; this table is then horizontally downsampled to give us the 4×4 QT shown in Table 4.2.

14	12	12	18	25	49	56	58
14	15	19	27	46	72	75	59
21	29	46	60	75	107	108	85
61	78	87	93	108	111	112	100

Table 4.1: Auxilliary QT obtained by vertically downsampling Table 2.1

13	15	37	57
15	23	59	67
25	53	91	97
70	90	110	106

Table 4.2: Auxilliary QT obtained by horizontally downsampling Table 4.1 above

This approach allows us to avoid the extra overhead of storing the two additional tables in the output file — we only have to store the primary 8×8 table. More importantly, it allows us to apply QT optimisation algorithms designed for JPEG to MJPEG.

In the case of perceptual coding, where the physical meaning of frequency coefficients is fundamental, one would properly optimise the additional QTs as well, and thus store them as separate entities in the output file.

These two additional QTs should also quantise their corresponding frequency coefficients with more or less the same severity as the primary QT does with its corresponding coefficients. We therefore multiply the DCT coefficients in the left and right strips by two before quantisation, since their magnitudes are roughly half as big as those of coefficients

in 8×8 DCT blocks. After dequantisation they are divided by two. The 4×8 blocks of hybrid coefficients in the top and bottom strips, on the other hand, are left unchanged because these coefficients are of roughly the same magnitude as coefficients in 8×8 DCT blocks.

Finally, entropy coding needs to be applied to these outer strips after quantisation. Just like the internal 8×8 frequency blocks, we form zigzag sequences from the coefficient blocks in these strips: the 4×8 blocks in the top and bottom strips are transformed to sequences of length 32, while the 4×4 blocks in the left and right strips are transformed to sequences of length 16. Once again, we use the standard Huffman tables of JPEG to encode these zigzag sequences.

4.3 Matlab Implementation

Just like JPEG, we implemented MJPEG in Matlab, specifically making use of the hybrid coefficients strategy. In Appendix B.1.2 the corresponding m-files are listed, with `mjpeg.m` and `mjpeg_dec.m` performing the encoding and decoding, respectively. Once again the encoder accepts as input an $m \times n$ image and a QT to quantise it with, and outputs the resulting matrix, say Y, of quantised coefficients. To decode, we input Y and the QT used during encoding to `mjpeg_dec`, which then returns the reconstructed image.

Since we encode by applying the 1D MDCT to the rows and columns of an image separately, and use the 1D IMDCT in a similar fashion to decode, the auxilliary functions `row_enc.m` and `row_dec.m` were created. `row_enc` forms transform blocks using 50% overlap, windows them, and passes each to the m-file `mdct.m`, which calculates a transform block's 1D MDCT. Similarly, `row_dec` passes blocks of frequency coefficients to the m-file `imdct.m`, windows the output, and then performs overlapping and adding. `row_enc` and `row_dec` are also the m-files where the window function is specified; the versions listed in Appendix B.1.2 make use of the sine window as an example.

Matlab does not have a built-in implementation of the 1D DCT, required to form the 4×8 blocks of hybrid coefficients in the top and bottom strips of matrix Y. Therefore,

the functions `dct1.m` and `idct1.m` were written to perform the necessary calculations.

The extra functionality of `dct2bytes` and `d2b` mentioned in Section 2.5 now also becomes clear: In order to calculate the file size resulting from encoding the three types of coefficient blocks contained in Y, `dct2bytes` needs to pass each portion of Y to `d2b`, one after the other. For each such portion `dct2bytes` indicates to `d2b` the dimensions of the frequency blocks contained therein by means of an option parameter. `d2b` then performs the required calculations accordingly.

4.4 A Preliminary Comparison

In order to compare MJPEG with JPEG, QTs are needed to compress test images. We could, for instance, adopt the standard JPEG table (together with its rescalings) for use in MJPEG, having already adopted JPEG's standard Huffman tables. A comparison making use of this table is shown in Figure 4.13 below. The 256×256 Lena image was first JPEG encoded using Table 2.1, resulting in a file size of 7590 bytes. Figure 4.13(a) shows its reconstruction, which has a PSNR equal to 32.9031 dB. The closest file size resulting from an MJPEG encoding (with the sine window) is obtained when rescaling Table 2.1 using $qual = 51.6$. This encoding has a file size of 7596 bytes and a corresponding PSNR of 33.3762 dB. Its reconstruction is shown in Figure 4.13(b). With a higher PSNR, we consider MJPEG's result to be slightly superior to that of JPEG.

These results are, however, not optimal in terms of PSNR. Table 2.1 is the result of psychovisual experiments conducted on the standard DCT, and should therefore be perceptually optimal for this transform. Hence, the PSNR of Figure 4.13(a) is not necessarily optimised by this table. Furthermore, rescaled versions of this QT are no longer perceptually optimal for the DCT, much less numerically. As a result, the PSNR of Figure 4.13(b), where a different transform (the MDCT) was also used, is most likely also not optimal.

(a) JPEG encoding: 7590 bytes, 32.9031 dB

(b) MJPEG encoding: 7596 bytes, 33.3762 dB

Figure 4.13: Comparison of JPEG and MJPEG encodings of Lena

To properly compare MJPEG with JPEG we turn to the design of optimised QTs. This means that, given an image to compress along with a target file size, we wish to design a QT that maximises the PSNR for the target file size. As stated in Section 1.2, one could also design QTs that maximise perceptual quality, or equivalently, minimise visible distortion — a paradigm known as perceptual coding. While we do not work within this paradigm, applying it to the MDCT will of course make for an equally interesting avenue of research. For this reason, we first discuss the basics of perceptual coding in the next chapter, before discussing our approach of maximising the PSNR in Chapter 6.

Chapter 5

QT Design Part 1: Perceptual Coding

In this chapter a brief overview of the basic concepts of perceptual coding is presented. We start by discussing the motivation for this coding paradigm, and describing the way in which perceptual quality is assessed.

5.1 Introduction

Perceptual coding of both images and audio is motivated by the fact that tradditional means of gauging the quality of an approximation, such as the PSNR, do not necessarily correlate well with perceived quality. Given two different encodings of an image (or sound file), both with the same PSNR, one might be visually (or aurally) indistinguishable from the original, while the other might exhibit noticeable deterioration. The example shown in Figure 5.1, though somewhat artificial, illustrates this point.

(a) JPEG encoding: 37.8818 dB

(b) Artificially perturbed version: 37.9201 dB

Figure 5.1: Illustration of the shortcomings of the PSNR as a quality measure

Figure 5.1(a) shows the reconstruction of a JPEG encoding of the 256×256 Lena image, using $qual = 85$. It is almost indistinguishable from the original shown in Appendix A, and has a PSNR equal to 37.8818 dB. By contrast, the image in Figure 5.1(b), while having a PSNR of 37.9201 dB, has a noticeable difference to the original. It was obtained by assigning a value of 100 to a block of pixels in Lena's face. Clearly, the image in Figure 5.1(a) can be considered visually superior to the one in Figure 5.1(b).

In other words, just because an encoding of an image (or sound file) has a high PSNR, we cannot assume that it will necessarily be of satisfactory visual (or aural) quality to an end user. Therefore, instead of maximising the PSNR, perceptual coding attempts to optimise visual (or aural) quality. In the case of perceptual image coding, this goal is formalised by the following problem statement:

> Given an image to compress, along with a target file size, quantise the frequency components such that the visual quality is maximised (the perceived error is minimised) for the target file size.

In many applications it is desirable that the encoded image be indistinguishable from the original (*i.e.* there is no perceived error). In such a case, we say that the encoding is *transparent* and refer to this process as *transparent coding*. A dual formulation of our problem statement is then:

> Given the requirement of transparent coding, quantise the frequency components such that the resulting file size is minimised, or equivalently, minimise the file size while ensuring that all resulting distortions remain invisible.

Any method that solves either of the above problems is referred to as *image dependent*, since it optimises the quality (or file size) of a particular image subject to the file size (or transparency) constraint. It does so by taking into consideration the characteristics of the image to be compressed. On the other hand, a technique that generates a quantisation table to transparently code all images is called *image independent* — no images are taken into consideration when calculating the QT. Table 2.1 is an example of a QT generated by such means.

5.2 Quality Assessment

Having formalised the problem statement above, we still need a method for measuring visual quality in order to evaluate the performance of competing techniques. The answer is intuitive: let human observers view the resulting encodings and decide for themselves how good the images look.

This is done via formal viewing tests: Trained subjects familiar with compression artefacts evaluate the results under specified viewing conditions using specified display equipment. This ensures that the process is scientific and that the test results are reproducible. In each case the viewers are shown both the original version of the image under consideration as well as a decoding of its compressed form. They then rate the perceived difference between the two, referred to as an *impairment*, on a 5-grade impairment scale. This scale was defined by the International Telecommunication Union, Radiocommunication Bureau (ITU-R), and is listed in Table 5.1 below, showing the quality assigned to each value.

Value	**Quality**	**Impairment**
5	Excellent	Imperceptible
4	Good	Perceptible, but not annoying
3	Fair	Slightly annoying
2	Poor	Annoying
1	Bad	Very annoying

Table 5.1: ITU-R 5-grade impairment scale as listed in [8]

Some form of statistical analysis is then applied to the given scores. For instance, the average of the scores for a particular encoding of an image can be calculated, yielding its *mean opinion score*.

When it comes to audio coding, this method of quality assessment has become the official means of comparing audio coding algorithms. As such, the guidelines for conducting formal listening tests are much stricter and have been formalised in [12]. Here, instead of two audio signals, subjects are given three audio signals to listen to, in what is known

as a "double-blind, triple-stimulus with hidden reference" test. Again the original signal, called the *reference*, is present and is known as such, but now of the remaining two, say A and B, one is the encoded version while the other is once again the reference. Furthermore, neither the listener nor the test administrator knows which is which, hence the term "double blind". The listener attempts to identify which of A and B is the copy of the reference, thereby grading it a 5, and then also grades the quality of the other.

This is done to facilitate a more rigorous statistical analysis. From the above two gradings the *subjective difference grade* (SDG) is calculated as

$$\text{SDG} = G_1 - G_2,$$

where G_1 and G_2 are the grades assigned to the encoding and the reference, respectively. Notice that in the case of non-transparent coding, the SDG will have a negative value when the listener correctly distinguishes between the reference and the encoding, while yielding a positive value otherwise. (In the case of transparent coding, listeners will roughly half of the time incorrectly distinguish between the two signals, but the SDG will in either case be 0.) Table 5.2, taken from [8], shows the relationship between the 5-grade scale of Table 5.1 and the SDG.

Impairment	**ITU-R Grade**	**SDG**
Imperceptible	5	0
Perceptible, but not annoying	4	-1
Slightly annoying	3	-2
Annoying	2	-3
Very annoying	1	-4

Table 5.2: Relationship between the 5-grade scale and the SDG

It is then the SDGs to which a more rigorous statistical analysis technique is applied.

Many more details on formal listening tests exist, and a more in-depth discussion can be found in [8].

5.3 Thresholds

In perceptual coding we utilise studies of human perception in the frequency domain. In both vision and hearing, human perception is a function of frequency — both the eye and ear have varying degrees of sensitivity to various frequencies. Figure 5.2, for instance, depicts what is known as the *threshold in quiet* in psychoacoustics.

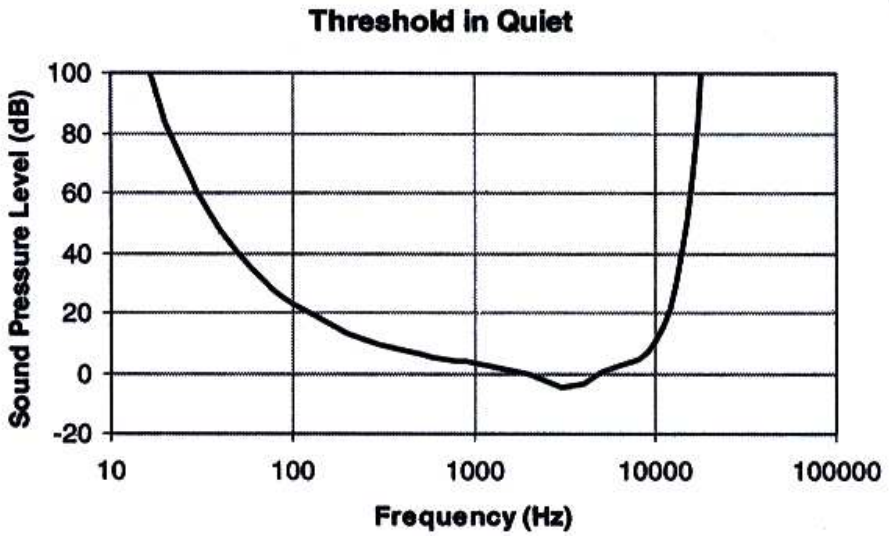

Figure 5.2: Threshold of human hearing as shown in [8]

Such a curve is generated by measuring the amplitude[1] at which audio signals of various frequencies become just noticeable. We observe that the human ear is more sensitive to mid-range frequencies than very high and very low frequencies. Alternatively, a sensitivity function, that measures sensitivity as a function of frequency, can be used, and would behave like a "flipped over" version of the curve above.

In the case of human vision, such sensitivity curves are conventionally used when illustrating the sensitivity of the eye to various spatial frequencies. A classic example, taken from [5], is shown in Figure 5.3, where contrast sensitivity[2] is plotted as a function of spatial frequency.

[1]The pressure, expressed in decibel units, exerted by sound waves is used to quantify their amplitude.

[2]Contrast refers to the change in intensity of visual input.

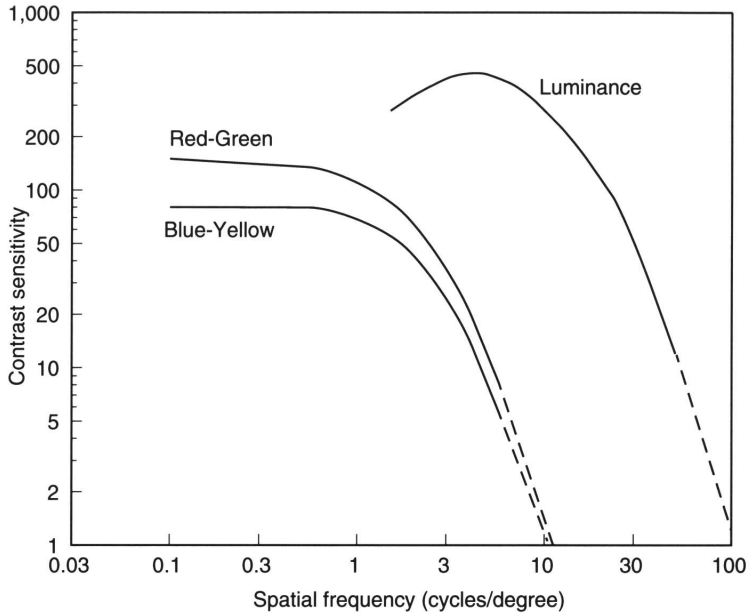

Figure 5.3: Classic contrast sensitivity curves for human vision [5]

Three sensitivity curves are shown: one for luminance, and two for so-called chrominance, since colour can be represented by a luminance and two chrominance components. The curve depicting luminance contrast sensitivity corresponds to measurements made by Van Nes and Bouman [13], while the two depicting contrast sensitivity for chrominance correspond to measurements made by Mullen [14]. From these curves we see that the eye is most sensitive to low spatial frequencies, and that sensitivity decreases as spatial frequency increases. Analogously to our discussion of Figure 5.2, the threshold curves for human vision will be "flipped over" versions of the curves shown in Figure 5.3 above.

In both vision and hearing the concept of thresholds is fundamental — if a signal of a particular frequency has an amplitude below that frequency's threshold, it is imperceptible. Thresholds can also be elevated due to phenomena known as *masking*, which we discuss in the next section. These elevated thresholds are referred to as *masked thresholds*, while the basic thresholds discussed thus far are sometimes called *base thresholds*.

Given the concept of thresholds, the achievement of transparent coding now becomes clear: Frequency components with magnitude below threshold can be discarded (quantised to

zero), since they are redundant. Non-redundant components are quantised such that the resulting quantisation error is below threshold, rendering it imperceptible.

A very important fact, however, is that the curves shown in Figure 5.3 are not unique. For each combination of *display luminance* (the brightness of the display device) and *veiling luminance* (the brightness of ones surroundings), different sensitivity curves, and thus different visibility thresholds, will be obtained. The combination of these two luminances is sometimes called the *total luminance*. As a result, a perceptual image coder will have to take into account the total luminance when calculating base thresholds[3]. By interpolating and extrapolating previous experimental data, Ahumada and Peterson contributed a model in [15] that does precisely this. It enables us to calculate luminance thresholds (as a function of frequency) for any realistic value of the total luminance. This model was then extended to colour components by Ahumada, Peterson and Watson in [16].

Once the base thresholds have been calculated, they can immediately be used to calculate a QT that will ensure transparent coding. As stated in Section 5.1, such an approach is called image independent. More sophisticated (image dependent) perceptual coders, on the other hand, also take advantage of the previously mentioned masking phenomena, which differ from image to image. By analysing the masking present in an image, such coders will calculate the masked thresholds from the base thresholds and thereby achieve better performance. Furthermore, an image dependent perceptual coder will also allow one to select a desired file size or visual quality.

5.4 Masking Phenomena and Competing Techniques

Masking occurs when the perceptibility of one signal (the *maskee*) is diminished due to the presence of another (the *masker*). In vision, two types of masking exist: *luminance* masking and *contrast* masking.

[3]This is in contrast to audio coding, where the base thresholds are always calculated from the data corresponding to Figure 5.2.

5.4.1 Luminance Masking

The model by Ahumada and Peterson mentioned above partially accounts for luminance masking, since screen brightness and environmental illumination affect the base thresholds. However, various regions of an image to be encoded also have varying brightness. The thresholds of the frequency components within a transform block will therefore be elevated by the luminance of that particular block.

Various models for computing this elevation exist. Watson's DCTune [17, 18, 19], for instance, uses a transform block's DC coefficient, denoted by c_{00}, as a measure of its luminance. The base thresholds, denoted by t_{ij}, are then elevated to say $\widehat{t}_{ij}$ according to the model

$$\widehat{t}_{ij} = t_{ij} \left(\frac{c_{00}}{\bar{c}_{00}} \right)^{a_T}, \quad i = 0, \ldots, 7, \; j = 0, \ldots, 7,$$

where $\bar{c}_{00}$ and a_T are constants defined in [17, 18, 19].

5.4.2 Contrast Masking

Each transform block in an image is a superposition of components of various frequencies[4], the amplitudes (contributions) of which are given by the output of the chosen transform. The more prominent of these components, namely those with larger amplitudes (coefficients), will have a masking effect on the others.

Once again, different models of this phenomenon exist. Both the model used in DCTune and the improved model in [20, 21] exclude the DC component from contrast masking. The reason for this is that its masking effect is already taken into account by luminance masking. Therefore, after applying a luminance masking model, potential maskers are identified among the AC components. Given such a masker, its coefficient denoted by c_M, the further elevated threshold, say m_{ij}, of a maskee is then calculated as

$$m_{ij} = \widehat{t}_{ij} \max \left(1, \; \left(f \frac{c_M}{\widehat{t}_{ij}} \right)^w \right),$$

where f and w are parameters defined in [20, 21].

[4] In the case of the DCT, each transform block is a superposition of the DCT basis functions.

For further examples of masking models, the reader is also referred to [22], [23, 24] and [25].

5.4.3 Competing Techniques

The way in which masked thresholds are used for quantisation differs from technique to technique. A distinction can be made between those perceptual coding techniques that are locally adaptive and those that are not.

Ideally, we would like to quantise each coefficient block using that block's own masked thresholds. This means that quantisation adapts from block to block, hence the term "locally adaptive". In doing so, we unfortunately no longer have only one quantisation table, and storing one for each transform block would neutralise any improvements gained.

A locally adaptive technique proposed by Karam and Höntsch [22] addresses this problem by using linear prediction to predict a block's QT based on the previous block's QT as well as that block's decoded data. Instead of storing an 8×8 QT, an 8×8 table of numbers needed to initialise the predictive technique is stored in the output file. It also allows the user to select a desired visual quality, and optimises the quantisation accordingly.

On the other hand, instead of locally adapting, a technique might retain the use of a single QT. DCTune, for example, "pools" the effects of all masked thresholds, thereby creating a single QT that minimises an image's file size for a given visual quality. In the special case of transparent coding, for instance, all quantisation noise will be below the pooled masked thresholds, while keeping the file size as small as possible.

Interestingly, the technique by Safranek and Tran [23, 24] is partially locally adaptive. Prior to generating a (single) QT, frequency components below their corresponding masked thresholds are set to zero. This approach is sometimes called a *zeroing strategy*, and it allows for improved performance when a single QT is used.

The one thing that image dependent perceptual coders have in common, though, is their relative ease of calculating QT entries. In each case the perceptual error is measured in a unit known as the *just-noticeable difference* (JND). By doing so, the requirement that

the perceptual error of a reconstructed image be smaller than, say ϵ, is equivalent to requiring the quantisation error in each frequency component, when converted to JND, to be smaller than ϵ. This means that each QT entry can be optimised individually by searching the set $\{1, \ldots, 255\}$. Additionally, since quantisation error increases monotonically with the magnitude of an entry, this search can be implemented using a binary search. This approach is unfortunately not valid when attempting to optimise numerical (objective) quality, as will be discussed in the next chapter. Consequently, perceptual coding algorithms have a significant advantage in terms of running time over algorithms that optimise numerical quality.

Finally, competing perceptual coding techniques can be compared by using the method of formal viewing tests described in Section 5.2 above. An example of such a comparison can be found in [22], where Karam and Hontsh's technique is compared with DCTune.

5.5 Perceptual Coding and the MDCT

Perceptual image coding is typically applied to DCT-based image compression techniques. Indeed, the threshold model of Ahumada and Peterson, as well as certain models of masking phenomena, specifically assume the use of the DCT. Therefore, applying this paradigm to the MDCT would not only involve choosing a perceptual coding technique, but also the adaptation of these models to this transform. Furthermore, the application of various perceptual coding techniques to the MDCT could be investigated to see which performs best. In the end, these results would then be compared with those obtained for the standard DCT when using the same perceptual coding techniques. Taking into consideration the fact that all such comparisons would be made by using formal viewing tests, one can see that this would make for quite an interesting research endeavour.

Chapter 6

QT Design Part 2: Optimising Numerical Quality

6.1 Introduction

Our approach to optimal quantisation is within the framework of optimising objective quality. This means that physical interpretations of frequency components can be discarded, and viewing conditions are not taken into consideration. It also means that we can view our design problem purely from an optimisation theoretical point of view.

A drawback, unfortunately, is that we can no longer "decouple" frequency components as done in perceptual coding. Requiring that each error in the frequency domain, whether relative or absolute, be below a certain tolerance ϵ and optimising the quantisation accordingly, will not yield the smallest file size for the resulting PSNR (or largest PSNR for the resulting file size). The reason for this being that different frequency components contribute differently to the numerical quality of an approximation. Each would require its own ϵ, the values of which are unknown *a priori*. As a result, the optimisation algorithms encountered in this paradigm are often significantly more time-consuming than

those utilised in perceptual coding[1].

Additionally, since quantisation takes place in the frequency domain, but the PSNR is calculated in the spatial domain, an optimisation algorithm would have to completely decode an image each time a candidate quantisation table is evaluated. This would slow down running time even further. Therefore a compromise is made: Instead of maximising the PSNR, the algorithms to be discussed minimise the mean-squared-error (MSE) in the frequency domain. Given the matrices Y and Y_{dq} of original and dequantised coefficients, respectively, both of dimensions $m \times n$, this error is defined as

$$E = \frac{1}{mn} \sum_{x=1}^{m} \sum_{y=1}^{n} [Y(x,y) - Y_{dq}(x,y)]^2. \tag{6.1}$$

Since the DCT is a linear transform, a minimised MSE in the frequency domain corresponds to a minimised MSE in the spatial domain. When rounding to form valid pixels, this correspondence is no longer exact, but still very good, meaning that a minimised value of E will also correspond very well to a maximised PSNR.

We are now ready to formalise our optimisation problem:

> Let $Q = [q_1, q_2, \ldots, q_{64}]$ denote a quantisation table with entries arranged in zigzag ordering. Then, given an image to encode and a target file size T (in bytes), minimise $E = E(Q)$, subject to the constraint
>
> $$100 \left(\frac{|B(Q) - T|}{T} \right) \leq \epsilon, \tag{6.2}$$
>
> where B denotes the file size (in bytes) obtained by using JPEG's standard Huffman tables, explained in Section 2.4.

Notice that constraint (6.2) requires the deviation of the file size from the target to not exceed ϵ %. Any candidate Q that satisfies the constraint is called a *feasible solution*. Here we choose $\epsilon = 0.1$. Also, due to our choice to derive the two additional QTs used

[1] RD-Opt [3, 4] performs such a decoupling by using a statistical analysis of an image's frequency components. By doing so, individual binary searches can again be used, but at the cost of achieving slightly suboptimal results.

by MJPEG from the primary one, as detailed in Section 4.2, this optimisation problem is equally applicable to both JPEG and MJPEG.

Due to the rounding that takes place during quantisation, the underlying formula for E as a function of Q is not differentiable. Hence we cannot apply classic analytical or numerical methods for solving constrained optimisation problems. Neither does this function possess continuous behaviour, meaning that algorithms such as Hooke-Jeeves and Nelder-Mead, which do not attempt numerical differentiation, but do require continuity, are also not applicable.

The above, coupled with the fact that the independent variables q_k $(k = 1, \ldots, 64)$ vary discretely, means that this is a textbook example of a *discrete optimisation* problem. In such problems candidate solutions form a finite *search space* that can, in principle, be searched through in finite time. The challenge posed by such problems is that the realistic ones have prohibitively large search spaces.

The search space in our problem is large indeed: with a QT consisting of 64 entries, each allowed to assume an integer value between 1 and 255, we have 255^{64} possible QTs. Searching through such a set is for all intents and purposes impossible.

When all else fails, one can always attempt to solve discrete optimisation problems with *genetic algorithms*. They can, however, still be very time-consuming and, fortunately, alternative approaches are possible for this particular problem. Central to this research is the greedy algorithm by Wu and Gersho [2], as well as its subsequent improvement by Fung and Parker [1].

6.2 Greedy Algorithm

The algorithm by Wu and Gersho [2] is a steepest-descent technique that, in light of the previous discussion, would not seem applicable to our problem. As such, it can only provide us with approximations to solutions, but given its greedy nature its application makes intuitive sense. Furthermore, its improvements over QTs such as Table 2.1 are significant, suggesting that it does indeed yield good approximations to the actual solutions.

We begin with an initial QT consisting of large values, each preferably at its maximum value of 255. For convenience, we introduce the notation $[[l]]$ to refer to the QT with entries all equal to l, meaning that

$$[[l]] = \begin{bmatrix} l & l & l & l & l & l & l & l \\ l & l & l & l & l & l & l & l \\ l & l & l & l & l & l & l & l \\ l & l & l & l & l & l & l & l \\ l & l & l & l & l & l & l & l \\ l & l & l & l & l & l & l & l \\ l & l & l & l & l & l & l & l \\ l & l & l & l & l & l & l & l \end{bmatrix}. \tag{6.3}$$

Therefore, the initial QT will be written as $[[255]]$.

The file size B resulting from using the above QT is the smallest we can possibly obtain, so we can assume that a realistic target file size will be larger. (The resulting error E will similarly be the largest possible error.) Replacing an entry in the quantisation table with a smaller value will typically result in a larger file size, say $\widehat{B}$ (and smaller error, say $\widehat{E}$), taking us one step closer to the target file size. In order to make the most of this step, we want the decrease in error to be as large as possible, while using as few extra bytes as possible. In other words, we want the quantity

$$\lambda = \frac{-\Delta E}{\Delta B} = \frac{E - \widehat{E}}{\widehat{B} - B}$$

to be as large as possible. Therefore, during each iteration, at each position k in the quantisation table, each possible change from the current entry q_k to the candidate

$$q \in \{1, 2, \ldots, q_k - 1\}$$

is temporarily implemented ($\widehat{B}$ and $\widehat{E}$ calculated) in the search for the largest value of λ, say λ^*. We will refer to this evaluation of a new file size and coding error for a candidate q as *probing*. The value q^* and the position k^* at which λ^* occurs are then the sought after optimal update and its location, respectively.

At the end of an iteration this optimal update is then made, resulting in a new QT, as well as new values of the file size B and error E. We repeat these iterations until B is no longer smaller than the target file size. The pseudocode in Algorithm 6.1 specifies the algorithm more formally.

Input: Target file size T
initialize QT: $Q = [[255]]$;
calculate B; calculate E;
while $B < T$ **do**
  $\lambda^* = 0$;
  for *k = 1 To 64* **do**
    $qq = Q(k)$;
    for *q = 1 To qq - 1* **do**
      $Q(k) = q$;
      calculate $\widehat{B}$; calculate $\widehat{E}$; $\lambda = \frac{E-\widehat{E}}{\widehat{B}-B}$;
      if $\lambda > \lambda^*$ **then**
        $\lambda^* = \lambda$; $k^* = k$; $q^* = q$; $B^* = \widehat{B}$; $E^* = \widehat{E}$;
      end
    end
    $Q(k) = qq$;
  end
  $Q(k^*) = q^*$; $B = B^*$; $E = E^*$;
end

Algorithm 6.1: The greedy algorithm by Wu and Gersho [2]

In the description of Algorithm 6.1 we have made the assumption that replacing a QT entry with a smaller value necessarily leads to a reduction in error and an increase in file size, thus resulting in a positive (and finite) value of λ. Exceptions do however exist and, while the algorithm is immune to them, some can be exploited to reduce running time. Let us consider each in turn:

1. $\Delta B = 0, -\Delta E > 0 \Rightarrow \lambda = \infty$:

   When replacing a QT entry with a smaller one, an encoding sometimes results that requires the same number of bytes, but has a smaller error than the previous encoding. The corresponding value of λ, namely ∞, will therefore be judged the best (assuming the previous best was finite) and no subsequent value of λ (not even ∞) will be able to beat it. This judgement is appropriate, since the encoding error is decreased without costing us any bytes. It would therefore be wasteful to continue probing once a value of ∞ is encountered. Even if we compared the values of $-\Delta E$ (decrease in error) for each such case in order to find the best "freebie", the first occurrence of ∞ will likely be the best. This is so because (a) subsequent probes within a specific frequency index k will be for larger values of q and cannot yield larger decreases in E, and (b) subsequent indices k more or less correspond to higher frequencies due to their zigzag ordering, and probing within them is thus unlikely to yield larger decreases in E for $\Delta B = 0$.

   Instead, upon encountering $\lambda = \infty$, we "break" out of the two FOR-loops (having found the λ^*, q^*, and k^* we were looking for) and finalise the current iteration.

2. $\Delta B = 0, -\Delta E = 0 \Rightarrow \lambda = \text{NaN}$[2]:

   This situation occurs when the kth coefficient of each frequency block is quantised to zero by entry q_k in the current QT, as well as by the value of q currently being probed.

   When this happens, no further probing is needed for this value of k, since subsequent (and larger) values of q will also quantise the coefficients involved to zero, and thus also give us $\lambda = \text{NaN}$. Therefore, the algorithm can also be modified to break out of the innermost FOR-loop when $\lambda = \text{NaN}$ is encountered. Note that no programming language would deem $\lambda = \text{NaN}$ larger than λ^*, meaning that the algorithm still functions properly when not testing for this case.

[2]NaN is a special symbol, meaning "not a number", assigned by certain programming languages to a number resulting from zero divided by itself.

3. $\Delta B > 0, -\Delta E = 0 \Rightarrow \lambda = 0$:

   In a situation like this, the investment of more bytes in an encoding has not led to a decrease in error. Appropriately, we have $\lambda = 0$, which will be "ignored" by the algorithm.

4. $\Delta B < 0, -\Delta E > 0 \Rightarrow \lambda < 0$:

   Due to the runlength/Huffman coding used by JPEG and MJPEG, the replacement of a QT entry with a smaller one sometimes yields a smaller coding file size. In such a case, the magnitude of ΔB is usually quite small. Notice that, since $\lambda < 0$, this case is irrelevant to Algorithm 6.1.

   To illustrate this rare occurrence, consider the following block of unquantised DCT coefficients from the 256×256 Plane image, shown in Appendix A. This frequency block, rounded to two decimals, is given by

$$F = \begin{array}{|cccccccc|} \hline 276.62 & 147.39 & 157.51 & -185.44 & 42.38 & 25.55 & 11.47 & -45.13 \\ 160.16 & 37.72 & -144.70 & 96.62 & 17.17 & -54.31 & 13.04 & 21.46 \\ 155.55 & -21.37 & -39.64 & 32.30 & -22.40 & 33.64 & -38.53 & 26.19 \\ 42.18 & -193.21 & 36.84 & 88.40 & -70.47 & 10.13 & 13.55 & -10.89 \\ -40.63 & -13.92 & 38.84 & -39.37 & 13.63 & -6.28 & 7.86 & -1.65 \\ -1.06 & 82.00 & 38.52 & -73.73 & 30.25 & 9.11 & 3.93 & -15.65 \\ 26.35 & 8.76 & -29.53 & 17.12 & -4.11 & 0.31 & -4.11 & 3.44 \\ -81.25 & -6.40 & -11.96 & -3.25 & 39.05 & -28.49 & -11.25 & 27.27 \\ \hline \end{array} .$$

   When quantising F with the quantisation table

$$Q = \begin{array}{|cccccccc|} \hline 26 & 34 & 33 & 29 & 36 & 30 & 49 & 31 \\ 32 & 36 & 31 & 30 & 32 & 38 & 36 & 58 \\ 31 & 33 & 29 & 33 & 43 & 34 & 46 & 49 \\ 38 & 28 & 30 & 41 & 34 & 41 & 48 & 71 \\ 32 & 37 & 43 & 37 & 52 & 59 & 71 & 69 \\ 36 & 34 & 44 & 46 & 64 & 57 & 68 & 88 \\ 37 & 50 & 63 & 61 & 71 & 68 & 70 & 80 \\ 48 & 52 & 84 & 59 & 79 & 64 & 70 & 75 \\ \hline \end{array} ,$$

we obtain F_q, given by

$$F_q = \begin{array}{|cccccccc|}\hline 11 & 4 & 5 & -6 & 1 & 1 & 0 & -1 \\ 5 & 1 & -5 & 3 & 1 & -1 & 0 & 0 \\ 5 & -1 & -1 & 1 & -1 & 1 & -1 & 1 \\ 1 & -7 & 1 & 2 & -2 & 0 & 0 & 0 \\ -1 & 0 & 1 & -1 & 0 & 0 & 0 & 0 \\ 0 & 2 & 1 & -2 & 0 & 0 & 0 & 0 \\ 1 & 0 & 0 & 0 & 0 & 0 & 0 & 0 \\ -2 & 0 & 0 & 0 & 0 & 0 & 0 & 0 \\ \hline \end{array}.$$

By replacing the entry $q_{38} = Q(7,3) = 63$ with the value 57, giving us

$$\widehat{Q} = \begin{array}{|cccccccc|}\hline 26 & 34 & 33 & 29 & 36 & 30 & 49 & 31 \\ 32 & 36 & 31 & 30 & 32 & 38 & 36 & 58 \\ 31 & 33 & 29 & 33 & 43 & 34 & 46 & 49 \\ 38 & 28 & 30 & 41 & 34 & 41 & 48 & 71 \\ 32 & 37 & 43 & 37 & 52 & 59 & 71 & 69 \\ 36 & 34 & 44 & 46 & 64 & 57 & 68 & 88 \\ 37 & 50 & \boxed{57} & 61 & 71 & 68 & 70 & 80 \\ 48 & 52 & 84 & 59 & 79 & 64 & 70 & 75 \\ \hline \end{array},$$

the quantised counterpart of F will now be

$$\widehat{F}_q = \begin{array}{|cccccccc|}\hline 11 & 4 & 5 & -6 & 1 & 1 & 0 & -1 \\ 5 & 1 & -5 & 3 & 1 & -1 & 0 & 0 \\ 5 & -1 & -1 & 1 & -1 & 1 & -1 & 1 \\ 1 & -7 & 1 & 2 & -2 & 0 & 0 & 0 \\ -1 & 0 & 1 & -1 & 0 & 0 & 0 & 0 \\ 0 & 2 & 1 & -2 & 0 & 0 & 0 & 0 \\ 1 & 0 & \boxed{-1} & 0 & 0 & 0 & 0 & 0 \\ -2 & 0 & 0 & 0 & 0 & 0 & 0 & 0 \\ \hline \end{array}.$$

Notice that $F_q(7,3) = 0$, while $\widehat{F}_q(7,3) = -1$.

Our somewhat unexpected phenomenon now occurs when we entropy code these two blocks. The zigzag sequences of F_q and $\widehat{F}_q$, say $\mathbf{z}$ and $\widehat{\mathbf{z}}$, respectively, are (in truncated form)

$$\mathbf{z} = \boxed{11}\boxed{4}\boxed{5}\cdots\boxed{\text{-2}}\boxed{0}\boxed{0}\boxed{\text{-2}}\cdots\boxed{0}\boxed{0}\boxed{0}$$

and

$$\widehat{\mathbf{z}} = \boxed{11}\boxed{4}\boxed{5}\cdots\boxed{\text{-2}}\boxed{0}\boxed{\text{-1}}\boxed{\text{-2}}\cdots\boxed{0}\boxed{0}\boxed{0}.$$

The first 36 entries of $\mathbf{z}$ and $\widehat{\mathbf{z}}$ are identical, ending with the same non-zero AC coefficient, namely -2. The same contribution to the file size, say p bits, is therefore made by these entries.

In the case of $\mathbf{z}$, the next two entries are zeroes preceding the subsequent non-zero coefficient. With this coefficient equal to -2, the symbol (**runlength**, **category**) = (2, 2) is formed, which has a Huffman code of 8-bit length. The contribution made to the file size by $\mathbf{z}$ thus far is now equal to $p + 8$ bits.

In the case of $\widehat{\mathbf{z}}$, on the other hand, the 38th entry is equal to -1, with the first of the abovementioned zeroes now preceding it. The symbol thereby formed is (**runlength**, **category**) = (1, 1), which has a Huffman code that is 4 bits long. The subsequent entry of -2, no longer preceded by any zeroes is now represented by (0, 2). The Huffman code for this symbol is 2 bits long. As a result, the first 39 entries of $\widehat{\mathbf{z}}$ add $p + 6$ bits to the file size, while those of $\mathbf{z}$ added $p + 8$ bits.

The remaining entries of $\mathbf{z}$ and $\widehat{\mathbf{z}}$ once again add an equal number of bits to the file size, meaning that $\widehat{\mathbf{z}}$ adds 2 fewer bits to the file size than $\mathbf{z}$.

While some transform blocks from this image do behave in the expected fashion when making the above change to Q (*i.e.* add more bits to the file size than before), most of them yield unchanged quantised coefficients in this particular case, thereby making the same contribution to the file size before and after changing Q to $\widehat{Q}$. The few transform blocks exhibiting the unexpected behaviour illustrated above,

happen to make more decreased contributions to the file size than the increased contributions made by the few behaving as expected.

In the end, the number of bits required to encode all quantised coefficients obtained by using Q is equal to 48041, while the number of bits required when using $\widehat{Q}$ is equal to 48040. Since storage space is allocated in bytes, the encoding resulting from using Q has a file size of $B = 6006+354 = 6360$ bytes, when taking into account the overhead mentioned in Section 2.5. The encoding resulting from using $\widehat{Q}$, however, has a file size of $\widehat{B} = 6005 + 354 = 6359$ bytes. Consequently, $\Delta B = \widehat{B} - B = -1$.

5. $\Delta B < 0, -\Delta E = 0 \Rightarrow \lambda = 0$:

   This case is similar to the previous one, with the addition of an (unexpected) occurrence of $-\Delta E = 0$, similar to that of case 3 above. With $\lambda = 0$, it has no effect on the algorithm.

Algorithm 6.1 is too time-consuming to be implemented in Matlab. Instead, we chose to implement it in C++, with the program reading in an image's frequency components from a mat-file created by Matlab. As an example of the algorithm's usage, consider its application to the JPEG encoding of the 256×256 Lena image, for the target file size of 8000 bytes. Starting with the quantisation table $Q = [[255]]$, the initial file size is $B = 1540$ bytes, and its corresponding error is $E = 375.7444$. The first few iterations yield "freebies". For instance, the table

$$Q = \begin{array}{|cccccccc|}\hline 252 & 255 & 255 & 255 & 255 & 255 & 255 & 255 \\ 255 & 255 & 255 & 255 & 255 & 255 & 255 & 255 \\ 255 & 255 & 255 & 255 & 255 & 255 & 255 & 255 \\ 255 & 255 & 255 & 255 & 255 & 255 & 255 & 255 \\ 255 & 255 & 255 & 255 & 255 & 255 & 255 & 255 \\ 255 & 255 & 255 & 255 & 255 & 255 & 255 & 255 \\ 255 & 255 & 255 & 255 & 255 & 255 & 255 & 255 \\ 255 & 255 & 255 & 255 & 255 & 255 & 255 & 255 \\ \hline \end{array}$$

results from the first iteration, where the file size is still $B = 1540$ bytes but the error is $E = 375.1606$.

The second to last table is

$$Q = \begin{array}{|cccccccc|}\hline 20 & 23 & 26 & 19 & 23 & 20 & 22 & 20 \\ 21 & 21 & 20 & 20 & 23 & 27 & 21 & 28 \\ 21 & 20 & 22 & 25 & 23 & 29 & 27 & 28 \\ 19 & 19 & 27 & 23 & 22 & 25 & 25 & 39 \\ 17 & 22 & 22 & 25 & 27 & 32 & 33 & 32 \\ 20 & 20 & 27 & 25 & 25 & 35 & 35 & 43 \\ 20 & 26 & 21 & 32 & 24 & 34 & 37 & 33 \\ 30 & 24 & 35 & 31 & 46 & 42 & 48 & 45 \\ \hline \end{array}$$

with coding file size $B = 7980$ bytes and error $E = 21.5000$. This leads to the table

$$Q = \begin{array}{|cccccccc|}\hline 20 & \boxed{21} & 26 & 19 & 23 & 20 & 22 & 20 \\ 21 & 21 & 20 & 20 & 23 & 27 & 21 & 28 \\ 21 & 20 & 22 & 25 & 23 & 29 & 27 & 28 \\ 19 & 19 & 27 & 23 & 22 & 25 & 25 & 39 \\ 17 & 22 & 22 & 25 & 27 & 32 & 33 & 32 \\ 20 & 20 & 27 & 25 & 25 & 35 & 35 & 43 \\ 20 & 26 & 21 & 32 & 24 & 34 & 37 & 33 \\ 30 & 24 & 35 & 31 & 46 & 42 & 48 & 45 \\ \hline \end{array} \tag{6.4}$$

being obtained in the subsequent iteration, where the transition from $q_2 = Q(1,2) = 23$ to 21 was deemed the most advantageous. The resulting file size is $B = 8000$ bytes, with corresponding error $E = 21.3941$, upon which the algorithm terminates.

Using Matlab, we find that the encoding produced by the final QT above has a PSNR of 34.8084 dB. By comparison, an encoding of 7995 bytes produced by a rescaling of the standard JPEG table, using $qual = 54.5$, has a PSNR of 33.2453 dB. Clearly, the QT obtained with Algorithm 6.1 is the superior table.

Even when implemented in C++, Algorithm 6.1 still takes too long. The QT in (6.4)

required roughly 6h15min to obtain when using an Intel Core 2 vPro at 3 GHz. For a larger target file size this would have taken even longer. Furthermore, the running time is also proportional to the size of the input image — a 512×512 image, for example, would slow things down by a factor of 4.

6.3 Bi-directional Greedy Algorithm

Algorithm 6.1 progresses in only one direction, namely from a file size lower than the target toward that target, via larger and larger file sizes. However, we could just as easily have started with an initial QT filled with 1s, and proceeded in the opposite direction. In other words, by starting with the largest possible file size B and smallest possible error E, one would now attempt to minimise

$$\lambda = \frac{\Delta E}{-\Delta B} = \frac{\widehat{E} - E}{B - \widehat{B}}$$

during each iteration, thereby incurring the smallest increase in error for the largest decrease in file size. This would continue until the current file size is no longer larger than the target.

From the above remark we see that both the maximising step in one direction and the minimising step in the opposite are equally valid. This is the basis for the improved algorithm proposed by Fung and Parker [1]. Rather than starting with an "extreme" QT, a more feasible (most likely sub-optimal) initial table is used. The new algorithm iteratively improves upon this table by probing in the appropriate direction, depending on whether the current file size is above or below the target. This means that if the current table yields a file size smaller than the target, the approach used in Algorithm 6.1 is taken: probing smaller QT entries and maximising λ. Otherwise, the dual approach is taken: probing larger QT entries and minimising λ. The pseudocode for the algorithm is given in Algorithm 6.2.

Input: Target file size T and initial table Q

calculate B; calculate E; $R_{max} = \infty$; $R_{min} = 0$;

while $R_{max} > R_{min}$ **do**

  if $B < T$ **then**

    $\lambda^* = 0$;

    for *k = 1 To 64* **do**

      $qq = Q(k)$;

      for *q = 1 To qq - 1* **do**

        $Q(k) = q$; calculate $\widehat{B}$; calculate $\widehat{E}$; $\lambda = \frac{E-\widehat{E}}{\widehat{B}-B}$;

        if $\lambda > \lambda^*$ **then**

          $\lambda^* = \lambda$; $k^* = k$; $q^* = q$; $B^* = \widehat{B}$; $E^* = \widehat{E}$;

        end

      end

      $Q(k) = qq$;

    end

    $R_{max} = \lambda^*$;

  else

    $\lambda^* = \infty$;

    for *k = 1 To 64* **do**

      $qq = Q(k)$;

      for *q = qq + 1 To 255* **do**

        $Q(k) = q$; calculate $\widehat{B}$; calculate $\widehat{E}$; $\lambda = \frac{\widehat{E}-E}{B-\widehat{B}}$;

        if $\lambda < \lambda^*$ *And* $\lambda > 0$ **then**

          $\lambda^* = \lambda$; $k^* = k$; $q^* = q$; $B^* = \widehat{B}$; $E^* = \widehat{E}$;

        end

      end

      $Q(k) = qq$;

    end

    $R_{min} = \lambda^*$;

  end

  $Q(k^*) = q^*$; $B = B^*$; $E = E^*$;

end

Algorithm 6.2: The bi-directional greedy algorithm by Fung and Parker [1]

The algorithm keeps track of the most recent maximised and minimised values of λ, which it stores in R_{max} and R_{min}, respectively. As long as the algorithm can improve upon the QT, R_{max} will be larger than R_{min}. Eventually, this condition ceases to hold, at which point the algorithm will repeatedly output the same sequence of tables, with a corresponding sequence of file sizes oscillating about the target file size. For this reason $R_{max} \leq R_{min}$ is used as the stopping condition.

Notice that the interpretations of many of the exceptional cases listed in the previous section, change when minimising λ in Algorithm 6.2. This is due to the changed order in which the file sizes and errors are subtracted, where we now expect ΔE and $-\Delta B$ to be positive. In particular, the interpretations of cases 1 and 3 will be inverted. Case 3, now reading $(-\Delta B > 0,\ \Delta E = 0 \Rightarrow \lambda = 0)$, will represent a "freebie", since the file size is reduced without incurring any increase in error; in case 1, now reading $(-\Delta B = 0,\ \Delta E > 0 \Rightarrow \lambda = \infty)$, an increased error has not lead to a decrease in file size. Case 1, with $\lambda = \infty$, will therefore be ignored by the second portion of Algorithm 6.2, and we could (at first glance) test for case 3 to detect "freebies".

However, case 4, where $\lambda < 0$, and case 5, where $\lambda = 0$, now need to be avoided. For this reason, the additional condition $(\lambda > 0)$ is used in the second portion of the algorithm, thereby also potentially throwing away valid "freebies". Fortunately, no such "freebies" have ever been observed (we specifically tested for them), so it seems that no harm is done. Lastly, the interpretation of case 2, where $\lambda = \text{NaN}$, remains the same, and we can once again test for it to optimise running time.

We now repeat the search for an optimised QT for the JPEG encoding of Lena, using a C++ implementation of this algorithm. The JPEG table obtained with $qual = 54.5$,

$$Q_J = \begin{array}{|cccccccc|}\hline 15 & 10 & 9 & 15 & 22 & 36 & 46 & 56 \\ 11 & 11 & 13 & 17 & 24 & 53 & 55 & 50 \\ 13 & 12 & 15 & 22 & 36 & 52 & 63 & 51 \\ 13 & 15 & 20 & 26 & 46 & 79 & 73 & 56 \\ 16 & 20 & 34 & 51 & 62 & 99 & 94 & 70 \\ 22 & 32 & 50 & 58 & 74 & 95 & 103 & 84 \\ 45 & 58 & 71 & 79 & 94 & 110 & 109 & 92 \\ 66 & 84 & 86 & 89 & 102 & 91 & 94 & 90 \\ \hline \end{array} \tag{6.5}$$

and used in the previous section, is feasible since it yields an encoding of 7995 bytes. We thus use it as our initial table. One of the last QTs output before oscillation occurs has a coding file size of $B = 7987$ bytes and error $E = 21.4616$. Thereafter the tables

$$Q_1 = \begin{array}{|cccccccc|}\hline 20 & 21 & 26 & 19 & 22 & 20 & 22 & 20 \\ 21 & 21 & 20 & 20 & 23 & 23 & 21 & 28 \\ 19 & 20 & 22 & 25 & 23 & 29 & 27 & 29 \\ 19 & 20 & 25 & 23 & 24 & 25 & 25 & 39 \\ 17 & 22 & 22 & 25 & 27 & 32 & 33 & 33 \\ 20 & 20 & 27 & 26 & 33 & 35 & 35 & 43 \\ 20 & 26 & 23 & 33 & 24 & 34 & 38 & 33 \\ 23 & 24 & 35 & 32 & 46 & 42 & 48 & 45 \\ \hline \end{array} \tag{6.6}$$

with $B = 7995$ bytes and $E = 21.4199$, and

$$Q_2 = \begin{array}{|cccccccc|}\hline 20 & 21 & 26 & 19 & 22 & 20 & 22 & 20 \\ 21 & 21 & 20 & 20 & 23 & 23 & 21 & 28 \\ 19 & 20 & 22 & 25 & 23 & 29 & 27 & 29 \\ 19 & \boxed{17} & 25 & 23 & 24 & 25 & 25 & 39 \\ 17 & 22 & 22 & 25 & 27 & 32 & 33 & 33 \\ 20 & 20 & 27 & 26 & 33 & 35 & 35 & 43 \\ 20 & 26 & 23 & 33 & 24 & 34 & 38 & 33 \\ 23 & 24 & 35 & 32 & 46 & 42 & 48 & 45 \\ \hline \end{array} \tag{6.7}$$

with $B = 8012$ bytes and $E = 21.3333$ are obtained, giving us $R_{max} = 333.8658$. Lastly, the algorithm again outputs Q_1, meaning that R_{min} is also equal to 333.8658, and it then terminates. In the absence of the stopping condition, the sequence $\{Q_1, Q_2, Q_1, \ldots\}$ would be generated indefinitely. Algorithm 6.2 is indeed an improvement over Algorithm 6.1, requiring roughly 2h37min to reach its final sequence of QTs for this particular example.

From such a final sequence, the table with coding file size closest to the target can be chosen as the final one, but it will not necessarily be feasible. Q_1, for instance, while feasible, could still be tweaked to yield an even closer file size by inspecting the difference between it and Q_2. This difference is between their 4th row, 2nd column entries, where the transitions from $Q_1(4,2) = 20$ to $Q_2(4,2) = 17$, and vice versa, take place. By instead choosing $q_{12} = 19$, the QT

$$Q = \begin{array}{|cccccccc|}\hline 20 & 21 & 26 & 19 & 22 & 20 & 22 & 20 \\ 21 & 21 & 20 & 20 & 23 & 23 & 21 & 28 \\ 19 & 20 & 22 & 25 & 23 & 29 & 27 & 29 \\ 19 & \boxed{19} & 25 & 23 & 24 & 25 & 25 & 39 \\ 17 & 22 & 22 & 25 & 27 & 32 & 33 & 33 \\ 20 & 20 & 27 & 26 & 33 & 35 & 35 & 43 \\ 20 & 26 & 23 & 33 & 24 & 34 & 38 & 33 \\ 23 & 24 & 35 & 32 & 46 & 42 & 48 & 45 \\ \hline \end{array}$$

is obtained, which yields an encoding with a file size of 8000 bytes, an error $E = 21.3967$, and a PSNR of 34.8085 dB. We can now better compare this table with the one found with Algorithm 6.1 in the previous section, shown in (6.4). Just as their entries differ only slightly, their respective encodings also have basically the same PSNR; hence we consider the two QTs to be equally valid.

We are of course free to start Algorithm 6.2 with any initial table; in particular, were we to start with the table $Q = [[255]]$, the actions of Algorithm 6.1 would be mimicked and its output reproduced. Consequently, Algorithm 6.2 is an extension of its predecessor.

6.3.1 Proposed Improvements

In general, different initial QTs result in slightly different but equally valid optimised QTs. The running times, however, can be vastly different. The reason for this is the fact that the number of iterations performed by Algorithm 6.2 is a function of the initial table. A well chosen initial table could reduce this number by being "close" to a final sequence of tables in a chronological sense. For instance, each table Q_{n+1} output by Algorithm 6.2 is closer to the final sequence than its predecessor Q_n, since using Q_{n+1} as initial table instead of Q_n would require one less iteration to reach the final sequence. The quantisation table

$$Q = \begin{array}{|cccccccc|}\hline 14 & 16 & 18 & 20 & 22 & 24 & 26 & 28 \\ 16 & 18 & 20 & 22 & 24 & 26 & 28 & 30 \\ 18 & 20 & 22 & 24 & 26 & 28 & 30 & 32 \\ 20 & 22 & 24 & 26 & 28 & 30 & 32 & 34 \\ 22 & 24 & 26 & 28 & 30 & 32 & 34 & 36 \\ 24 & 26 & 28 & 30 & 32 & 34 & 36 & 38 \\ 26 & 28 & 30 & 32 & 34 & 36 & 38 & 40 \\ 28 & 30 & 32 & 34 & 36 & 38 & 40 & 42 \\ \hline \end{array},$$

for instance, is closer to a final sequence than Q_J, shown in (6.5) and used as initial QT in the example above, was. By instead using Q as initial table and repeating the experiment, Algorithm 6.2 now requires more or less 1h27min to reach a final sequence of QTs.

Furthermore, the entries in Q are also closer to the entries in the final tables obtained with it than the entries in Q_J are to the entries in Q_1 and Q_2, shown in (6.6) and (6.7), respectively. This means that we can significantly reduce the number of candidate values to probe when using Q, thereby reducing the amount of work done during each iteration of the algorithm. The same final sequence of QTs can for instance be obtained by only probing the 20 candidate values above or below each entry during a particular iteration, depending on the direction being probed in. This reduces the running time to approximately 17min. If we do the same in the case of Q_J, however, the tables Q_1 and Q_2 will not be obtained, but an inferior final sequence instead.

A well chosen initial QT should therefore also minimise the number of values, say w, to probe in Algorithm 6.2. We will refer to this number as the *probing width*. Its use is formally described in Algorithm 6.3, which is a modification of Algorithm 6.2. Note that, by choosing $w = 254$, any result obtained with Algorithm 6.2 can be reproduced with Algorithm 6.3.

Input: Target file size T, initial table Q and probing width w

calculate B; calculate E; $R_{max} = \infty$; $R_{min} = 0$;

while $R_{max} > R_{min}$ **do**

  if $B < T$ **then**

    $\lambda^* = 0$;

    for k = *1 To 64* **do**

      $qq = Q(k)$; $qqq = \max(qq - w,\ 1)$;

      for q = *qqq To qq - 1* **do**

        $Q(k) = q$; calculate $\widehat{B}$; calculate $\widehat{E}$; $\lambda = \frac{E-\widehat{E}}{\widehat{B}-B}$;

        if $\lambda > \lambda^*$ **then**

          $\lambda^* = \lambda$; $k^* = k$; $q^* = q$; $B^* = \widehat{B}$; $E^* = \widehat{E}$;

        end

      end

      $Q(k) = qq$;

    end

    $R_{max} = \lambda^*$;

  else

    $\lambda^* = \infty$;

    for k = *1 To 64* **do**

      $qq = Q(k)$; $qqq = \min(qq + w,\ 255)$;

      for q = *qq + 1 To qqq* **do**

        $Q(k) = q$; calculate $\widehat{B}$; calculate $\widehat{E}$; $\lambda = \frac{\widehat{E}-E}{B-\widehat{B}}$;

        if $\lambda < \lambda^*$ *And* $\lambda > 0$ **then**

          $\lambda^* = \lambda$; $k^* = k$; $q^* = q$; $B^* = \widehat{B}$; $E^* = \widehat{E}$;

        end

      end

      $Q(k) = qq$;

    end

    $R_{min} = \lambda^*$;

  end

  $Q(k^*) = q^*$; $B = B^*$; $E = E^*$;

end

Algorithm 6.3: Proposed improved algorithm utilising a probing width w

The challenge now becomes choosing an appropriate initial table for an input image and target file size — one that will allow us to use as narrow a probing width as possible in order to minimise running time. While Fung and Parker do propose a formula for calculating initial tables in [1], their tables will often have entries of 255 in high frequency positions. Based on the discussion above, arriving at properly optimised QTs from such initial tables would require too much probing. Conversely, using a narrow probing width in conjunction with an initial QT calculated with the abovementioned formula would yield an inferior output table.

Instead, we propose an alternative method for calculating initial QTs, with a detailed account given in the next chapter. Also, an additional performance increase is gained by using two separate probing widths, one for QT entries in lower frequency positions and one for entries in higher frequency positions. From our experiments, detailed in Section 7.4, we found that we could further reduce the probing width for lower frequency entries and still obtain the same results. For this reason, QT entries are numbered and processed in zigzag ordering, as formulated in the problem statement in Section 6.1 and the subsequent descriptions of the greedy algorithms. By doing so, we can easily process lower frequency entries using their probing width first, followed by higher frequency entries being processed using their probing width. This partitioning is illustrated in Figure 6.1, where the first 28 entries in zigzag order, constituting the shaded upper triangle, are chosen as the lower frequency entries.

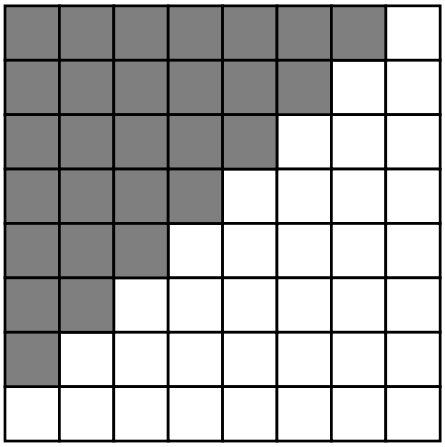

Figure 6.1: Partitioning of QT entries into lower and higher frequencies, enabling the use of two probing widths

6.4 Genetic Algorithms

Earlier in this chapter we mentioned that any discrete optimisation problem can be addressed with a genetic algorithm (GA). While not nearly a viable alternative to the previous algorithms, as we shall see shortly, a GA might be useful as a preprocessing stage to Algorithm 6.3, in an attempt to reduce its running time. That is, after calculating an initial QT, a GA might be able to improve upon it, thereby giving us an even better table to start Algorithm 6.3 with.

GAs are based on the fundamentals of evolutionary biology. Starting with an initial population of approximate solutions, each iteration replaces the population (current generation) with a new one, the next generation, by simulating natural selection. In other words, those solutions with higher fitness are more likely to reproduce than those with lower fitness. The basic outline of a typical GA is shown in Algorithm 6.4.

Input: **old_pop** = initial population of size n

Input: *total* = number of iterations to perform

for $i = 1$ *To total* **do**

  for $k = 1$ *To* n **do**

    calculate fitness of **old_pop**(k);

  end

  for $k = 1$ *By 2 To* n **do**

    randomly select $parent_1$ and $parent_2$ by utilising fitness;

    generate offspring $child_1$ and $child_2$;

    `(* insert in new population *)`

    new_pop$(k) = child_1$;

    new_pop$(k+1) = child_2$;

  end

  `(* new population becomes old population for next iteration *)`

  old_pop = **new_pop**;

end

Output fittest member of final population;

Algorithm 6.4: The basics of a typical genetic algorithm

The initial population is chosen as a set of randomly generated members of the search space. No rigorous guidelines for choosing its size n exist, with reported sizes ranging from anywhere between 20 or 30 to several thousand. The number of iterations performed by a GA is likewise chosen heuristically, and is usually at least 50. These iterations are referred to as *generations*. With both a large population and many generations potentially required to obtain an adequate solution to a particular problem, GAs can be quite time-consuming. They are therefore not competitive with Algorithm 6.3 and are only of interest here in the context of preprocessing.

In the next few subsections, we briefly describe the operations that take place in a GA, such as the fitness calculation, selection of parents, and simulation of reproduction. These discussions are limited to our application of a GA to optimal quantisation, and do not constitute a proper introduction. For further details, we refer the reader to [26].

6.4.1 The Fitness Function

In a GA the fitness of a candidate solution is a measure of how well it solves the underlying optimisation problem. This is quantified by using a *fitness function*, which is always derived from the function to be optimised, called the *object function*. In unconstrained maximisation problems, we can simply use the object function as the fitness function, while using its negative or inverse as the fitness function in unconstrained minimisation problems.

Recalling our problem statement in Section 6.1, the function we wish to minimise is the error E in the frequency domain. If this problem was unconstrained, the fitness f of a quantisation table Q could for instance be chosen as

$$f(Q) = \frac{1}{E(Q)}.$$

Our problem is constrained though, so we also have to penalise deviation from constraint (6.2). If we do not, the table $Q = [[1]]$ (which always yields the smallest error) will always be deemed the fittest. By virtue of (6.2), a candidate solution Q yielding a file size B will be penalised if $B > 1.001T$ or $B < 0.999T$. The deviation (in percentage) is therefore calculated as

$$dev(Q) = \begin{cases} 100\left(\dfrac{B(Q) - 1.001T}{1.001T}\right), & B > 1.001T, \\ 100\left(\dfrac{0.999T - B(Q)}{0.999T}\right), & B < 0.999T, \\ 0, & \text{otherwise.} \end{cases} \tag{6.8}$$

Using this deviation, a new object function is created, say $cost(Q)$, given by

$$cost(Q) = E(Q) + c.dev(Q), \quad c > 0. \tag{6.9}$$

The number c is known as the *penalty parameter* and is used to ensure proper penalisation of infeasibility.

For calculating c, the adaptive method proposed in [27] was chosen. During each iteration

of the GA the current value of c, say c_i, is modified for the next generation according to

$$c_{i+1} = c_i \left(\frac{BFC}{BIC} \right). \tag{6.10}$$

Here BFC refers to the lowest cost belonging to a feasible solution (the best feasible cost), while BIC refers to the lowest cost belonging to an infeasible solution (the best infeasible cost). As a result, the penalty parameter will be scaled up if deviation from our constraint is not sufficiently penalised, and down if deviation is over-penalised.

For the initial value of c we use the "interior method" proposed in [27], where an initial value much higher than the expected proper value is chosen. The value used in our C++ implementation of a GA is 35.

Finally, our fitness function is once again chosen as the inverse of the object function, meaning that

$$f(Q) = \frac{1}{cost(Q)}. \tag{6.11}$$

6.4.2 Natural Selection

During a typical iteration of a GA the fitness of each member of the current population is calculated using the chosen fitness function. As shown in Algorithm 6.4, pairs of these members are then randomly selected, by utilising their fitness, to reproduce. Several selection methods exist, among others the basic fitness-proportionate method that we chose. This method is called *roulette wheel sampling*, and can be implemented by partitioning the probability interval $[0,\ 1]$ into n subintervals, where n is the size of the population. Each member of the population is then assigned its own subinterval, $[a_k,\ b_k)$, the width of which is proportional to that member's fitness.

In each case the upper limit b_k is calculated as

$$b_k = \sum_{j=1}^{k} \frac{f(Q_j)}{f_{tot}},$$

where Q_j is the jth member of the current generation and f_{tot} is the total fitness

$$f_{tot} = \sum_{j=1}^{n} f(Q_j).$$

Each lower limit a_k, on the other hand, is equal to the previous subinterval's upper limit, *i.e.* $a_k = b_{k-1},\ k \geq 2$, and $a_1 = 0$. For example, if the first member has fitness $f = 10$ and $f_{tot} = 100$, then its subinterval will be $[a_1,\ b_1) = [0,\ 0.1)$. Then, if the second member has fitness $f = 5$, its subinterval is $[a_2,\ b_2) = [0.1,\ 0.15)$, etc. By now generating a random number between 0 and 1, a member can be selected by determining which subinterval the random number belongs to.

In a practical implementation one would only store the upper limits b_k, and calculate them using the recursion formula

$$\begin{aligned} b_1 &= \frac{f(Q_1)}{f_{tot}}, \\ b_k &= b_{k-1} + \frac{f(Q_k)}{f_{tot}}, \quad k \geq 2. \end{aligned} \tag{6.12}$$

6.4.3 Genetic Operators

Once two members have been selected, say $parent_1$ and $parent_2$, two new approximate solutions, say $child_1$ and $child_2$, are constructed, thereby simulating reproduction. Two genetic operators are utilised during this process, namely *crossover* and *mutation*. We explain them by using a pair of QTs as an example. Let these tables be

$parent_1 =$

1	2	3	4	5	6	7	8
9	10	11	12	13	14	15	16
17	18	19	20	21	22	23	24
25	26	27	28	29	30	31	32
33	34	35	36	37	38	39	40
41	42	43	44	45	46	47	48
49	50	51	52	53	54	55	56
57	58	59	60	61	62	63	64

and

$$parent_2 = \begin{array}{|cccccccc|}\hline 65 & 66 & 67 & 68 & 69 & 70 & 71 & 72 \\ 73 & 74 & 75 & 76 & 77 & 78 & 79 & 80 \\ 81 & 82 & 83 & 84 & 85 & 86 & 87 & 88 \\ 89 & 90 & 91 & 92 & 93 & 94 & 95 & 96 \\ 97 & 98 & 99 & 100 & 101 & 102 & 103 & 104 \\ 105 & 106 & 107 & 108 & 109 & 110 & 111 & 112 \\ 113 & 114 & 115 & 116 & 117 & 118 & 119 & 120 \\ 121 & 122 & 123 & 124 & 124 & 126 & 127 & 128 \\ \hline \end{array} .$$

In a GA the digital representation of an approximate solution (population member) constitutes its set of genes. For a QT each entry is a gene, and for this example we number them from left to right, top to bottom. During crossover $child_1$ and $child_2$ are constructed from the genes (entries) of both $parent_1$ and $parent_2$ by randomly selecting a *crossover point*, say r. The first r genes of $parent_1$ and remaining $64 - r$ genes of $parent_2$ are concatenated to form $child_1$, while $child_2$ is formed from the concatenation of the first r genes of $parent_2$ with the remaining $64 - r$ genes of $parent_1$.

For example, if $r = 10$, we will have

$$child_1 = \begin{array}{|cccccccc|}\hline 1 & 2 & 3 & 4 & 5 & 6 & 7 & 8 \\ 9 & 10 & 75 & 76 & 77 & 78 & 79 & 80 \\ 81 & 82 & 83 & 84 & 85 & 86 & 87 & 88 \\ 89 & 90 & 91 & 92 & 93 & 94 & 95 & 96 \\ 97 & 98 & 99 & 100 & 101 & 102 & 103 & 104 \\ 105 & 106 & 107 & 108 & 109 & 110 & 111 & 112 \\ 113 & 114 & 115 & 116 & 117 & 118 & 119 & 120 \\ 121 & 122 & 123 & 124 & 124 & 126 & 127 & 128 \\ \hline \end{array}$$

and

$$child_2 = \begin{array}{|cccccccc|}\hline 65 & 66 & 67 & 68 & 69 & 70 & 71 & 72 \\ 73 & 74 & 11 & 12 & 13 & 14 & 15 & 16 \\ 17 & 18 & 19 & 20 & 21 & 22 & 23 & 24 \\ 25 & 26 & 27 & 28 & 29 & 30 & 31 & 32 \\ 33 & 34 & 35 & 36 & 37 & 38 & 39 & 40 \\ 41 & 42 & 43 & 44 & 45 & 46 & 47 & 48 \\ 49 & 50 & 51 & 52 & 53 & 54 & 55 & 56 \\ 57 & 58 & 59 & 60 & 61 & 62 & 63 & 64 \\ \hline \end{array} .$$

This particular implementation of crossover is termed *single-point* crossover, and is the approach we chose. Other approaches, such as two-point crossover, are explained in [26].

Crossover need not necessarily take place: In general, a *crossover probability* p_c can be used to determine whether or not crossover takes place. If it does not (*i.e.* a random number between 0 and 1 is not smaller than p_c), $child_1$ and $child_2$ are chosen as exact replicas of their parents. Since p_c is usually chosen to be at least 0.75, we simply chose $p_c = 1$ for our implementation.

After $child_1$ and $child_2$ have been created, the mutation operator comes into play. It can replace a gene in a randomly selected position with a randomly selected new value. To determine when a mutation takes place, a parameter p_m, called the *mutation probability*, is used. This number is usually quite small and can for instance be $p_m = 0.05$. If a random number between 0 and 1 is not smaller than p_m, mutation does not take place. In general, mutation can be applied to each gene with probability p_m. Here, for each child in turn, we apply it only once.

If, for example, $child_2$ above were to undergo a mutation, a random integer between 1 and 64 would be generated to select the gene undergoing the mutation. We would then generate a random integer between 1 and 255 to determine the new value of the mutated gene. If the randomly selected gene was at position was 24 and its new value was 200,

then we would have

$$child_2 = \begin{array}{|cccccccc|}\hline 65 & 66 & 67 & 68 & 69 & 70 & 71 & 72 \\ 73 & 74 & 11 & 12 & 13 & 14 & 15 & 16 \\ 17 & 18 & 19 & 20 & 21 & 22 & 23 & 200 \\ 25 & 26 & 27 & 28 & 29 & 30 & 31 & 32 \\ 33 & 34 & 35 & 36 & 37 & 38 & 39 & 40 \\ 41 & 42 & 43 & 44 & 45 & 46 & 47 & 48 \\ 49 & 50 & 51 & 52 & 53 & 54 & 55 & 56 \\ 57 & 58 & 59 & 60 & 61 & 62 & 63 & 64 \\ \hline \end{array} .$$

In the end, the new members $child_1$ and $child_2$ are placed in a new population that will replace the current one. For this reason, reproduction is performed $\frac{n}{2}$ times per iteration to obtain a new population of n members.

6.4.4 Convergence

As Algorithm 6.4 suggests, a tradditional stopping condition is not used in a GA. Instead, the algorithm is run for a large number of generations. Upon termination the fittest member of the final population will be chosen as the best approximation to the sought after solution. What happens when convergence takes place, is that all members of the population will be (roughly) the same. We can therefore inspect the members of the final population to see whether or not convergence has occurred. If it has not, we can always "resume" the algorithm, using the final population as the new initial population.

Since each new generation completely replaces the one preceding it, the fittest member of a particular generation is not necessarily fitter than, or even as fit as, the one from the previous generation. Rather, it is the average fitness of the population that generally increases from generation to generation. If we do not wish to lose the fittest member, we can let it survive: after generating a new population, one can randomly select a member from it to be replaced by the fittest member from the previous generation. This approach is called *elitism*, and we chose to use it in our implementation.

6.5 C++ Implementation

As we saw in Section 6.3.1, Algorithm 6.3 retains the workings of Algorithms 6.1 and 6.2 as subsets, therefore only its implementation is discussed here. We intend to use the algorithm to obtain optimised QTs for both JPEG and MJPEG so as to compare results; hence, two C++ implementations were created. For brevity, only the implementation for MJPEG, `qt_m.cc`, is listed in Appendix B.2. Its JPEG counterpart, `qt.cc`, is very similar.

Each program reads in a mat-file of unquantised frequency components created by Matlab. Such files are created by applying either `my_jpeg.m` or `mjpeg.m` (whichever is applicable) to an image, with quantisation disabled, and saving the output. For instance, `qt_m` will read in an image's unquantised MDCT coefficients. These coefficients are stored in the $m \times n$ matrix Y, where m and n are also the dimensions of the original image.

Both programs store their QTs in the same left-to-right, top-to-bottom format as matrix Y, making quantisation and dequantisation as efficient as possible. In order to still process QT entries in zigzag ordering, both programs use an array $\mathbf{z}$ of indices arranged in this ordering to reconcile the indexing. In other words, QT entries are now addressed as $Q(\mathbf{z}(k))$ rather than $Q(k)$ during the main algorithm.

The two probing widths mentioned in Section 6.3.1 are used, with the one used for lower frequency entries called lo, and the one used for higher frequency entries called hi. To use these two probing widths, each of the outer FOR-loops of Algorithm 6.3 are separated into two new ones. The first of these processes the first 28 QT entries using lo, while the second processes the remaining entries using hi.

As was discussed in Section 6.2, our implementations test for the special cases of $\lambda = \infty$ and $\lambda = \text{NaN}$ in order to break out of the appropriate FOR-loops when necessary. Some other aspects of note are the functions `qdq`, `dct2bytes`, `d2b` and `calc_error`. Function `qdq` performs quantisation and dequantisation (utilising $m \times n$ matrices Y_q and Y_{dq}); functions `dct2bytes` and `d2b` behave in exactly the same way as their respective Matlab counterparts; and `calc_error` uses Y and Y_{dq} to calculate the error E defined in (6.1). In

the case of program `qt_m` the primary QT is also downsampled to form the two auxilliary QTs before each call to `qdq`. This task is performed by the function `down_Q`.

Both programs also contain an implementation of our proposed method for calculating initial QTs. The user can choose, via an input option, whether to directly supply the main algorithm with such an obtained table (option 0), or to first attempt to improve the table with a genetic algorithm (option 1). In addition, by choosing option 2, this stage can be skipped and Algorithm 6.3 will start with an initial table specified in function `init_Q`. This allows us to generate the output of Algorithms 6.1 and 6.2.

Our implemented genetic algorithm can be found in function `ga`, which is called after the construction of an initial population. The adaptive method used for calculating the penalty parameter, described in Section 6.4.1, relies on the presence of at least one feasible solution in the initial population. For this reason, before constructing an initial population, we ensure the feasibility of our initial QT by prompting the user to make slight modifications to its entries if it happens to be infeasible. The resulting table, say Q, is then used to construct an initial population and is also included as a member of that population. By assuming that Q is a good initial table and subsequently restricting the search in Algorithm 6.3 with probing widths, the GA's search space is also reduced. We therefore generate an initial population by randomly adding or subtracting integer values from the entries in Q, within the limits set by the probing widths.

As stated in Section 6.4.2, selection is implemented by using roulette wheel sampling; the function responsible for searching the probability intervals assigned to population members is `find_pos`. Function `mate` then performs the crossover and mutation operators described in Section 6.4.3, and places the resulting offspring in the next generation. Note that, since the search space is reduced by using probing widths, we also limit the intervals from which mutated genes are selected accordingly. At the end of each iteration, the elitist approach mentioned in Section 6.4.4 is employed: the fittest QT from the current generation survives by replacing a randomly selected QT from the next generation.

Lastly, when the GA has finished, the final generation's fittest table is chosen as the new initial QT for Algorithm 6.3.

Chapter 7

Modelling and Predicting Initial Tables

We saw in the previous chapter that the choice of initial QTs plays a central role in minimising the running time of Algorithm 6.3. In this chapter we propose a method for generating good initial tables.

7.1 Linear Models

As we discussed in Section 6.3.1, we would ideally like initial tables to be as "close" as possible to the optimised tables that will be obtained using them. One aim of doing so is to hopefully reduce the number of iterations needed by Algorithm 6.3. The other advantage is the reduction in probing width to be achieved. A good initial table $\widetilde{Q}$ should therefore be "close" to the final table Q in the sense that

$$||Q - \widetilde{Q}||_\infty = \max_{1 \leq k \leq 64} |q_k - \widetilde{q}_k| \tag{7.1}$$

should be small. Less formally, we could also say that a good initial table should mimic the trends of the final table. Looking at the optimised tables shown in Figure 7.1, obtained for some JPEG encodings of 256×256 Lena, there indeed seem to be trends to exploit.

13	14	16	15	15	14	18	14
13	15	16	15	16	15	15	17
13	16	15	17	16	15	17	15
14	14	16	13	13	18	17	15
13	15	15	14	18	17	18	14
17	14	14	17	16	15	18	18
13	13	17	15	15	17	15	18
14	16	16	16	18	17	18	19

(a) $B = 10900$ bytes

17	18	20	16	18	20	22	20
18	19	20	19	22	20	21	21
19	20	18	20	21	21	23	20
16	17	20	21	20	19	21	26
16	22	19	20	22	20	24	25
19	20	22	20	21	20	26	22
18	25	17	20	21	27	31	26
23	24	19	19	32	29	33	45

(b) $B = 9015$ bytes

25	33	29	26	32	27	34	29
26	26	29	32	29	33	35	39
22	31	33	28	35	31	39	36
29	28	31	33	39	39	37	44
24	32	38	37	36	38	52	39
32	34	40	37	49	51	43	61
41	39	45	54	60	53	61	63
39	35	56	56	55	67	65	75

(c) $B = 6342$ bytes

Figure 7.1: Optimised QTs for the Lena image, listed in decreasing file size order

Not only do the entries of these tables become larger as the file size is decreased, they also seem to have a roughly bi-linear or "planar" behaviour, with gradients increasing with decreasing file size. This means that we should be able to approximate these tables fairly well with 2-variable functions of the form

$$\widetilde{Q}(m,n) = c_1(m+n) + c_0, \qquad m = 0,\ldots,7,\ n = 0,\ldots,7. \tag{7.2}$$

By using the 2-norm

$$||Q - \widetilde{Q}||_2 = \sqrt{\sum_{k=1}^{64}(q_k - \widetilde{q}_k)^2} \tag{7.3}$$

rather than the ∞-norm in (7.1), we can easily obtain least squares solutions for c_0 and c_1. The resulting approximations for (a), (b), and (c) in Figure 7.1 are listed in Figure 7.2 below, with their entries rounded to form valid QTs.

14	14	14	14	15	15	15	16
14	14	14	15	15	15	16	16
14	14	15	15	15	16	16	16
14	15	15	15	16	16	16	16
15	15	15	16	16	16	16	17
15	15	16	16	16	16	17	17
15	16	16	16	16	17	17	17
16	16	16	16	17	17	17	18

(a) $\widetilde{Q} = 0.2813(m+n) + 13.5781$

15	16	17	18	19	20	21	22
16	17	18	19	20	21	22	23
17	18	19	20	21	22	23	24
18	19	20	21	22	23	24	25
19	20	21	22	23	24	25	26
20	21	22	23	24	25	26	27
21	22	23	24	25	26	27	28
22	23	24	25	26	27	28	29

(b) $\widetilde{Q} = 1.0015(m+n) + 14.5521$

17	20	23	27	30	33	36	39
20	23	27	30	33	36	39	43
23	27	30	33	36	39	43	46
27	30	33	36	39	43	46	49
30	33	36	39	43	46	49	52
33	36	39	43	46	49	52	56
36	39	43	46	49	52	56	59
39	43	46	49	52	56	59	62

(c) $\widetilde{Q} = 3.2292(m+n) + 16.8646$

Figure 7.2: Least squares approximations of QTs in Figure 7.1

We see that these approximations are indeed good ones, with the gradient c_1 in particular exhibiting the expected behaviour. While these least-squares models might not minimise the ∞-norm, this is a small price to pay for the ease of computation they provide.

What is needed now is some way to predict the parameters c_0 and c_1 when presented with an input image and target file size. To investigate how optimised QTs and their

corresponding least-squares models vary for different file sizes and different images, we stored and analysed the output generated by both `qt.cc` and `qt_m.cc` for three images. These images were Lena, Bridge and Plane, all of dimensions 256×256 and shown in Appendix A, and for `qt_m` the sine window was used. In each case the programs were started with an initial table filled with 1s, made use of a uniform probing width of $w = 254$, and were given a target file size of 4000 bytes — thereby mimicking the behaviour of Algorithm 6.1 in the "opposite" direction. Had we started from the "normal" direction, with initial tables filled with values of 255, and large target file sizes, many of the optimised tables corresponding to lower file sizes would have had entries of 255 amongst other two-digit entries. Our linear model would be a poor fit for such tables. Starting from this "opposite" direction, on the other hand, results in much better behaved, yet equally valid, optimised QTs.

7.2 Prediction Strategy

One finding from the analysis mentioned above, is that the parameter c_0 (and thus the first entry of a model) does not necessarily increase monotonically with decreasing file size. The tables shown in Figures 7.3 and 7.4 below, once again taken from the JPEG encodings of Lena, and accompanied by their respective models, are an example of this observation. The same is true of the gradient c_1, but we found that the combined effect of c_0 and c_1 is always such that the higher frequency entries do increase monotonically with decreasing file size, in particular those on the co-main diagonal.

22	23	28	26	30	24	30	24
26	26	26	26	26	33	25	28
21	27	32	27	29	29	28	35
25	24	27	29	34	33	25	44
24	25	26	27	34	33	52	39
22	28	27	30	33	38	43	43
35	28	23	44	60	53	44	49
39	25	35	33	55	42	65	45

(a) $B = 7034$ bytes

17	19	21	24	26	28	30	33
19	21	24	26	28	30	33	35
21	24	26	28	30	33	35	37
24	26	28	30	33	35	37	40
26	28	30	33	35	37	40	42
28	30	33	35	37	40	42	44
30	33	35	37	40	42	44	46
33	35	37	40	42	44	46	49

(b) $\widetilde{Q} = 2.2872(m+n) + 16.6615$

Figure 7.3: For the Lena image: (a) An optimised QT and (b) its corresponding least-squares model

25	23	28	26	31	25	30	29
26	26	26	29	26	33	32	28
21	29	32	28	29	29	39	35
25	24	27	29	34	35	26	44
24	25	26	27	34	33	52	39
22	28	27	31	33	38	43	43
36	28	27	44	60	53	61	63
39	33	35	33	55	67	65	45

(a) $B = 6880$ bytes

15	18	21	24	26	29	32	34
18	21	24	26	29	32	34	37
21	24	26	29	32	34	37	40
24	26	29	32	34	37	40	42
26	29	32	34	37	40	42	45
29	32	34	37	40	42	45	48
32	34	37	40	42	45	48	51
34	37	40	42	45	48	51	53

(b) $\widetilde{Q} = 2.6979(m+n) + 15.4583$

Figure 7.4: For the Lena image: (a) An optimised QT for a higher file size than the one shown in Figure 7.3(a), and (b) its least-squares model possessing a smaller first entry than the one shown in Figure 7.3(b)

As it turns out, these co-main diagonal values can be, at least roughly, predicted for an input image and target file size. Thanks to the symmetry brought by our choice of modelling function, they have the same value, which can be used as an alternate parameter

in (7.2). This means that we can recast our model to look as follows:

$$\widetilde{Q}(m,n) = k_1(m+n-7) + k_0, \qquad m = 0,\ldots,7,\ n = 0,\ldots,7, \tag{7.4}$$

where k_0 will determine the entries on the co-main diagonal, and k_1 will have the same value as c_1.

The model in Figure 7.2(a), for example, will be transformed from

$$\widetilde{Q}(m,n) = 0.2813(m+n) + 13.5781$$

to

$$\widetilde{Q}(m,n) = 0.2813(m+n-7) + 15.5472.$$

Notice that k_0 and k_1 have now become the parameters we wish to predict. In this new form, the gradient k_1 can be thought of as a rotation applied about the co-main diagonal to the table $[[k_0]]$, using the notation defined by (6.3). By predicting k_0, we would also be predicting the table $[[k_0]]$ to which k_1 will be applied. We therefore turn to such "constant" tables in this endeavour. The hope is that the value $\widehat{k}_0$ for which the table $[[\widehat{k}_0]]$ gives a coding file size closest to the target, will be a good approximation to k_0. As a consequence, $\widehat{k}_0$ has to be restricted to integer values between 1 and 255, since quantising with floating-point numbers makes no sense when our file size calculations assume the storage of an 8-bit integer quantisation table in the output file. However, this restriction also has the benefit of limiting the search to a finite number of candidates.

With $\widehat{k}_0$ now an integer, we can just as well use it as a prediction for the co-main diagonal entries instead, to which we will henceforth refer as *diag*. This will enable us to approximate (predict) k_1: By investigating how k_1 varies for each value of *diag*, a list of approximate gradients $\widehat{k}_1$ can be maintained and indexed by $\widehat{k}_0$. In other words, upon obtaining $\widehat{k}_0$ the approximate gradient will be

$$\widehat{k}_1 = \text{list\_of\_gradients}(\widehat{k}_0), \tag{7.5}$$

making

$$\widehat{Q}(m,n) = \widehat{k}_1(m+n-7) + \widehat{k}_0, \qquad m = 0,\ldots,7,\ n = 0,\ldots,7 \tag{7.6}$$

our predicted initial table.

Let us see how this approach fares when applied to the tables (a), (b) and (c) in Figure 7.1, using their respective coding file sizes as the target file size T in each case. Firstly, table (a) has a resulting file size of 10900 bytes, and was approximated by table (a) in Figure 7.2, which has a value of *diag* equal to 16. By JPEG encoding Lena with the tables $[[1]], [[2]], \ldots, [[255]]$, we find that the table $[[16]]$ gives the closest file size of 10681 bytes. Therefore $\widehat{k}_0 = 16$. By comparison, the tables $[[15]]$ and $[[17]]$ give file sizes of 11165 bytes and 10248 bytes, respectively. In general, the sequence of tables $[[1]], [[2]], \ldots, [[255]]$ will result in successively lower file sizes, meaning that the sequence of values

$$|B(Q) - T|, \quad Q = [[1]], \ldots, [[255]]$$

is convex. Consequently, a golden ratio search can be used to find $\widehat{k}_0$, thereby significantly reducing the amount of work involved.

Returning to our example, we obtain a value of $\widehat{k}_0 = 21$ for $T = 9015$ bytes corresponding to table (b) in Figure 7.1; its approximation has co-main diagonal entries equal to 22, as we saw in Figure 7.2(b). Lastly, the target file size of 6342 bytes belonging to table (c) in Figure 7.1 results in $\widehat{k}_0 = 34$, while the actual co-main diagonal values of Figure 7.2(c) were 39.

The above example gives a snapshot of our findings from analysing the data from the three test images mentioned earlier. In general, $\widehat{k}_0$ accurately recovers the co-main diagonal up until roughly $diag = 18$ for the JPEG encodings, and $diag = 16$ for the MJPEG encodings, after which it starts "lagging" behind more and more. This relationship between $\widehat{k}_0$ and *diag* is summarised in Table 7.1 below, for the case of the JPEG encodings. It shows, for each image, the actual values of *diag* corresponding to values of $\widehat{k}_0$ obtained. The number of occurrences of each value of *diag* corresponding to a particular $\widehat{k}_0$ is listed in brackets.

$\widehat{k}_0$	**Lena**	**Plane**	**Bridge**
10	10(43), 11(5)	10(46)	10(53)
11	11(40), 12(5)	10(2), 11(41)	10(4), 11(46)
12	12(40), 13(9)	11(1), 12(47)	11(4), 12(39)
13	13(41), 14(6)	12(1), 13(39)	12(5), 13(42)
14	14(35), 15(9)	14(43)	13(3), 14(40)
15	15(27)	14(1), 15(31)	14(3), 15(35)
16	15(1), 16(30), 17(1)	15(1), 16(41)	15(3), 16(41)
17	17(26), 18(2)	17(34), 18(3)	16(3), 17(32)
18	18(31), 19(8)	18(20), 19(2)	18(36), 19(3)
19	19(9), 20(19)	19(27), 20(1)	19(30), 20(7)
20	20(8), 21(16)	20(29), 21(1)	20(24), 21(7)
21	21(3), 22(19)	21(29), 22(4)	21(17), 22(14)
22	22(5), 23(13), 24(5)	22(18), 23(12)	22(15), 23(13)
23	24(10), 25(16)	23(20), 24(4)	23(21), 24(11)
24	25(3), 26(14)	24(21), 25(9)	24(4), 25(23)
25	27(21), 28(1)	25(20), 26(6)	25(3), 26(19)
26	28(21)	26(3), 27(16), 28(4)	26(2), 27(20), 28(10)
27	29(11), 30(11)	28(12), 29(8)	28(7), 29(20)
28	30(8), 31(14)	29(11), 30(13)	29(1), 30(21), 31(7)
29	32(20)	30(2), 31(13), 32(4)	31(6), 32(10), 33(9), 34(1)
30	32(3), 33(8), 34(8)	33(13), 34(5)	34(19), 35(3)
31	34(7), 35(6), 36(5)	34(12), 35(3)	35(17), 36(13)
32	36(15), 37(8)	35(4), 36(14)	36(7), 37(9)
33	37(3), 38(8), 39(6)	36(6), 37(12)	37(7), 38(12)
34	39(15), 40(1)	37(1), 38(12)	38(1), 39(14), 40(4)
35	40(9)	38(5), 39(14), 40(1)	40(11), 41(7), 42(3)
36	40(4), 41(11)	40(18), 41(3)	42(8), 43(5)

Table 7.1: The relationship between $\widehat{k}_0$ and *diag* for the JPEG encodings of the three images (*continued on next page*)

$\widehat{k}_0$	**Lena**	**Plane**	**Bridge**
37	42(9), 43(6), 44(3)	41(10), 42(4)	43(5), 44(12), 45(5)
38	44(14)	42(4), 43(12)	45(9), 46(16)
39	45(10)	44(9), 45(4)	46(3), 47(16)
40	45(2), 46(16)	45(3), 46(10), 47(5)	47(1), 48(3), 49(11), 50(2)
41	46(1), 47(10)	47(10), 48(7)	50(14)
42	47(3), 48(9)	48(7), 49(6)	50(1), 51(14), 52(4)
43	49(5), 50(2)	49(3), 50(7)	52(2), 53(8), 54(5)
44	50(9)	50(6), 51(7)	54(9), 55(6)
45	51(5) , 52(5)	51(6) , 52(7)	55(8)
46	52(2), 53(6), 54(6)	52(2), 53(8)	
47	54(1), 55(5)	53(1), 54(7), 55(7)	

Table 7.1: The relationship between $\widehat{k}_0$ and *diag* for the JPEG encodings of the three images (*continued*)

For both JPEG and MJPEG we chose to limit our linear models to values of *diag* between 10 and 55. In the case of JPEG, this limits the values of $\widehat{k}_0$ to the set $\{10, \ldots, 47\}$, as seen in Table 7.1. The reasons for these limits are as follows: On the one hand, models with co-main diagonal entries of 9 and lower tend to have very small gradients. The example QT below, taken from the JPEG encodings of Bridge and shown alongside its least squares model, clearly illustrates this.

9	10	10	10	9	9	9	9
11	10	10	9	9	9	9	8
10	10	9	9	9	9	8	9
10	9	9	10	9	9	10	9
10	9	9	10	10	10	9	9
9	9	9	9	10	10	9	10
9	8	9	10	11	9	10	10
10	8	10	9	9	9	11	13

(a) $B = 25769$ bytes

9	9	9	9	9	9	9	9
9	9	9	9	9	9	9	9
9	9	9	9	9	9	9	9
9	9	9	9	9	9	9	10
9	9	9	9	9	9	10	10
9	9	9	9	9	10	10	10
9	9	9	9	10	10	10	10
9	9	9	10	10	10	10	10

(b) $\widetilde{Q} = 0.0298(m+n) + 9.2292$

Figure 7.5: For the Bridge image: (a) An optimised QT corresponding to a large file size, and (b) its least-squares model possessing a small gradient

With such small gradients one could just as well use $[[\widehat{k}_0]]$ as initial table upon obtaining $\widehat{k}_0$, for $\widehat{k}_0 = 1, \ldots, 9$. File sizes yielding such low values of $\widehat{k}_0$ are also very large and probably outside the scope of practical usage. With a very strong correlation between $\widehat{k}_0 = 10$ and $diag = 10$ (almost no instances of $\widehat{k}_0 = 9$ mapped to $diag = 10$, and vice versa), we chose these values as the lower limits.

On the other hand, optimised QTs only exhibit planar behaviour up to a certain point. Eventually, low file size QTs start deviating from this pattern, as the table

$$Q = \begin{array}{|cccccccc|}\hline 33 & 26 & 33 & 30 & 39 & 34 & 38 & 40 \\ 33 & 31 & 28 & 33 & 38 & 46 & 38 & 77 \\ 28 & 29 & 38 & 40 & 44 & 59 & 86 & 77 \\ 34 & 34 & 41 & 47 & 47 & 92 & 88 & 90 \\ 28 & 42 & 43 & 49 & 82 & 105 & 90 & 88 \\ 46 & 44 & 57 & 67 & 97 & 87 & 84 & 76 \\ 39 & 54 & 74 & 91 & 72 & 96 & 67 & 79 \\ 67 & 70 & 91 & 84 & 81 & 81 & 93 & 63 \\ \hline \end{array},$$

also taken from the JPEG encodings of Bridge, suggests. This table gives a file size of 8442 bytes and has a least squares model with $diag = 59$. We can see that the largest entries are no longer confined to only the highest frequencies — they now also show up in positions slightly below the co-main diagonal. Applying the same models to such tables would still give us larger and larger gradients, but the resulting approximations would no longer be satisfactory. With this behaviour tending to occur in tables whose corresponding models have values of $diag$ larger than 55, we chose to only model up to this point. For our JPEG models the largest value of $\widehat{k}_0$ to map to $diag = 55$ was 47, hence the use of it as a lower limit. Instances of $\widehat{k}_0 = 47$ mapping to values of $diag$ larger than 55 are not listed in Table 7.1, since they are not applicable, which is why the last two entries in the third column are empty. Also note that, since the file sizes yielding values of $\widehat{k}_0$ larger than 47 (and/or values of $diag$ larger than 55) are quite small, they are again probably outside the scope of practical usage.

As mentioned previously, the correlation between the co-main diagonal values $diag$ and gradients k_1 was also analysed, enabling us to predict approximate gradients $\widehat{k}_1$. For now these analyses (for both JPEG and sine window MJPEG) are only based on the data from the Lena image, but have yielded good results as will be seen in Section 7.4. The findings for the JPEG case are summarised in Table 7.2, where the second column lists the smallest and largest values k_1 assumed for each of the relevant values of $diag$. The approximate gradients $\widehat{k}_1$ are then taken as the midpoints of the resulting intervals.

diag	**Range**	**Approximate gradient $\widehat{k}_1$**
10	[0.2723, 0.3170]	0.2946
11	[0.2426, 0.3601]	0.3014
12	[0.2708, 0.3914]	0.3311
13	[0.4018, 0.4896]	0.4457
14	[0.3929, 0.4613]	0.4271
15	[0.2664, 0.4390]	0.3527
16	[0.2589, 0.3021]	0.2805

Table 7.2: The relationship between $diag$ and $\widehat{k}_1$ obtained from the JPEG encodings of Lena (*continued on next page*)

diag	**Range**	**Approximate gradient $\widehat{k}_1$**
17	[0.2813, 0.3780]	0.3297
18	[0.3497, 0.5119]	0.4308
19	[0.5045, 0.7798]	0.6422
20	[0.7545, 0.8259]	0.7902
21	[0.9420, 1.0104]	0.9762
22	[0.9405, 1.0253]	0.9829
23	[1.0298, 1.3170]	1.1734
24	[1.3542, 1.6235]	1.4889
25	[1.6280, 1.8304]	1.7292
26	[1.7932, 1.9152]	1.8542
27	[1.8438, 1.9420]	1.8929
28	[1.8973, 1.9702]	1.9337
29	[1.8884, 2.0551]	1.9718
30	[2.1652, 2.3110]	2.2381
31	[2.1935, 2.3095]	2.2515
32	[2.2693, 2.3542]	2.3118
33	[2.2753, 2.4182]	2.3468
34	[2.6027, 2.7530]	2.6779
35	[2.7098, 2.8750]	2.7924
36	[2.8051, 2.9107]	2.8579
37	[2.9211, 2.9479]	2.9345
38	[2.9137, 3.2262]	3.0700
39	[3.2262, 3.3348]	3.2805
40	[3.0208, 3.2083]	3.1145
41	[3.0744, 3.1458]	3.1101
42	[3.1563, 3.3571]	3.2567
43	[3.4107, 3.5149]	3.4628

Table 7.2: The relationship between *diag* and $\widehat{k}_1$ obtained from the JPEG encodings of Lena (*continued on next page*)

diag	**Range**	**Approximate gradient $\widehat{k}_1$**
44	[3.5089, 3.6295]	3.5692
45	[3.3839, 3.5134]	3.4486
46	[3.4182, 3.5774]	3.4978
47	[3.3125, 3.4003]	3.3564
48	[3.2813, 3.3527]	3.3170
49	[3.2604, 3.2693]	3.2649
50	[3.2887, 3.3601]	3.3244
51	[3.2173, 3.2470]	3.2321
52	[3.2619, 3.3408]	3.3014
53	[3.3289, 3.5699]	3.4494
54	[3.4762, 3.5640]	3.5201
55	[3.6429, 3.7723]	3.7076

Table 7.2: The relationship between *diag* and $\widehat{k}_1$ obtained from the JPEG encodings of Lena (*continued*)

Given the large discrepancies between larger values of $\widehat{k}_0$ and *diag* seen in Table 7.1, we would rather not index Table 7.2 with such a $\widehat{k}_0$ and end up with the wrong approximate gradient. Instead, the following approach is used: Upon obtaining say $\widehat{k}_0 = 45$ for some target file size, we now know from Table 7.1 that the actual value of *diag* should have been somewhere between 51 and 55. We just need some way of picking one of them. We therefore try out each of the candidate models

$$\widehat{Q} = 3.2321(m + n - 7) + 51,$$

$$\widehat{Q} = 3.3014(m + n - 7) + 52,$$

$$\widehat{Q} = 3.4494(m + n - 7) + 53,$$

$$\widehat{Q} = 3.5201(m + n - 7) + 54,$$

$$\widehat{Q} = 3.7076(m + n - 7) + 55,$$

encoding the image with each, in the hope that the one corresponding to the correct value of *diag* will yield a file size closest to the target. If not, the model that does will hopefully correspond to a good approximation to the actual *diag*. The following QT, from the JPEG encodings of Lena, leads to such a case.

33	34	42	36	40	32	55	51
38	35	38	36	36	41	45	59
32	41	42	42	43	42	53	41
38	39	47	48	41	48	71	62
38	49	46	52	55	59	52	57
56	41	58	72	68	72	63	61
44	65	56	54	81	73	61	63
65	53	73	56	86	67	65	75

(a) $B = 5171$ bytes

29	32	35	39	42	45	49	52
32	35	39	42	45	49	52	55
35	39	42	45	49	52	55	58
39	42	45	49	52	55	58	62
42	45	49	52	55	58	62	65
45	49	52	55	58	62	65	68
49	52	55	58	62	65	68	72
52	55	58	62	65	68	72	75

(b) $\widetilde{Q} = 3.2798(m + n) + 28.8698$

Figure 7.6: An example optimised QT, along with its corresponding model to facilitate an example of our prediction strategy

Using its resulting file size of 5171 bytes as the target, $\widehat{k}_0 = 45$ is obtained. Hence, we encode Lena with each of the candidate models above, obtaining the file sizes 5295, 5235, 5188, 5128, and 5091 bytes, respectively. This means that the model

$$\widehat{Q} = 3.4494(m + n - 7) + 53$$

will be chosen, since its corresponding file size of 5188 bytes is closest to the target. While this is not the ideal model with $diag = 52$, it is at least one of its closest neighbours, as we had hoped. Consequently, the predicted initial QT will be

$$\widehat{Q} = \begin{array}{|cccccccc|}\hline 29 & 32 & 36 & 39 & 43 & 46 & 50 & 53 \\ 32 & 36 & 39 & 43 & 46 & 50 & 53 & 56 \\ 36 & 39 & 43 & 46 & 50 & 53 & 56 & 60 \\ 39 & 43 & 46 & 50 & 53 & 56 & 60 & 63 \\ 43 & 46 & 50 & 53 & 56 & 60 & 63 & 67 \\ 46 & 50 & 53 & 56 & 60 & 63 & 67 & 70 \\ 50 & 53 & 56 & 60 & 63 & 67 & 70 & 74 \\ 53 & 56 & 60 & 63 & 67 & 70 & 74 & 77 \\ \hline \end{array} .$$

We use this approach for all values of $\widehat{k}_0$ larger than 18. Instead of using (7.5) and (7.6), the choice of model described above is made by evaluating

$$\widehat{k}_1 = \text{list\_of\_gradients}(diag) \tag{7.7}$$

and

$$\widehat{Q}(m,n) = \widehat{k}_1(m+n-7) + diag, \qquad m = 0,\ldots,7,\ n = 0,\ldots,7, \tag{7.8}$$

for the appropriate candidate values of $diag$. These candidates are listed in Table 7.3 (formed by condensing the data contained in Table 7.1) for each of the relevant values of $\widehat{k}_0$.

$\widehat{k}_0$	*diag*
19	19, 20
20	20, 21
21	21, 22
22	22, 23, 24
23	23, 24, 25
24	24, 25, 26
25	25, 26, 27
26	26, 27, 28
27	28, 29, 30
28	29, 30, 31
29	30, 31, 32, 33
30	32, 33, 34, 35
31	34, 35, 36
32	35, 36, 37
33	36, 37, 38, 39
34	37, 38, 39, 40
35	38, 39, 40, 41, 42
36	40, 41, 42, 43
37	41, 42, 43, 44, 45
38	42, 43, 44, 45, 46
39	44, 45, 46, 47
40	45, 46, 47, 48, 49, 50
41	46, 47, 48, 49, 50
42	47, 48, 49, 50, 51, 52
43	49, 50, 51, 52, 53, 54
44	50, 51, 52, 53, 54, 55
45	51, 52, 53, 54, 55
46	52, 53, 54, 55
47	53, 54, 55

Table 7.3: Candidate values of *diag* for each $\widehat{k}_0$ in the case of JPEG

For values of $\widehat{k}_0$ between 10 and 18, we proceed as initially planned, using (7.5) and (7.6), and ignoring the minor discrepancies between $\widehat{k}_0$ and *diag*. The QT in Figure 7.1(a), for instance, gave a value of $\widehat{k}_0 = 16$, as we saw earlier, and its linear model in Figure 7.2(a) had a value of *diag* also equal to 16. By indexing Table 7.2 with this $\widehat{k}_0$, we obtain $\widehat{k}_1 = 0.2805$ as approximate gradient. In other words, we have as initial QT

$$\widehat{Q} = 0.2805(m + n - 7) + 16,$$

which looks as follows:

$$\widehat{Q} = \begin{array}{|cccccccc|}\hline 14 & 14 & 15 & 15 & 15 & 15 & 16 & 16 \\ 14 & 15 & 15 & 15 & 15 & 16 & 16 & 16 \\ 15 & 15 & 15 & 15 & 16 & 16 & 16 & 17 \\ 15 & 15 & 15 & 16 & 16 & 16 & 17 & 17 \\ 15 & 15 & 16 & 16 & 16 & 17 & 17 & 17 \\ 15 & 16 & 16 & 16 & 17 & 17 & 17 & 17 \\ 16 & 16 & 16 & 17 & 17 & 17 & 17 & 18 \\ 16 & 16 & 17 & 17 & 17 & 17 & 18 & 18 \\ \hline \end{array}.$$

This table compares very favourably with the one from the original model in Figure 7.2(a).

Finally, we also list the tables summarising the findings for the sine window MJPEG encodings of the test images. Firstly, the counterpart to Table 7.1, Table 7.4, shows the relationship between $\widehat{k}_0$ and *diag* for this case. Here our choice to limit our models to values of *diag* between 10 and 55 causes $\widehat{k}_0$ to be limited to the set $\{10, \ldots, 46\}$. This table's condensed version, and counterpart to Table 7.3, is shown in Table 7.5. Lastly, Table 7.6 is the counterpart to Table 7.2 and shows the analysis of the gradients for this case.

$\widehat{k}_0$	**Lena**	**Plane**	**Bridge**
10	10(44), 11(4)	10(50)	10(44)
11	11(43), 12(10)	10(2), 11(50)	10(5), 11(41)
12	12(32), 13(8)	12(44)	11(7), 12(47)
13	13(31), 14(11)	12(2), 13(41)	12(2), 13(44)
14	14(27), 15(16)	14(38)	13(4), 14(42)
15	15(24), 16(8)	14(3), 15(36)	14(3), 15(32)
16	16(22), 17(11)	15(7), 16(31)	15(3), 16(44)
17	17(18), 18(13)	16(4), 17(29)	16(2), 17(30), 18(1)
18	18(18), 19(13)	18(32)	18(29), 19(4)
19	19(6), 20(19)	18(2), 19(32)	19(26), 20(10)
20	20(7), 21(18)	20(33), 21(4)	20(19), 21(7)
21	21(5), 22(17)	21(20), 22(13)	21(26), 22(9)
22	22(3), 23(13), 24(14)	22(3), 23(20)	22(21), 23(13)
23	24(8), 25(9), 26(11)	24(24), 25(1)	23(15), 24(13)
24	26(4), 27(20)	25(18), 26(8)	24(12), 25(14)
25	27(5), 28(19)	26(15), 27(9)	25(7), 26(25)
26	29(20), 30(2)	27(13), 28(15)	26(3), 27(22)
27	30(19)	28(7), 29(15)	28(20), 29(5)
28	30(3), 31(10), 32(10)	29(5), 30(14)	29(18), 30(15)
29	32(3), 33(10)	30(1), 31(10), 32(6)	30(7), 31(19), 32(1)
30	33(11), 34(9)	33(11), 34(12), 35(4)	32(15), 33(4)
31	34(7), 35(8)	35(8), 36(12)	33(10), 34(18)
32	35(12), 36(3)	36(3), 37(13)	34(1), 35(18), 36(2)
33	36(6), 37(9), 38(5)	37(5), 38(5)	36(15)
34	38(12), 39(4)	38(4), 39(8)	36(2), 37(9), 38(6)
35	39(10), 40(8)	39(12), 40(9)	38(1), 39(17), 40(9)
36	40(7), 41(7), 42(6)	40(12), 41(9), 42(1)	40(12), 41(8)

Table 7.4: The relationship between $\widehat{k}_0$ and *diag* for the MJPEG encodings of the three images (*continued on next page*)

$\widehat{k}_0$	**Lena**	**Plane**	**Bridge**
37	42(5), 43(6), 44(9)	42(11), 43(2)	41(6), 42(10), 43(6)
38	44(5), 45(6), 46(6)	43(8), 44(6)	43(2), 44(15), 45(3)
39	46(2), 47(7), 48(6)	44(4), 45(11), 46(6)	45(18)
40	49(11)	46(1), 47(9), 48(3)	46(10), 47(12)
41	49(4), 50(6)	48(12)	47(5), 48(9)
42	50(6), 51(5)	48(3), 49(12), 50(1)	48(7), 49(13)
43	51(5), 52(5)	50(16)	49(7), 50(8)
44	52(8)	51(8)	50(2), 51(5), 52(12)
45	52(2), 53(7)	52(10), 53(7)	52(2), 53(14)
46	53(3), 54(1), 55(4)	53(7), 54(2), 55(6)	54(7), 55(4)

Table 7.4: The relationship between $\widehat{k}_0$ and *diag* for the MJPEG encodings of the three images (*continued*)

$\widehat{k}_0$	*diag*
17	17, 18
18	18, 19
19	19, 20
20	20, 21
21	21, 22
22	22, 23, 24
23	23, 24, 25, 26
24	24, 25, 26, 27
25	25, 26, 27, 28
26	26, 27, 28, 29, 30
27	28, 29, 30
28	29, 30, 31, 32
29	30, 31, 32, 33
30	32, 33, 34, 35
31	33, 34, 35, 36
32	34, 35, 36, 37
33	36, 37, 38
34	36, 37, 38, 39
35	38, 39, 40
36	40, 41, 42
37	41, 42, 43, 44
38	43, 44, 45, 46
39	44, 45, 46, 47, 48
40	46, 47, 48, 49
41	47, 48, 49, 50
42	48, 49, 50, 51
43	49, 50, 51, 52
44	50, 51, 52
45	52, 53
46	53, 54, 55

Table 7.5: Candidate values of *diag* for each $\widehat{k}_0$ in the case of MJPEG

diag	**Range**	**Approximate gradient $\widehat{k}_1$**
10	[0.2485, 0.3452]	0.2969
11	[0.3274, 0.4107]	0.3690
12	[0.3943, 0.4866]	0.4405
13	[0.3899, 0.4747]	0.4323
14	[0.4420, 0.4896]	0.4658
15	[0.4658, 0.5253]	0.4955
16	[0.5179, 0.6503]	0.5841
17	[0.5670, 0.6994]	0.6332
18	[0.6696, 0.7738]	0.7217
19	[0.7470, 0.8244]	0.7857
20	[0.8378, 0.9628]	0.9003
21	[0.8839, 1.0342]	0.9590
22	[0.9747, 1.0952]	1.0350
23	[1.0759, 1.4702]	1.2731
24	[1.4003, 1.5342]	1.4672
25	[1.6414, 1.9271]	1.7843
26	[1.9271, 2.2009]	2.0640
27	[2.2054, 2.2440]	2.2247
28	[2.2753, 2.4271]	2.3512
29	[2.2946, 2.4435]	2.3690
30	[2.2426, 2.3795]	2.3110
31	[2.3482, 2.4836]	2.4159
32	[2.4836, 2.6533]	2.5685
33	[2.5476, 2.6131]	2.5804
34	[2.5521, 2.7188]	2.6354
35	[2.5223, 2.7068]	2.6145
36	[2.5491, 2.6086]	2.5789

Table 7.6: The relationship between *diag* and $\widehat{k}_1$ obtained from the MJPEG encodings of Lena (*continued on next page*)

diag	**Range**	**Approximate gradient $\widehat{k}_1$**
37	[2.8839, 2.9286]	2.9063
38	[2.9494, 3.0714]	3.0104
39	[3.0193, 3.2411]	3.1302
40	[3.1310, 3.1726]	3.1518
41	[3.1607, 3.3199]	3.2403
42	[3.4107, 3.5193]	3.4650
43	[3.4732, 3.7827]	3.6280
44	[3.7440, 3.8363]	3.7902
45	[3.8750, 4.0342]	3.9546
46	[3.9360, 4.0342]	3.9851
47	[3.8929, 4.0595]	3.9762
48	[4.2738, 4.4449]	4.3593
49	[4.1845, 4.4301]	4.3073
50	[4.1131, 4.2292]	4.1711
51	[4.0208, 4.2143]	4.1175
52	[3.8185, 4.0208]	3.9196
53	[3.7054, 3.8080]	3.7567
54	[3.7827, 3.7827]	3.7827
55	[4.2515, 4.4063]	4.3289

Table 7.6: The relationship between *diag* and $\widehat{k}_1$ obtained from the MJPEG encodings of Lena (*continued*)

7.3 C++ Implementation Revisited

Our proposed strategy for predicting initial QTs was incorporated into our C++ implementations to be used by Algorithm 6.3. Picking up where Section 6.5 left off, our

description is with respect to the program `qt_m.cc`.

First of all, the value $\widehat{k}_0$, represented by the variable $kk0$, is obtained by evaluating the file sizes resulting from using tables $[[1]], [[2]], \ldots, [[255]]$. This search is implemented by using a golden ratio search, and is performed by the function `gr`. Given that values of $\widehat{k}_0$ are here limited to the set $\{10, \ldots, 46\}$ (as described in the previous section), the program will exit if $kk0$ is outside this set.

Next, if $kk0$ is between 10 and 16, it is directly used to index the list of gradients shown in Table 7.6. This list is stored in the array **gradient**, and the obtained approximate gradient $\widehat{k}_1$ is represented by the variable $kk1$.

If, on the other hand, $kk0$ is larger than 17, the function `get_gradient` is called. This function evaluates candidate models for relevant values of *diag* and $\widehat{k}_1$, using the approach described by (7.7) and (7.8). The candidate values of *diag* listed in Table 7.5 are implicitly stored in the matrix $k2diag$ by storing the first value of *diag* corresponding to each $\widehat{k}_0$ in the matrix's first row, and the number of candidate values for each $\widehat{k}_0$ in the second row. Furthermore, to construct each candidate model, the function `plane_Q` is used. The *diag* and gradient values eventually decided upon are then stored in $kk0$ and $kk1$, respectively.

Lastly, having obtained $kk0$ and $kk1$ by either of these two methods, the initial QT is calculated from them by calling function `plane_Q`.

Notice that, apart from the candidate values of *diag* listed in Table 7.5, we have also included additional candidates to consider in $k2diag$. This ensures that the number of modifications required to make the initial QT feasible is small. For example, a value of $\widehat{k}_0 = 45$ will be obtained when inputting the Bridge image's frequency components (obtained by using the sine window) to `qt_m`, along with a target file size of 9000 bytes. Given the choices of *diag* in Table 7.5 (52 and 53), the values $diag = 52$ and $\widehat{k}_1 = 3.9196$ will be chosen, resulting in the initial QT

$$\widehat{Q} = \begin{array}{|cccccccc|}\hline 25 & 28 & 32 & 36 & 40 & 44 & 48 & 52 \\ 28 & 32 & 36 & 40 & 44 & 48 & 52 & 56 \\ 32 & 36 & 40 & 44 & 48 & 52 & 56 & 60 \\ 36 & 40 & 44 & 48 & 52 & 56 & 60 & 64 \\ 40 & 44 & 48 & 52 & 56 & 60 & 64 & 68 \\ 44 & 48 & 52 & 56 & 60 & 64 & 68 & 72 \\ 48 & 52 & 56 & 60 & 64 & 68 & 72 & 76 \\ 52 & 56 & 60 & 64 & 68 & 72 & 76 & 79 \\ \hline \end{array}.$$

This table yields an encoding with file size $B = 8552$ bytes and would require many modifications to become feasible. In order to not destroy the characteristics of the model, one might subtract a value of 1 from each entry of $\widehat{Q}$ until a file size close enough to 9000 bytes is reached. But then we could just as well have tested the model corresponding to a slightly lower value of $diag$ instead. The value $diag = 50$, with corresponding gradient $\widehat{k}_1 = 4.1711$, for instance, yields the initial QT

$$\widehat{Q} = \begin{array}{|cccccccc|}\hline 21 & 25 & 29 & 33 & 37 & 42 & 46 & 50 \\ 25 & 29 & 33 & 37 & 42 & 46 & 50 & 54 \\ 29 & 33 & 37 & 42 & 46 & 50 & 54 & 58 \\ 33 & 37 & 42 & 46 & 50 & 54 & 58 & 63 \\ 37 & 42 & 46 & 50 & 54 & 58 & 63 & 67 \\ 42 & 46 & 50 & 54 & 58 & 63 & 67 & 71 \\ 46 & 50 & 54 & 58 & 63 & 67 & 71 & 75 \\ 50 & 54 & 58 & 63 & 67 & 71 & 75 & 79 \\ \hline \end{array},$$

which results in a much closer coding file size of $B = 9004$ bytes. For this reason a few extra candidate values of $diag$ are included in $k2diag$ for each $\widehat{k}_0$.

Of course, these initial QTs do not actually need to be feasible when directly starting Algorithm 6.3 with one of them (as opposed to first running a genetic algorithm), but we nevertheless enforce it for two reasons. Firstly, since an initial QT must be feasible when constructing an initial population for a GA, it makes sense to use the same feasible initial QT when directly starting Algorithm 6.3, so as to properly compare the running times of

each approach. Secondly, enforcing feasibility allows us to compare the PSNR obtained using a feasible initial QT with the PSNR obtained using an optimised QT. This gives us an additional useful measure of how "close" an initial QT is to an optimal one, and we utilise it in the next section when testing our models.

7.4 Testing the Models

To investigate how well our models reduce the work needed to be done by Algorithm 6.3, we tested their MJPEG implementation on the three images Lena, Plane and Bridge. In particular, these tests were performed for the case of using the sine window. By varying the target file size, we started Algorithm 6.3 with each obtainable initial QT, running it for various probing widths in each case. By doing so, we found the smallest values of lo and hi required to reach the appropriate optimised QTs for each value of $diag$.

Consider, for example, the data shown in Table 7.7, which is an excerpt from Table C.2 in Appendix C. Here we have the results corresponding to $diag = 23$ for the Plane image.

diag **T (bytes)**	**Widths** **B (bytes)** **PSNR**	**Widths** **B (bytes)** **PSNR**	**Widths** **B (bytes)** **PSNR**	**$lo = 1$, $hi = 1$** **B (bytes)** **PSNR**	**Initial QT** **B (bytes)** **PSNR**
23	$lo = 4$, $hi = 10$	$lo = 3$, $hi = 10$	$lo = 4$, $hi = 5$		
10346	10343	10346	10346	10347	10350
	34.9386 dB	34.9291 dB	34.9325 dB	34.8856 dB	34.7462 dB

Table 7.7: Excerpt from Table C.2, illustrating a sensitivity analysis for the Plane image when $diag = 23$

In the first column we list the target file size T used to generate the results, in this case 10346 bytes. For each case we generated a QT using large but equal probing widths (such as $lo = hi = 50$) and then decreased them in steps of 5, each time repeating the experiment. We thereby determined the smallest (multiple of 5) uniform probing width

that still results in the same QT. Once this value was found, we assigned it to hi and, in the same fashion, then attempted to decrease lo even further. In both cases, once a value of 5 was reached, further decrements were made in steps of 1. As the second column of Table 7.7 shows, these smallest values were found to be $lo = 4$ and $hi = 10$, for $diag = 23$. In other words, as long as $lo \geq 4$ and $hi \geq 10$, Algorithm 6.3 will generate a QT yielding an encoding with file size $B = 10343$ bytes and PSNR equal to 34.9386 dB.

Moreover, the third and fourth columns also list the decreases (if any) in quality resulting from using the next-best values of lo and hi, respectively — thereby giving us a sensitivity analysis. From these columns in Table 7.7 we see that the decreases are quite small. This is in general the case, for all three images and all values of $diag$, as chronicled in Tables C.1 to C.3 in Appendix C.

In Figure 7.7 we show a graphical summary of the minimised probing widths as functions of $diag$. Figure 7.7(a) shows the results found for lo for each image, while Figure 7.7(b) shows the results for hi. For low- to almost mid-range values of $diag$ our models do a good job of minimising the probing widths, with values of lo staying below 10 up until $diag = 40$, and values of hi typically not exceeding 20 until $diag = 30$. The only exceptions are at $diag = 24$ and $diag = 25$ for Lena. For higher values of $diag$, lo peaks at 14; on the other hand, values of hi vary significantly for mid- to upper-range values of $diag$, though never exceeding 35.

The results shown in Figure 7.7 provide a rule of thumb for choosing probing widths as functions of $diag$. Upon obtaining a value of $diag$ between 10 and 15, for instance, an implementation might use $lo = 3$ and $hi = 4$. On the other hand, for values of $diag$ between, say, 35 and 55, a conservative estimate of $lo = 15$ and $hi = 35$ might be used.

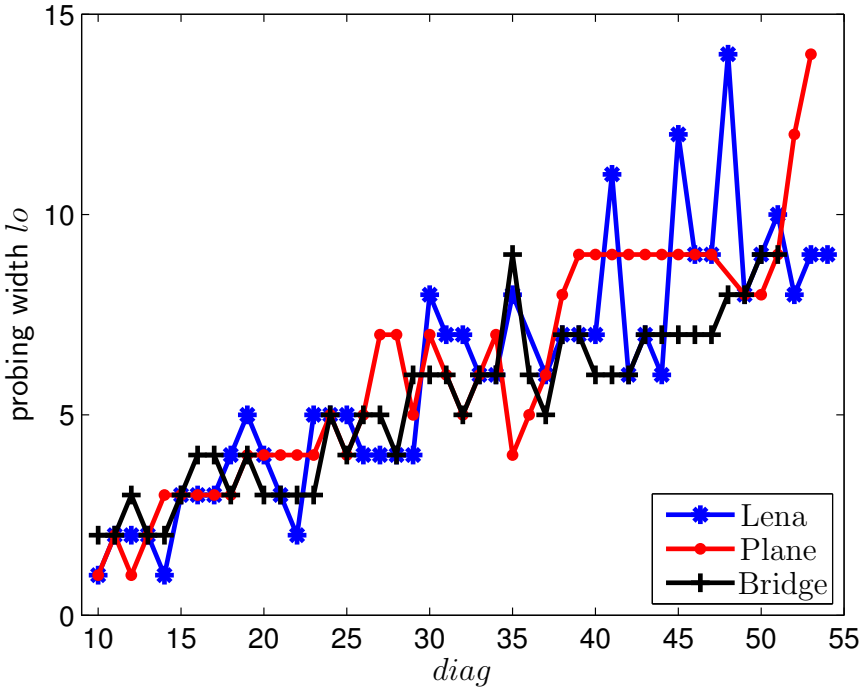

(a) Behaviour of probing width lo

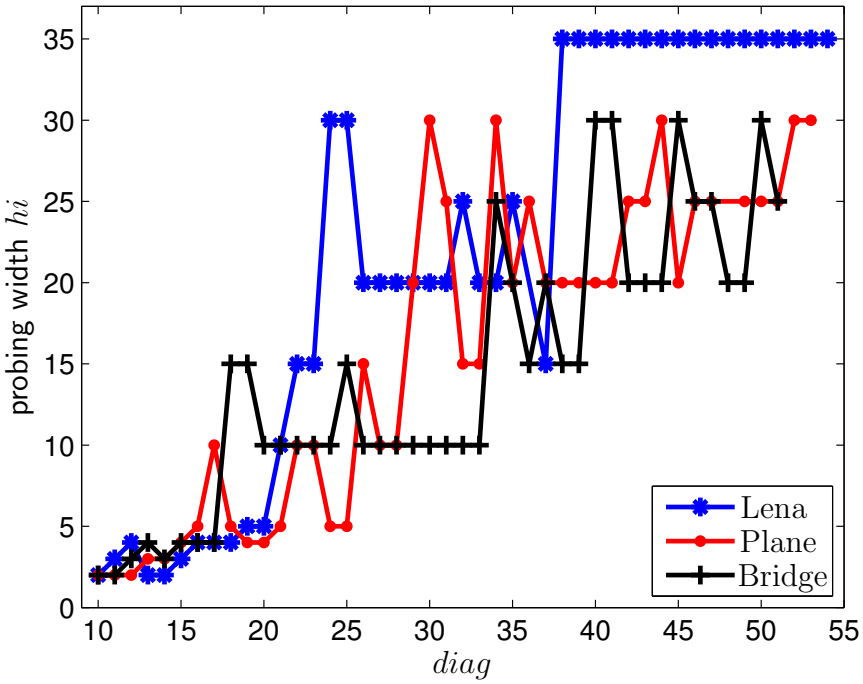

(b) Behaviour of probing width hi

Figure 7.7: Minimised probing widths as functions of $diag$

It is also interesting to investigate the results obtained by letting Algorithm 6.3 do the least amount of work per iteration, *i.e.* choosing $lo = hi = 1$. Such a result can be seen in the fifth column of Table 7.7. We observe that this "short-cut" approach increases the PSNR from 34.7462 dB (obtained with the feasible initial QT) to 34.8856 dB, more than half the total increase from 34.7462 dB to the optimal 34.9386 dB. The magnitudes of increases in PSNR made this way do of course taper off slightly as the required optimal probing widths increase, but never to the point of insignificance. Once again, these results are fully documented in Tables C.1 to C.3.

The progression of PSNR values for various probing widths and fixed values of *diag* can also be plotted from the rows of the tables in Appendix C, providing us with a graphical depiction of our sensitivity analysis. Such curves are shown in Figure 7.8 for selected values of *diag* in the case of Lena. Data points are calculated by using the best PSNR corresponding to each value of *hi* and subtracting the PSNR corresponding to the initial QT from each. For $diag = 12$, for instance, shown in Figure 7.8(a), we obtain the first data point by subtracting 39.2889 dB from 39.4128 dB, giving us the increase in PSNR resulting from using $lo = hi = 1$, or equivalently, a uniform probing width of $w = 1$. The second data point represents the increase in PSNR obtained by using $lo = 2$ and $hi = 3$, or $w = 3$, etc. From these curves in Figure 7.8 we see that small increases in PSNR are generally made from one probing width to the next. Conversely, this means that the PSNR degrades gracefully as probing widths are reduced beyond their minimal values.

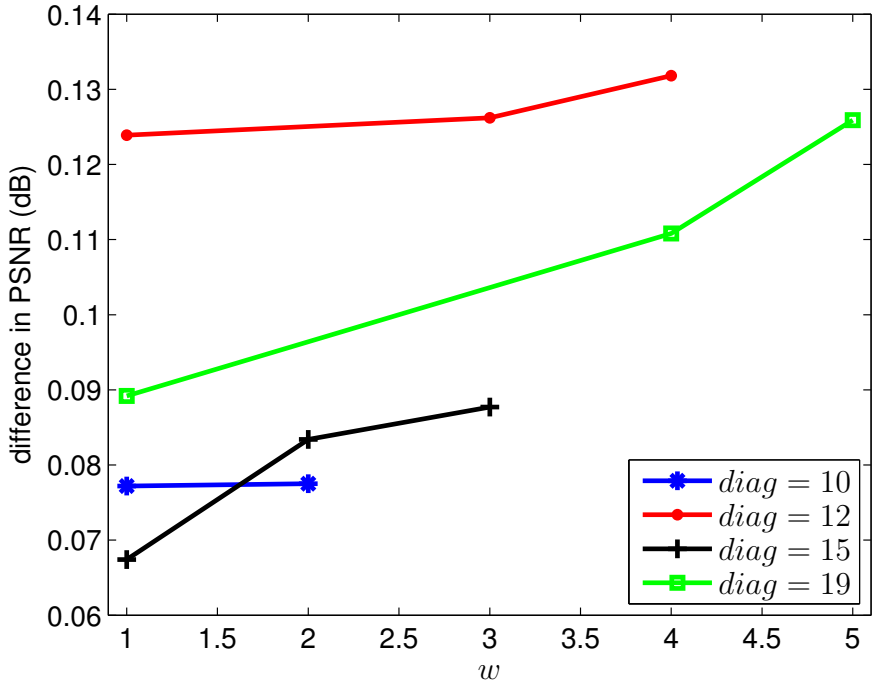

(a) Results for lower-range values of *diag*

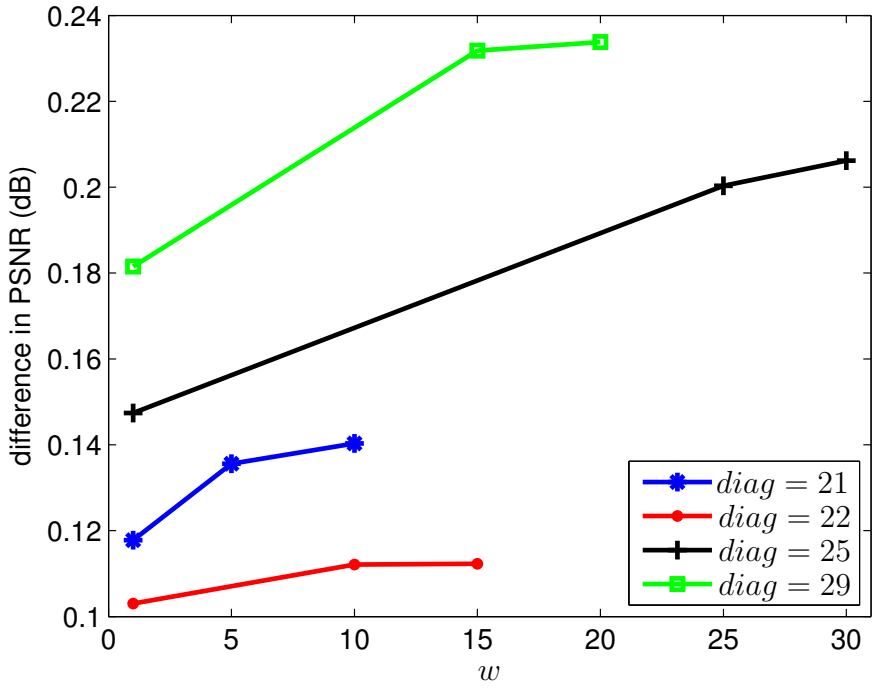

(b) Results for mid-range values of *diag*

Figure 7.8: Sensitivities of PSNR to various probing widths for the Lena image (*continued on next page*)

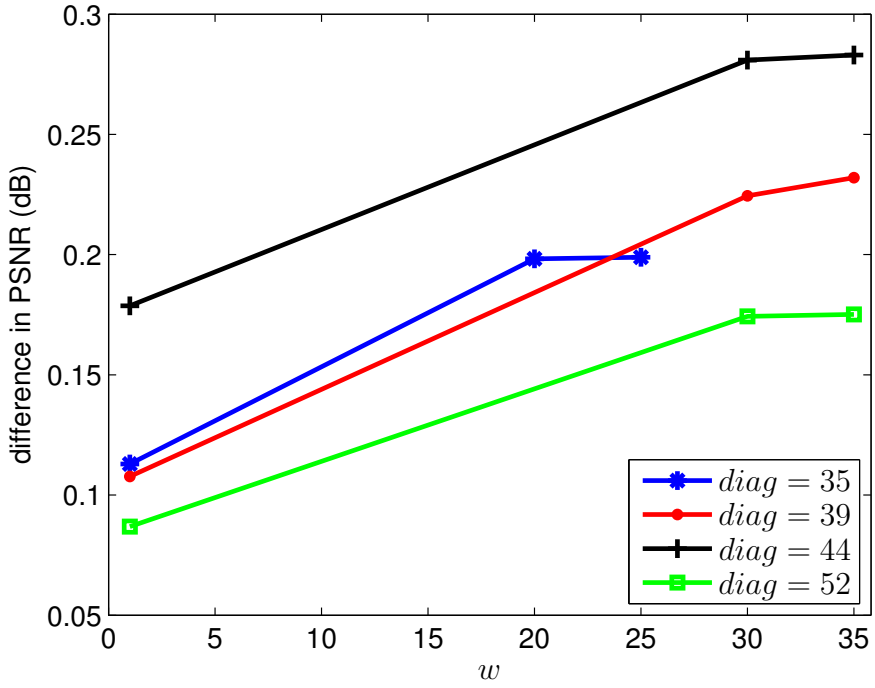

(c) Results for upper-range values of *diag*

Figure 7.8: Sensitivities of PSNR to various probing widths for the Lena image (*continued*)

Apart from aiding in our sensitivity analysis, the results yielded by the initial QTs shown in the last column of Tables C.1 to C.3 also serve another purpose. By comparing them with the results yielded by optimal QTs (shown in the second column), we can gauge how "close" our initial QTs are to the optimal ones. Figure 7.9 below shows the results of this analysis, where the differences in obtained PSNR are plotted as a function of *diag* for each of the three images. Notice that these differences are generally quite small and only exceed 0.3 dB in the three instances $diag = 26$, $diag = 27$ and $diag = 29$, for the Plane image.

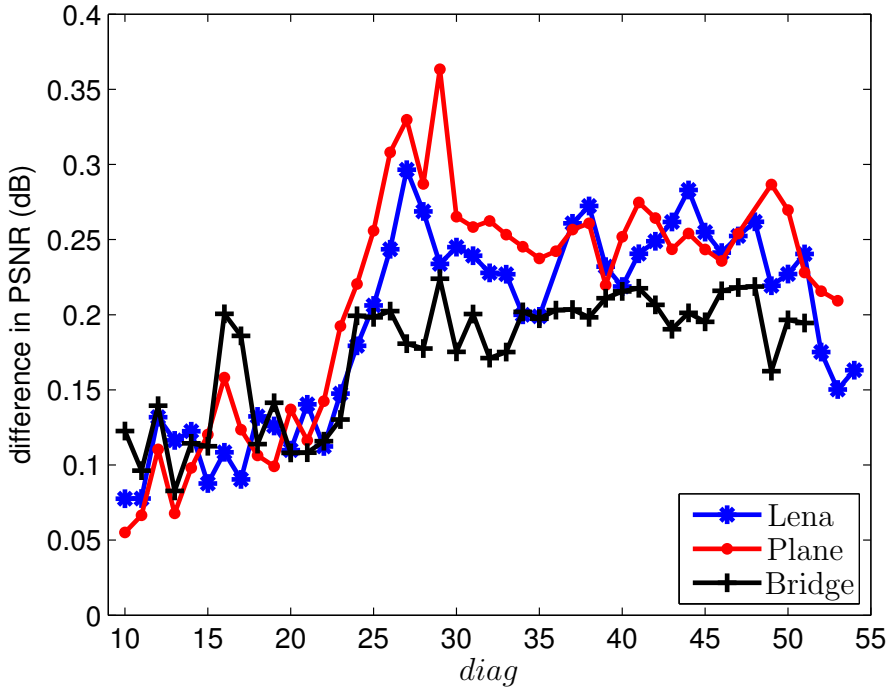

Figure 7.9: Differences between PSNR obtained with optimised and initial QTs

So far we have not listed any of the minimised running times required to obtain the results listed in the second column of Tables C.1 to C.3, corresponding to optimal probing widths. Since we are also interested in the effects a genetic algorithm might have on running times, we now list some side-by-side comparisons.

Tables 7.8 to 7.10 show the running times required to generate 5 selected results for each image compared with those required when first running a GA before Algorithm 6.3. Once again, an Intel Core 2 Vpro at 3 GHz was used throughout. In each case the GA was run for 200 generations, using a population of size 100, and its contribution to the running time was taken into account. Furthermore, the relevant value of lo was used when generating an initial population, and also to limit the extent of genetic mutations.

	Algorithm 6.3			GA + Algorithm 6.3		
T (bytes)	Duration	B (bytes)	PSNR	Duration	B (bytes)	PSNR
4979	15min	4981	31.5955 dB	14min	4981	31.6037 dB
5658	16min30s	5657	32.4900 dB	15min	5657	32.4875 dB
6150	19min30s	6151	33.0743 dB	19min30s	6151	33.0698 dB
6508	19min30s	6508	33.4900 dB	21min30s	6509	33.4930 dB
7248	13min	7248	34.3136 dB	13min	7250	34.3179 dB

Table 7.8: Running times: Lena

	Algorithm 6.3			GA + Algorithm 6.3		
T (bytes)	Duration	B (bytes)	PSNR	Duration	B (bytes)	PSNR
5847	19min	5846	30.5416 dB	22min	5845	30.5473 dB
6421	17min	6420	31.1682 dB	16min	6421	31.1694 dB
6918	15min30s	6919	31.7029 dB	19min30s	6918	31.7008 dB
7565	13min	7567	32.3397 dB	16min	7565	32.3365 dB
8319	9min30s	8320	33.0640 dB	11min	8320	33.0577 dB

Table 7.9: Running times: Plane

	Algorithm 6.3			GA + Algorithm 6.3		
T (bytes)	Duration	B (bytes)	PSNR	Duration	B (bytes)	PSNR
8672	22min	8672	28.4536 dB	18min30s	8669	28.4483 dB
9740	18min	9741	29.1037 dB	21min	9742	29.1128 dB
10506	22min30s	10508	29.5610 dB	23min30s	10507	29.5558 dB
11632	13min30s	11634	30.2028 dB	14min30s	11634	30.2030 dB
13252	8min	13250	31.1517 dB	9min	13250	31.1693 dB

Table 7.10: Running times: Bridge

From the first row of Table 7.8, for example, we see that the result listed in Table C.1 for $diag = 54$, using $lo = 9$ and $hi = 35$, required roughly 15min to be obtained. By comparison, roughly 14min were required to obtain an optimised QT when using a GA prior to Algorithm 6.3, while still using the same probing widths. Since the two approaches yield two different optimised QTs, the resulting file size and PSNR for each approach are also listed.

In most cases, unfortunately, the reduction made to the running time of Algorithm 6.3 is outweighed by the running time of the GA, meaning that their combined running time is longer than that of Algorithm 6.3 by itself. Reducing the number of generations would reduce the running time of the GA, but could also diminish the quality of the final population's fittest member. Conversely, increasing the number of generations could further reduce the running time of Algorithm 6.3, but would also increase the running time of the GA. The same is true of a reduction/increase in population size.

Further research would be required to determine the population size and number of generations that would optimise these trade-offs, and thus the total running time. As such, the results in the second column of Tables 7.8 to 7.10 are preliminary, although they do show promise. We discuss this further in Section 8.4, when outlining future research.

Chapter 8

Experimental Results

Now that we have a means to generate good initial tables for Algorithm 6.3, we proceed to investigate the merits of MJPEG relative to JPEG when using optimised QTs. There are many window functions to choose from when using the MDCT — the existence of one yielding results superior to those yielded by all others would be extremely advantageous. Without it, the user would need to select one by trial-and-error each time an image is to be compressed. For this reason, we also investigate the effects of several window functions on the coding results. Notice that, in order to satisfy the perfect reconstruction requirement (3.11), all windows (except for the sine window) are subjected to the normalisation procedure shown in (3.12).

8.1 Window Functions

In addition to the window functions described in Section 3.2, several others exist that are included in Matlab's signal processing toolbox. Of these, some are unfortunately defined to have the value of zero as their first and last entries — an undesirable attribute in the context of our application, since the first and last samples of transform blocks will play no role in the MDCT. Consequently, those windows will not yield competitive results, and have been excluded here. The seven remaining window functions are the Gaussian, Chebyshev, Triangular, Parzen, Nuttall, Hamming and Blackman-Harris windows; their

definitions can be found in their respective built-in Matlab implementations.

Table 8.1 shows a typical set of results obtained when comparing MJPEG using the above window functions to JPEG. These results were generated for the 256×256 Bridge image, using a target file size of $T = 22739$ bytes. Like the Kaiser-Bessel Derived (KBD) window, the Gaussian and Chebyshev windows have a parameter determining their shape. In the definitions provided in the Matlab documentation, the Gaussian window's parameter is denoted by a, while that of the Chebyshev window is denoted by r. The optimal value of each parameter must be found heuristically, involving the repeated use of Algorithm 6.3. For the particular case shown here, they were found to be roughly $\alpha = 1.625$, $a = 2.9375$ and $r = 75$.

Technique	$\boldsymbol{B}$ **(bytes)**	**PSNR**
Optimised JPEG	22741	37.3789 dB
Sine	22746	37.4207 dB
Hanning	22739	37.4255 dB
KBD ($\alpha = 1.625$)	22741	37.4236 dB
Gaussian ($a = 2.9375$)	22738	37.3813 dB
Chebyshev ($r = 75$)	22739	37.4017 dB
Triangular	22739	37.1221 dB
Parzen	22740	37.2919 dB
Nuttall	22738	37.1943 dB
Hamming	22737	37.2946 dB
Blackman-Harris	22745	37.1886 dB

Table 8.1: Example comparison of coding results yielded by several window functions with that of JPEG

What is typical about these results is the fact that the seven additional window functions yield results inferior to those yielded by the three window functions described in Section 3.2. Therefore, the comparison of results in the next section does not include these seven window functions.

As will be seen in the next section, the sine window often outperforms the Hanning and KBD windows, but unfortunately, as Table 8.1 shows, not always. A question that arises is whether or not an optimal window function can be designed. Moreover, even if the sine window consistently outperformed the others, we would still want to know whether or not an even better one could be designed. This is once again an optimisation problem, only this time not a discrete one, as described below.

We ideally seek a window function $\mathbf{w} = [w_1, \ldots, w_{16}]$ that maximises the PSNR of all MJPEG encodings, but to practically solve the problem we can only optimise $\mathbf{w}$ for one encoding at a time. Since MJPEG uses symmetric windows, we can write $\mathbf{w}$ as

$$\mathbf{w} = [w_1, \ldots, w_8, w_8, \ldots, w_1], \tag{8.1}$$

thereby halving the number of independent variables. Furthermore, due to the perfect reconstruction requirement (3.11), entries w_5 to w_8 must satisfy

$$\begin{aligned} w_5 &= \sqrt{1 - w_4^2} \\ w_6 &= \sqrt{1 - w_3^2} \\ w_7 &= \sqrt{1 - w_2^2} \\ w_8 &= \sqrt{1 - w_1^2}\,. \end{aligned} \tag{8.2}$$

Therefore, only the variables w_1 to w_4 are independent. Let them be denoted by

$$\mathbf{x} = [w_1, w_2, w_3, w_4]. \tag{8.3}$$

We also require the sequence $w_1, \ldots, w_8$ to be monotonically increasing — from (8.2) we conclude that the values of w_1 to w_4 should not exceed $\frac{1}{\sqrt{2}}$.

As a result, the optimisation problem reads as follows:

> Given a window function specified by $\mathbf{x}$ in (8.3), an image's frequency components obtained by using $\mathbf{x}$, and a target file size, maximise the PSNR $= \mathrm{PSNR}(\mathbf{x})$ of the encoding obtained with Algorithm 6.3, subject to
>
> $$w_1 \leq w_2 \leq w_3 \leq w_4$$
> $$w_1, \ldots, w_4 \ \in \ [0,\ \tfrac{1}{\sqrt{2}}].$$

With w_1 to w_4 varying continuously and the PSNR not being differentiable (due to the rounding involved in quantisation), we attempt to solve this problem using the Nelder-Mead algorithm. Since the PSNR is also discontinuous as a result of rounding, this algorithm will eventually break down. Nevertheless, any improvement over results yielded by the other window functions will do.

The Nelder-Mead algorithm, described in [28], maintains a list of approximate solutions $\mathbf{x}_1, \ldots, \mathbf{x}_{N+1}$, where N is the number of independent variables in the optimisation problem. These vectors are sorted according to their associated function values, from best to worst. In our case this sorting will be

$$\mathrm{PSNR}(\mathbf{x}_1) \geq \mathrm{PSNR}(\mathbf{x}_2) \geq \mathrm{PSNR}(\mathbf{x}_3) \geq \mathrm{PSNR}(\mathbf{x}_4) \geq \mathrm{PSNR}(\mathbf{x}_5). \tag{8.4}$$

During each iteration the algorithm will attempt to replace the worst vector $\mathbf{x}_{N+1}$ with a better one according to formulas and conditions described in [28]. If successful, the new list of vectors is again sorted, and we proceed to the next iteration. Otherwise, the convergence breaks down and the algorithm terminates.

For our problem, we used the 256×256 Lena image and a target file size of $T = 14839$ bytes. The initial vectors $\mathbf{x}_1$ to $\mathbf{x}_5$ were chosen on the boundary of the feasible region as

$$\begin{aligned}
\mathbf{x}_1 &= [0, 0, \tfrac{1}{\sqrt{2}}, \tfrac{1}{\sqrt{2}}] \\
\mathbf{x}_2 &= [0, 0, 0, \tfrac{1}{\sqrt{2}}] \\
\mathbf{x}_3 &= [0, \tfrac{1}{\sqrt{2}}, \tfrac{1}{\sqrt{2}}, \tfrac{1}{\sqrt{2}}] \\
\mathbf{x}_4 &= [\tfrac{1}{\sqrt{2}}, \tfrac{1}{\sqrt{2}}, \tfrac{1}{\sqrt{2}}, \tfrac{1}{\sqrt{2}}] \\
\mathbf{x}_5 &= [0, 0, 0, 0].
\end{aligned}$$

Here we have numbered the vectors to satisfy (8.4); their respective function values are

$$\begin{aligned}
\mathrm{PSNR}(\mathbf{x}_1) &= 34.6499\mathrm{dB} \\
\mathrm{PSNR}(\mathbf{x}_2) &= 34.1350\mathrm{dB} \\
\mathrm{PSNR}(\mathbf{x}_3) &= 33.5805\mathrm{dB} \\
\mathrm{PSNR}(\mathbf{x}_4) &= 31.9478\mathrm{dB}
\end{aligned}$$

$$\text{PSNR}(\mathbf{x}_5) \;=\; 31.4014\text{dB}.$$

After several iterations the algorithm eventually broke down. The best vector in the final list was

$$\mathbf{x}_1 = [0.09499651018430,\ 0.27268735998118,\ 0.45773112675032,\ 0.63149105950318]$$

with $\text{PSNR}(\mathbf{x}_1) = 40.2651$ dB. Let us refer to the window function constructed from $\mathbf{x}_1$, using (8.1) and (8.2), as the Nelder-Mead1 window.

This window does indeed yield improved results over the sine window for this image and target file size: While the sine window yields an encoding with a file size of 14840 bytes and a PSNR of 40.2454 dB, the Nelder-Mead1 window yields an encoding with a file size of 14841 bytes and a PSNR of 40.2651 dB. Moreover, this window consistently outperforms the sine window for the Lena image, as will be seen in the next section. However, the Nelder-Mead1 window performs worse than the sine window for the 256×256 Plane and 512×512 Peppers (also shown in Appendix A) images, as will also be seen. This means that the Nelder-Mead1 window is not the best for all images, and that such a best window does not exist.

To see what an optimised window function for the Plane image (for a particular file size) would be, we repeated the Nelder-Mead algorithm for this image. The target file size used was $T = 15904$ bytes, and the initial vectors $\mathbf{x}_1$ to $\mathbf{x}_5$ were chosen to be the same as in the previous experiment. This time the best vector in the final list was

$$\mathbf{x}_1 = [0.09917235114230,\ 0.28849462155593,\ 0.47112393494117,\ 0.63470224125757]$$

with $\text{PSNR}(\mathbf{x}_1) = 39.2748$ dB. We refer to the window function constructed from this $\mathbf{x}_1$ as the Nelder-Mead2 window. Once again, it improves upon the sine window for the image and target file size in question. The sine window yields an encoding with a file size of 15901 bytes and a PSNR of 39.2636 dB, while the Nelder-Mead2 window yields an encoding with a file size of 15905 bytes and a PSNR of 39.2748 dB.

In the next section we provide a detailed comparison of results obtained using the sine, Hanning and KBD windows, as well as the Nelder-Mead1 and Nelder-Mead2 windows.

8.2 Compression Results

Using the five window functions chosen in the previous section, four test images were encoded at various file sizes to compare the performance of MJPEG to JPEG. These images were Lena, Plane, Bridge and Peppers, shown in Appendix A, and all results were generated using Algorithm 6.3.

In Figure 8.1 the differences between the obtained PSNR of each instance of MJPEG and that of JPEG are plotted versus compression ratio for each image. Compression ratios are calculated by dividing obtained file sizes by canonical file sizes, such as $256 \times 256 = 65536$ bytes for a 256×256 image. From Figures 8.1(a), (b) and (d) one can see that the sine window outperforms the Hanning and KBD windows for the Lena, Plane and Peppers images.

In many instances the optimal parameter for the KBD window was found to be roughly $\alpha = 1.625$. In the remaining instances the best value was typically $\alpha = 1.5$, while $\alpha = 1.625$ was then the second best. For this reason, the curves for the KBD window are all plotted for $\alpha = 1.625$. Only in the case of the Bridge image (see Figure 8.1(c)) does the KBD window perform competitively. Also, not only does the sine window not perform the best here, it actually performs the worst of the three windows, since the Hanning window also outperforms it. A drawback of the KBD window, however, is the fact that the optimal value of its parameter α does not remain constant. For its second (and worst) data point in Figure 8.1(c), $\alpha = 1.625$ is actually not optimal. A value of $\alpha = 1.5$ yields the best PSNR increase for this compression ratio, namely 0.053 dB. Had this increase been yielded by $\alpha = 1.625$, the KBD window would have uniformly outperformed the sine and Hanning windows for this image.

The performance of the Nelder-Mead1 and Nelder-Mead2 windows is also quite interesting. As mentioned in the previous section, the Nelder-Mead1 window consistently performs the best for the Lena image, as can be seen in Figure 8.1(a). As also stated, it unfortunately fails to outperform the sine window for the Plane and Peppers images. This can be seen in Figures 8.1(b) and (d). The Nelder-Mead2 window, on the other hand, manages to

equal or slightly better the performance of the sine window on most occasions for these two images. Furthermore, it compares quite well with the Nelder-Mead1 window in the case of the Lena image, even overtaking it for higher compression ratios. Only in the case of the Bridge image is the Nelder-Mead1 window the best choice. Here it is only beaten by the KBD window at the third data point.

Another aspect of note is the fact that optimised MJPEG does not always outperform optimised JPEG. This can first of all be seen in Figure 8.1(d) for the Peppers image, where only the results obtained with the sine and Nelder-Mead2 windows are superior to JPEG. These improvements are also quite small initially. Even worse, from Figure 8.1(b) we see that the best MJPEG results for the Plane image take a long time to catch up to JPEG. In Figures 8.2 and 8.3 one can see these results only catching up for high compression ratios.

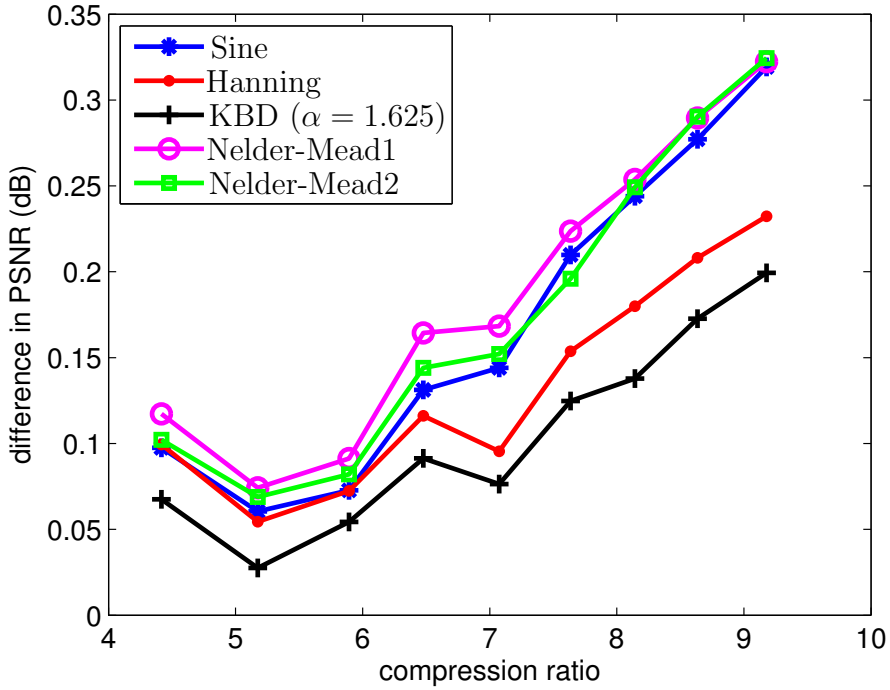

(a) Window performance: Lena

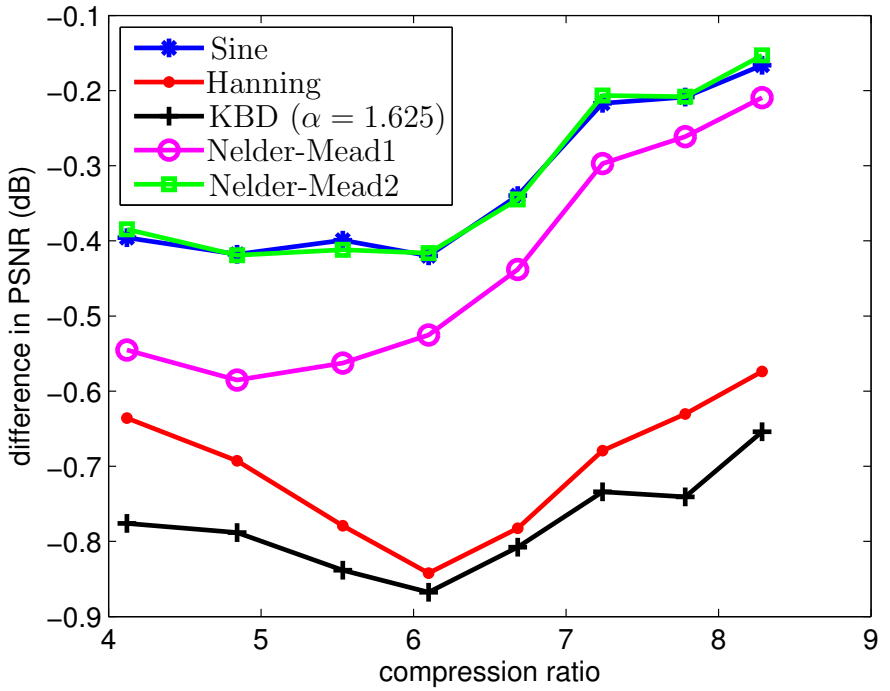

(b) Window performance: Plane

Figure 8.1: Comparison of window function performance for each test image (*continued on next page*)

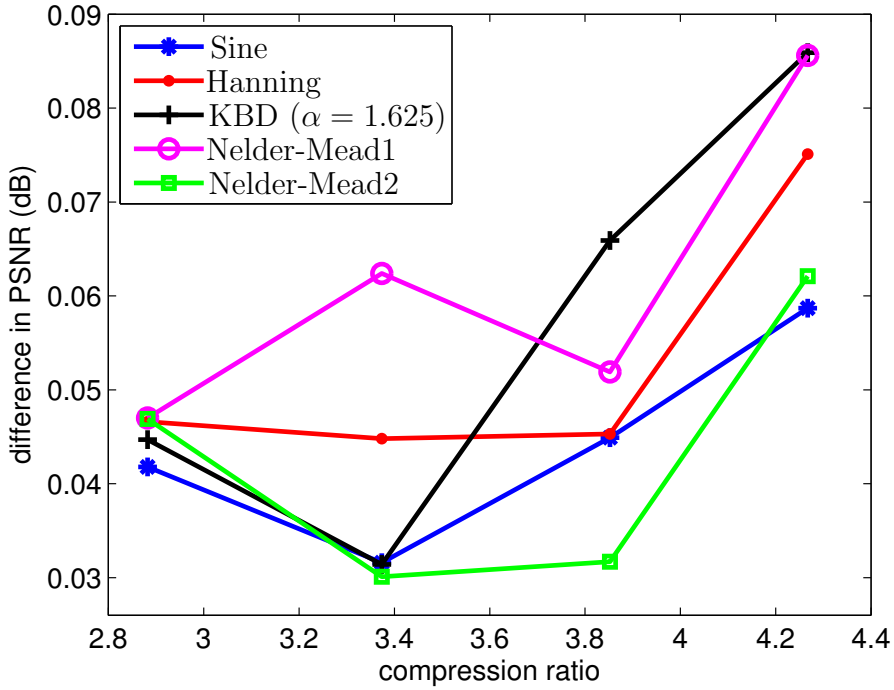

(c) Window performance: Bridge

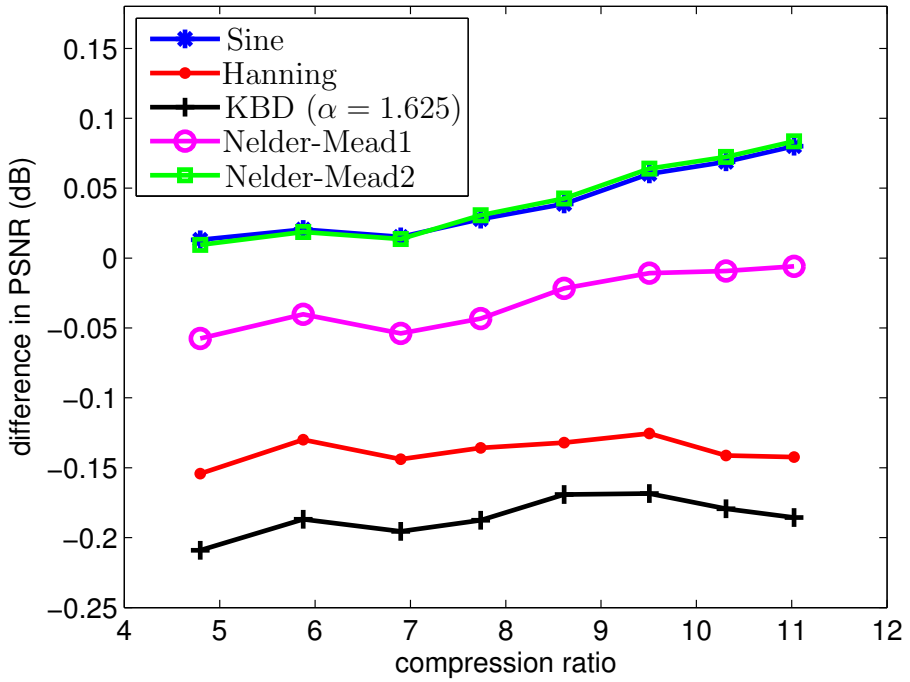

(d) Window performance: Peppers

Figure 8.1: Comparison of window function performance for each test image (*continued*)

The best results obtained for optimised MJPEG are also plotted in Figure 8.2, along with the results obtained for optimised and standard JPEG, for each of the four test images. The MJPEG results shown for the Lena, Plane and Peppers images correspond to those shown for the Nelder-Mead2 window in Figure 8.1 for each respective image. Those shown for the Bridge image, on the other hand, correspond to the results shown for the Nelder-Mead1 window in Figure 8.1(c). Having selected the best window function for each image, the additional data points in Figure 8.2's curves were generated to also investigate the performance of these windows for higher compression ratios. For the sake of interest, results obtained with standard JPEG are plotted to illustrate the improvements in PSNR that can be made by using optimal quantisation.

As the curves suggest, even when optimised MJPEG struggles against optimised JPEG, it eventually yields improved results for higher compression ratios. Since these improvements are initially quite small (or even non-existent in the case of the Plane image), and therefore difficult to see in Figure 8.2, the corresponding differences in PSNR are plotted in Figure 8.3 for each image. Notice that improvements of roughly 0.5 dB are achieved for the Lena and Peppers images at high compression ratios[1]. Furthermore, even the differences for the Plane image eventually reach roughly 0.1 dB for a high compression ratio.

[1]Higher compression ratios can be achieved for Peppers, since its dimensions are 512×512.

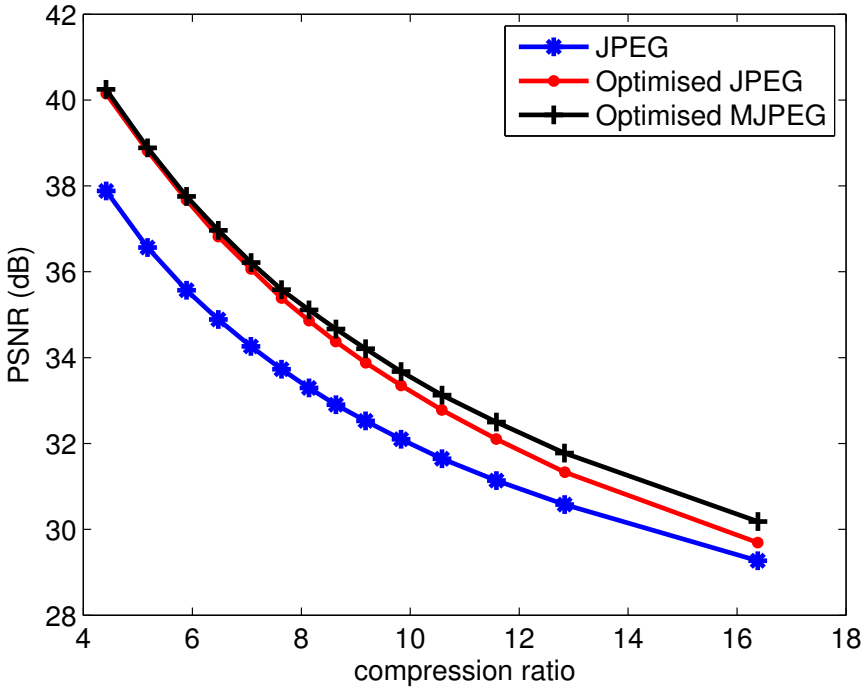

(a) Performance comparison: Lena

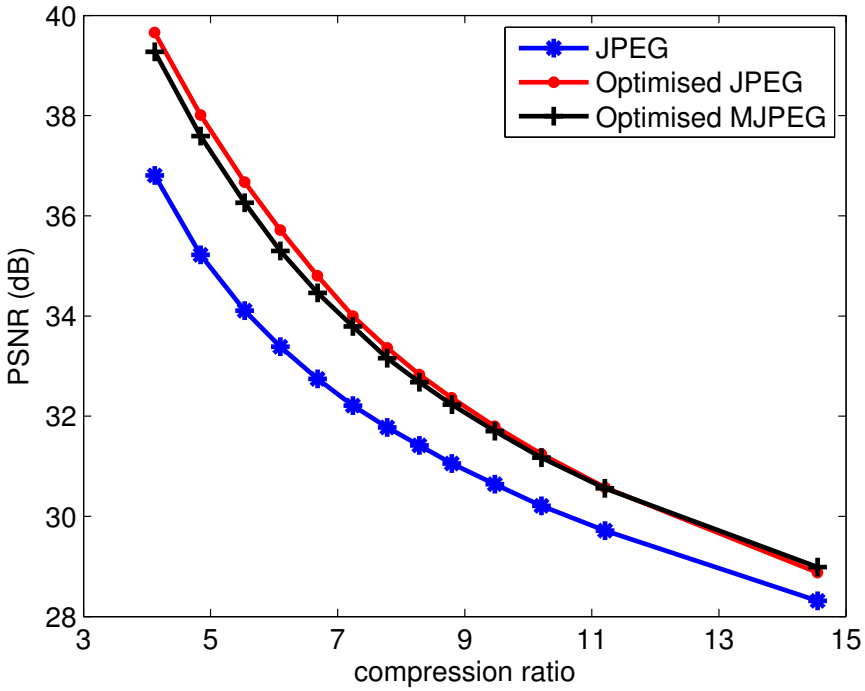

(b) Performance comparison: Plane

Figure 8.2: Comparison of the best MJPEG results with those of JPEG for each test image (*continued on next page*)

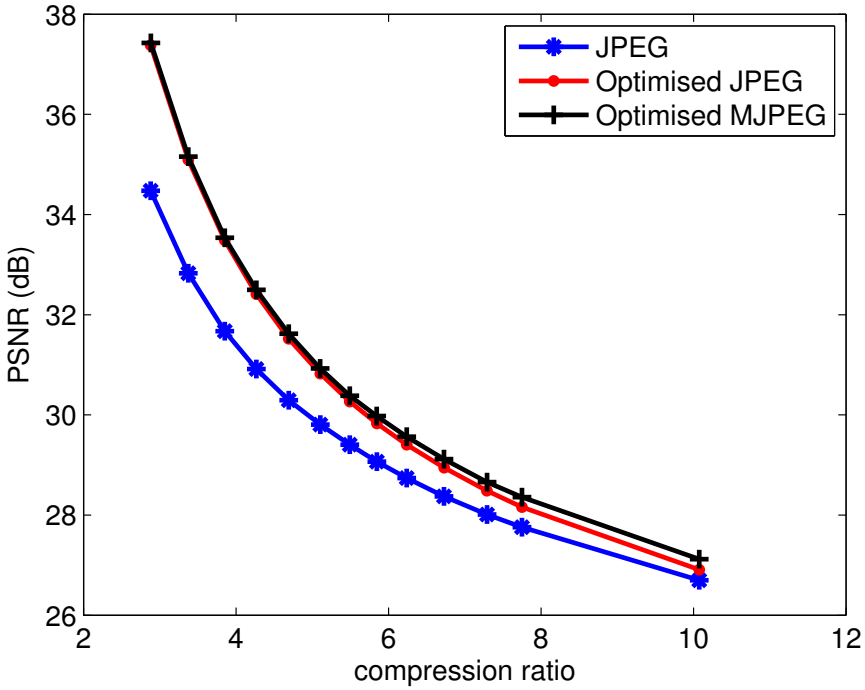

(c) Performance comparison: Bridge

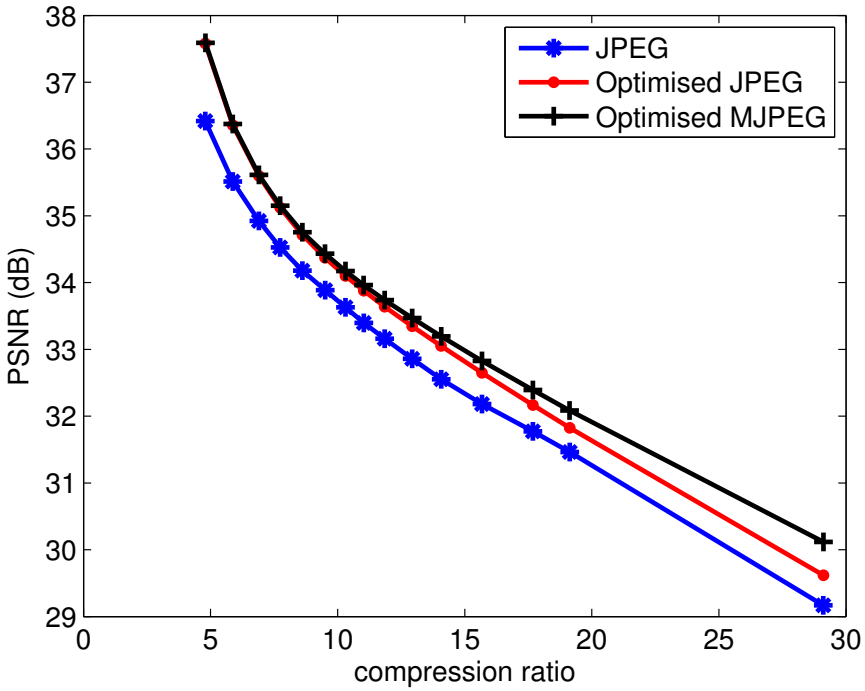

(d) Performance comparison: Peppers

Figure 8.2: Comparison of the best MJPEG results with those of JPEG for each test image (*continued*)

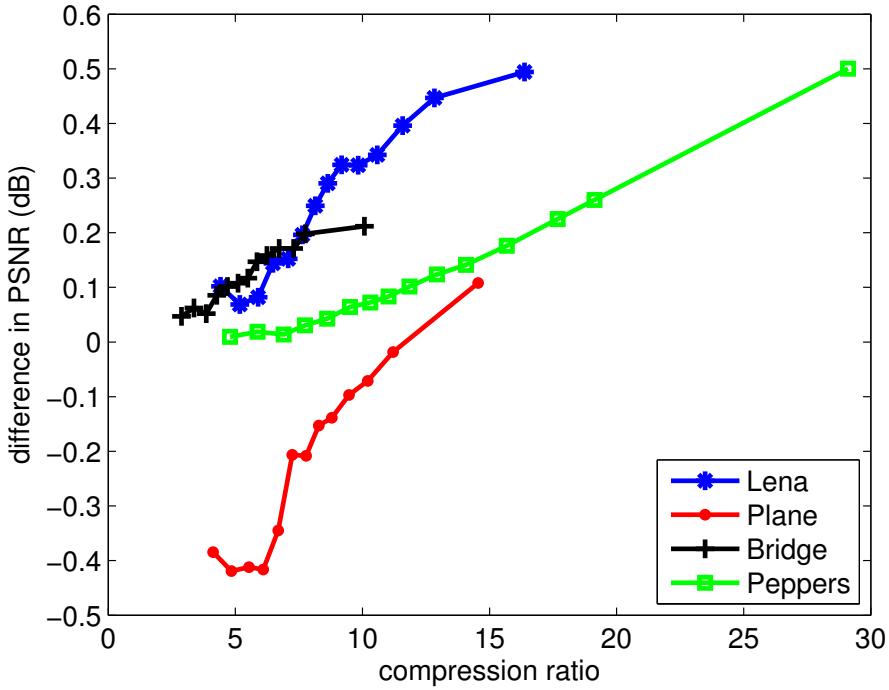

Figure 8.3: Differences in obtained PSNR for optimised MJPEG and optimised JPEG

We lastly also show the decodings corresponding to the last data points of the optimised JPEG and MJPEG results depicted in Figure 8.2, for each test image. These decodings are shown in Figures 8.4 to 8.7, where subfigure (a) of each depicts the relevant reconstructed optimised JPEG encoding, and subfigure (b) the relevant reconstructed optimised MJPEG encoding. In each case, besides possessing a slightly higher PSNR, the reconstructed MJPEG encodings exhibit fewer blocking artefacts than their JPEG counterparts. Ringing artefacts, which can occur around prominent edges in an image, are unfortunately equally visible in both encodings of each image.

(a) JPEG encoding: 4001 bytes, 29.6906 dB

(b) MJPEG encoding with Nelder-Mead2: 4000 bytes, 30.1849 dB

Figure 8.4: Reconstructed low-fidelity encodings of Lena

(a) JPEG encoding: 4504 bytes, 28.8793 dB

(b) MJPEG encoding with NelderMead2: 4503 bytes, 28.9872 dB

Figure 8.5: Reconstructed low-fidelity encodings of Plane

(a) JPEG encoding: 6505 bytes, 26.9080 dB

(b) MJPEG encoding with NelderMead1: 6505 bytes, 27.1197 dB

Figure 8.6: Reconstructed low-fidelity encodings of Bridge

(a) JPEG encoding: 9005 bytes, 29.6165 dB

(b) MJPEG encoding with Nelder-Mead2: 9005 bytes, 30.1167 dB

Figure 8.7: Reconstructed low-fidelity encodings of Peppers

8.3 Conclusions

As stated in Chapter 1, the motivating factor for this research was the question of whether improvements in PSNR could be gained by replacing JPEG's standard DCT with a windowed MDCT. As we saw in the previous section, improvements were indeed gained, but not as significant as one might have hoped.

When it comes to the choice of a window function, we would recommend either the consistent usage of the Nelder-Mead2 window, or allowing the user to choose between the Nelder-Mead1 and Nelder-Mead2 windows. One reason for the first option is the fact that the Nelder-Mead2 window performed consistently well for three of the four test images considered. The other reason is the fact that it is beneficial to not require the user to heuristically select a window function.

The Nelder-Mead1 window, on the other hand, performed very well for the Bridge image. It might therefore be a good idea to include it as a selectable window for cases where the Nelder-Mead2 window performs poorly. One drawback is of course the fact that an image would have to be encoded (and decoded) twice so that the user can select the superior encoding. Another is the fact that an additional parameter would have to be included in an output file to indicate which window function was utilised.

These drawbacks are not severe though: at worst only one additional byte of overhead would be added to an output file to signify the choice of window, and one additional encoding seems a small inconvenience compared to hopefully obtaining the best coding result each time.

8.4 Future Research

As we saw in Section 7.4, the use of a genetic algorithm in conjunction with Algorithm 6.3 can potentially lead to a reduction in their combined running time. For this to happen consistently and optimally, however, the optimal choice of population size and number of generations must still be investigated. Furthermore, our choice of selection scheme,

namely roulette wheel sampling, is very basic. Alternative approaches, such as tournament selection, exist and sometimes lead to more rapid convergence. An investigation therefore also needs to be conducted into the optimal choice of selection scheme.

Also, the optimal quantisation results presented in this chapter can be further improved. While not employed here, the zeroing strategy briefly mentioned in Section 5.4.3 is equally applicable to both perceptual coding and the optimisation of PSNR. Whereas this strategy is implemented in perceptual coding by setting coefficients that are below their corresponding masked thresholds to zero, it is implemented in the alternate paradigm by setting coefficients to zero that do not contribute enough to objective quality to justify encoding them. In [29] for instance, Crouse and Ramchandran combined the zeroing of coefficients with the greedy algorithm of Wu and Gersho [2] (Algorithm 6.1) to achieve improved results. One could similarly combine a zeroing strategy with Algorithm 6.3, thereby improving the coding results presented in this chapter.

Appendix A

Test Images

Figure A.1: Lena

Figure A.2: Plane

Figure A.3: Bridge

Figure A.4: Peppers

Appendix B

Source Code

B.1 M-files

B.1.1 JPEG

```
function Y = my_jpeg(X, Q)

X = double(X);                          % just in case
[m, n] = size(X);

for k = 1:8:m
    for l = 1:8:n
        A = X(k:k + 7, l:l + 7) - 128;  % level shift
        F = dct2(A);                    % transform
        F = round(F./Q);                % quantise
        Y(k:k + 7, l:l + 7) = F;
    end
end


function X = my_jpeg_dec(Y, Q)

[m, n] = size(Y);

for k = 1:8:m
    for l = 1:8:n
        F = Y(k:k + 7, l:l + 7);
        F = F.*Q;                   % dequantise
        A = round(idct2(F) + 128);  % inverse transform and level shift
        X(k:k + 7, l:l + 7) = A;
    end
end


function Q = jpeg_qt(qual)

if qual <= 50
    a = 50/qual;
```

```
else
    a = 2 - qual/50;
end

% luminance quantisation table
Q(1,:) = [16 11 10 16 24 40 51 61];
Q(2,:) = [12 12 14 19 26 58 60 55];
Q(3,:) = [14 13 16 24 40 57 69 56];
Q(4,:) = [14 17 22 29 51 87 80 62];
Q(5,:) = [18 22 37 56 68 109 103 77];
Q(6,:) = [24 35 55 64 81 104 113 92];
Q(7,:) = [49 64 78 87 103 121 120 101];
Q(8,:) = [72 92 95 98 112 100 103 99];

Q = round(a*Q);             % scale quantisation table
Q = max(Q, 1);              % minimum value is 1
Q = min(Q, 255);            % maximum value is 255


function bytes = dct2bytes(Y, opt)

if opt == 0
    bytes = d2b(Y, 1);
else
    bytes = d2b(Y(5:end-4, 5:end-4), 1);
    bytes = bytes + d2b(Y(:, 1:4), 2);
    bytes = bytes + d2b(Y(:, end-3:end), 2);
    bytes = bytes + d2b(Y(1:4, 5:end-4), 3);
    bytes = bytes + d2b(Y(end-3:end, 5:end-4), 3);
end

bytes = bytes + 354;


function bytes = d2b(Y, opt)

if opt == 1                 % 8x8 blocks
    steps = 8;
    max_pos = 64;
    offset1 = 7; offset2 = 7;
elseif opt == 2             % 4x4 blocks
    steps = 4;
    max_pos = 16;
    offset1 = 3; offset2 = 3;
else                        % 4x8 blocks
    steps = 8;
    max_pos = 32;
    offset1 = 3; offset2 = 7;
end

% DC huffman table
hdc = [2 3 3 3 3 3 4 5 6 7 8 9];

% AC huffman table
hac(1,:) = [2 2 3 4 5 7 8 10 16 16];
```

```
hac(2,:) = [4 5 7 9 11 16 16 16 16 16];
hac(3,:) = [5 8 10 12 16 16 16 16 16 16];
hac(4,:) = [6 9 12 16 16 16 16 16 16 16];
hac(5,:) = [6 10 16 16 16 16 16 16 16 16];
hac(6,:) = [7 11 16 16 16 16 16 16 16 16];
hac(7,:) = [7 12 16 16 16 16 16 16 16 16];
hac(8,:) = [8 12 16 16 16 16 16 16 16 16];
hac(9,:) = [9 15 16 16 16 16 16 16 16 16];
hac(10,:) = [9 16 16 16 16 16 16 16 16 16];
hac(11,:) = [9 16 16 16 16 16 16 16 16 16];
hac(12,:) = [10 16 16 16 16 16 16 16 16 16];
hac(13,:) = [10 16 16 16 16 16 16 16 16 16];
hac(14,:) = [11 16 16 16 16 16 16 16 16 16];
hac(15,:) = [16 16 16 16 16 16 16 16 16 16];
hac(16,:) = [16 16 16 16 16 16 16 16 16 16];

[m, n] = size(Y);

bits = 0;
prev = 0;                   % initial prediction for DC
for k = 1:steps:m
    for l = 1:steps:n
        A = Y(k:k + offset1, l:l + offset2);
        A = zigzag(A, opt);
        % trailing zeroes
        pos = max_pos;
        while (pos ~= 1) & (A(pos) == 0)
            pos = pos - 1;
        end

        % differential DC coding
        ddc = A(1) - prev;
        category = ceil(log2(abs(ddc) + 1));
        bits = bits + hdc(category + 1);
        bits = bits + category;
        prev = A(1);

        if pos == 1
            % EOB 1010
            bits = bits + 4;
        else
            % non-zero AC coefficients
            index = 2;
            count = 0;
            while index ~= pos + 1
                while A(index) == 0
                    count = count + 1;
                    index = index + 1;
                    % take care of 16 or more zeroes
                    if count == 16
                        count = 0;
                        % ZRL = 11 bits
                        bits = bits + 11;
                    end
```

```
                end
                category = ceil(log2(abs(A(index)) + 1));
                bits = bits + hac(count + 1, category);
                bits = bits + category;
                count = 0;
                index = index + 1;
            end
            % EOB 1010
            bits = bits + 4;
        end
    end
end
bytes = ceil(bits/8);


function psnr = decibels(X, XX)

[m, n] = size(X);
MSE = sum(sum((X - XX).^2))/(m*n);
psnr = 10*log10(65025/MSE);
```

B.1.2 MJPEG

```
function Y = mjpeg(X, Q)

X = double(X);      % just in case
X = X - 128;        % level shift

[m, n] = size(X);

% calculate frequency components

for k = 1:m
    f(k,:) = row_enc(X(k,:));
end

for k = 1:(n-8)
    F(:,k) = row_enc(f(:,k)')';
end
F = F/4;

for k = 1:4:m
    left(k:k+3,:) = dct2(X(k:k+3, 1:4));
    right(k:k+3,:) = dct2(X(k:k+3, end-3:end));
end
left = 2*left;
right = 2*right;

for l = 1:8:(n-8)
    temp = f(1:4, l:l+7);
    top(:, l:l+7) = [dct1(temp(:,1)) dct1(temp(:,2))...
                     dct1(temp(:,3)) dct1(temp(:,4))...
                     dct1(temp(:,5)) dct1(temp(:,6))...
                     dct1(temp(:,7)) dct1(temp(:,8))];
```

```
    temp = f(end-3:end, l:l+7);
    bottom(:, l:l+7) = [dct1(temp(:,1)) dct1(temp(:,2))...
                        dct1(temp(:,3)) dct1(temp(:,4))...
                        dct1(temp(:,5)) dct1(temp(:,6))...
                        dct1(temp(:,7)) dct1(temp(:,8))];
end

% down-sampled quantisation tables

q2(1,:) = round(mean(Q(1:2,:)));
q2(2,:) = round(mean(Q(3:4,:)));
q2(3,:) = round(mean(Q(5:6,:)));
q2(4,:) = round(mean(Q(7:8,:)));

q1(:,1) = round(mean(q2(:, 1:2),2));
q1(:,2) = round(mean(q2(:, 3:4),2));
q1(:,3) = round(mean(q2(:, 5:6),2));
q1(:,4) = round(mean(q2(:, 7:8),2));

% quantise middle (m-8 x n-8)
for k = 1:8:(m-8)
    for l = 1:8:(n-8)
        F(k:k+7, l:l+7) = F(k:k+7, l:l+7)./Q;
    end
end

% quantise left and right (m x 4)
for k = 1:4:m
    left(k:k+3, :) = left(k:k+3, :)./q1;
    right(k:k+3, :) = right(k:k+3, :)./q1;
end

% quantise top and bottom (4 x n-8)
for l = 1:8:(n-8)
    top(:, l:l+7) = top(:, l:l+7)./q2;
    bottom(:, l:l+7) = bottom(:, l:l+7)./q2;
end

Y = [top ; F ; bottom];
Y = [left Y right];
Y = round(Y);


function X = mjpeg_dec(Y, Q)

left = Y(:, 1:4);
right = Y(:, end-3:end);
Y(:, 1:4) = [];
Y(:, end-3:end) = [];
top = Y(1:4, :);
bottom = Y(end-3:end, :);
Y(1:4, :) = [];
Y(end-3:end, :) = [];

[m, n] = size(Y);
```

```
% down-sampled quantisation tables

q2(1,:) = round(mean(Q(1:2,:)));
q2(2,:) = round(mean(Q(3:4,:)));
q2(3,:) = round(mean(Q(5:6,:)));
q2(4,:) = round(mean(Q(7:8,:)));

q1(:,1) = round(mean(q2(:, 1:2),2));
q1(:,2) = round(mean(q2(:, 3:4),2));
q1(:,3) = round(mean(q2(:, 5:6),2));
q1(:,4) = round(mean(q2(:, 7:8),2));

% dequantise middle (m x n)
for k = 1:8:m
    for l = 1:8:n
        Y(k:k+7, l:l+7) = 4*Y(k:k+7, l:l+7).*Q;
    end
end

% dequantise left and right (m+8 x 4)
for k = 1:4:(m+8)
    left(k:k+3, :) = idct2(0.5*left(k:k+3, :).*q1);
    right(k:k+3, :) = idct2(0.5*right(k:k+3, :).*q1);
end

% dequantise top and bottom (4 x n)
for l = 1:8:n
    temp = top(:, l:l+7).*q2;
    top(:, l:l+7) = [idct1(temp(:,1)) idct1(temp(:,2))...
                     idct1(temp(:,3)) idct1(temp(:,4))...
                     idct1(temp(:,5)) idct1(temp(:,6))...
                     idct1(temp(:,7)) idct1(temp(:,8))];
    temp = bottom(:, l:l+7).*q2;
    bottom(:, l:l+7) = [idct1(temp(:,1)) idct1(temp(:,2))...
                        idct1(temp(:,3)) idct1(temp(:,4))...
                        idct1(temp(:,5)) idct1(temp(:,6))...
                        idct1(temp(:,7)) idct1(temp(:,8))];
end

% invert

for k = 1:n
    F(:,k) = row_dec(Y(:,k)', top(:,k)', bottom(:,k)')';
end

for k = 1:(m+8)
    X(k,:) = row_dec(F(k,:), left(k,:), right(k,:));
end

X = round(X) + 128;
```

```
function f = row_enc(x)

n = length(x);
w = sin(pi*((0:15) + 0.5)/16);
f = [];

for k = 1:8:(n-8)
    f = [f mdct(x(k:k+15).*w)];
end


function x = row_dec(f, left, right)

n = length(f);
w = sin(pi*((0:15) + 0.5)/16);
x = zeros(1, n + 8);

for k = 1:8:n
    x(k:k+15) = x(k:k+15) + imdct(f(k:k+7)).*w;
end

x(1:4) = left;
x(5:8) = x(5:8) + fliplr(left).*w(5:8).*w(13:16);
x(5:8) = x(5:8)./(w(5:8).^2);

x(end-3:end) = right;
x(end-7:end-4) = x(end-7:end-4) - fliplr(right).*w(1:4).*w(9:12);
x(end-7:end-4) = x(end-7:end-4)./(w(9:12).^2);


function X = mdct(x)

N = length(x); n0 = N/4 + 1/2;
for k = 0:N/2-1
    X(k + 1) = sum(x.*cos(2*pi*((0:N-1) + n0)*(k + 0.5)/N));
end


function x = imdct(X)

N = 2*length(X); n0 = N/4 + 1/2;
for n = 0:N-1
    x(n + 1) = sum(X.*cos(2*pi*(n + n0)*((0:N/2-1) + 0.5)/N));
end
x = 4*x/N;


function y = dct1(x)

x = x';
y(1) = 0.5*sum(x)/sqrt(2);
y(2) = 0.5*sum(x.*cos((1:2:7)*pi/8));
y(3) = 0.5*sum(x.*cos((1:2:7)*pi/4));
y(4) = 0.5*sum(x.*cos((1:2:7)*3*pi/8));
y = y';
```

```
function x = idct1(y)

y = y';
c = [1/sqrt(2) 1 1 1];
x(1) = sum(c.*y.*cos((0:3)*pi/8));
x(2) = sum(c.*y.*cos((0:3)*3*pi/8));
x(3) = sum(c.*y.*cos((0:3)*5*pi/8));
x(4) = sum(c.*y.*cos((0:3)*7*pi/8));
x = x';
```

B.2 C++ Implementation

```
#include <iostream>
#include <math.h>
#include <time.h>

using std::cout;
using std::cin;
using std::endl;

double target;
const int m = 256;
const int n = 256;
const int lower = 5;
const int upper = 5;
const int pop_size = 100;    // size of population
const int total = 200;       // number of generations
double Y[m][n];              // frequency components
double Yq[m][n];             // Y quantised
double Ydq[m][n];            // Y dequantised
double zz[64];               // zigzag sequence used in all 3 cases
double gradient[46];         // gradient values, indexed by diag values - 10
int k2diag[2][30];           // corrects kk0 values to diag values, indexed by kk0 - 17
int old_pop[pop_size][64];   // old population
int new_pop[pop_size][64];   // new population
int z[64];                   // indices of Q in zigzag ordering
int Q[64];                   // quantisation table
int q1[16];                  // downsampled 4x4 quantisation table
int q2[32];                  // downsampled 4x8 quantisation table
int hdc[12];                 // huffman dc
int hac[16][10];             // huffman ac
int kk0;                     // diag value
double kk1;                  // gradient value


void show_Q(int* q)
{
    int pos;

    for (pos = 0 ; pos < 64 ; pos++)
    {
        if (fmod(pos, 8) == 0)
```

```
        {
            cout << endl;
        }
        cout << q[pos] << " ";
    }
    cout << endl;
}


void mate(int parent1, int parent2, int k)
{
    int pos;
    double r;

    // crossover
    r = rand();
    r = r/RAND_MAX;
    r = round(62*r);
    // first portion
    for (pos = 0 ; pos <= r ; pos++)
    {
        new_pop[k][pos] = old_pop[parent1][pos];
        new_pop[k + 1][pos] = old_pop[parent2][pos];
    }
    // second portion
    for (pos = int(r) + 1 ; pos < 64 ; pos++)
    {
        new_pop[k][pos] = old_pop[parent2][pos];
        new_pop[k + 1][pos] = old_pop[parent1][pos];
    }

    // mutation
    r = rand();
    r = r/RAND_MAX;
    if (r < 0.05)
    {
        r = rand();
        r = r/RAND_MAX;
        r = round(63*r);
        pos = int(r);
        r = rand();
        r = r/RAND_MAX;
        new_pop[k][pos] = new_pop[k][pos] + int(round(2*lower*r - lower));
        new_pop[k][pos] = int(fmax(new_pop[k][pos], 1));
        new_pop[k][pos] = int(fmin(new_pop[k][pos], 255));
    }
    r = rand();
    r = r/RAND_MAX;
    if (r < 0.05)
    {
        r = rand();
        r = r/RAND_MAX;
        r = round(63*r);
        pos = int(r);
```

```
        r = rand();
        r = r/RAND_MAX;
        new_pop[k + 1][pos] = new_pop[k + 1][pos] + int(round(2*lower*r - lower));
        new_pop[k + 1][pos] = int(fmax(new_pop[k + 1][pos], 1));
        new_pop[k + 1][pos] = int(fmin(new_pop[k + 1][pos], 255));
    }
}


void copy_table(int* q1, int* q2)
{
    int k;

    for (k = 0 ; k < 64 ; k++)
    {
        q2[k] = q1[k];
    }
}


void update_pop()
{
    int k;

    for (k = 0 ; k < pop_size ; k++)
    {
    copy_table(new_pop[k], old_pop[k]);
    }
}


int find_pos(double* p, double r)
{
    int k = 0;

    while (r >= p[k])
    {
        k++;
    }
    return k;
}


void down_Q(int* q)
{
    // downsample quantisation table
    int pos;

    for (pos = 0 ; pos < 8 ; pos++)
    {
        q2[pos] = int(round(double(q[pos] + q[pos + 8])/2));
        q2[pos + 8] = int(round(double(q[pos + 16] + q[pos + 24])/2));
        q2[pos + 16] = int(round(double(q[pos + 32] + q[pos + 40])/2));
        q2[pos + 24] = int(round(double(q[pos + 48] + q[pos + 56])/2));
```

```
    }

    for (pos = 0 ; pos < 4 ; pos++)
    {
        q1[pos] = int(round(double(q2[2*pos] + q2[2*pos + 1])/2));
        q1[pos + 4] = int(round(double(q2[2*pos + 8] + q2[2*pos + 9])/2));
        q1[pos + 8] = int(round(double(q2[2*pos + 16] + q2[2*pos + 17])/2));
        q1[pos + 12] = int(round(double(q2[2*pos + 24] + q2[2*pos + 25])/2));
    }
}


void qdq(int* q)
{
    // quantises and dequantises
    int row, column, pos;

    // middle
    for (row = 4 ; row < m - 4 ; row++)
    {
        for (column = 4 ; column < n - 4 ; column++)
        {
            pos = int(8*fmod(row - 4, 8) + fmod(column - 4, 8));
            Yq[row][column] = round(Y[row][column]/q[pos]);
            Ydq[row][column] = Yq[row][column]*q[pos];
        }
    }

    // left
    for (row = 0 ; row < m ; row++)
    {
        for (column = 0 ; column < 4 ; column++)
        {
            pos = int(4*fmod(row,4) + column);
            Yq[row][column] = round(Y[row][column]/q1[pos]);
            Ydq[row][column] = Yq[row][column]*q1[pos];
        }
    }

    // right
    for (row = 0 ; row < m ; row++)
    {
        for (column = n - 4 ; column < n ; column++)
        {
            pos = int(4*fmod(row,4) + fmod(column,4));
            Yq[row][column] = round(Y[row][column]/q1[pos]);
            Ydq[row][column] = Yq[row][column]*q1[pos];
        }
    }

    // top
    for (row = 0 ; row < 4 ; row++)
    {
        for (column = 4 ; column < n - 4 ; column++)
```

```
    {
            pos = int(8*row + fmod(column - 4, 8));
            Yq[row][column] = round(Y[row][column]/q2[pos]);
            Ydq[row][column] = Yq[row][column]*q2[pos];
        }
    }

    // bottom
    for (row =  m - 4 ; row < m ; row++)
    {
    for (column = 4 ; column < n - 4 ; column++)
        {
            pos = int(8*fmod(row,4) + fmod(column - 4, 8));
            Yq[row][column] = round(Y[row][column]/q2[pos]);
            Ydq[row][column] = Yq[row][column]*q2[pos];
        }
    }
}


double calc_error()
{
    int row, column;
    double E;

    E = 0;

    for (row = 0 ; row < m ; row++)
    {
        for (column = 0 ; column < n ; column++)
        {
            E = E + pow(Y[row][column] - Ydq[row][column], 2);
        }
    }

    return E/(m*n);
}


void zigzag(int row, int column, int opt)
{
    switch (opt)
    {
    case 1 : // 8x8 blocks
        zz[0] = Yq[row][column]; zz[1] = Yq[row][column + 1];
        zz[2] = Yq[row + 1][column]; zz[3] = Yq[row + 2][column];
        zz[4] = Yq[row + 1][column + 1]; zz[5] = Yq[row][column + 2];
        zz[6] = Yq[row][column + 3]; zz[7] = Yq[row + 1][column + 2];
        zz[8] = Yq[row + 2][column + 1]; zz[9] = Yq[row + 3][column];
        zz[10] = Yq[row + 4][column]; zz[11] = Yq[row + 3][column + 1];
        zz[12] = Yq[row + 2][column + 2]; zz[13] = Yq[row + 1][column + 3];
        zz[14] = Yq[row][column + 4]; zz[15] = Yq[row][column + 5];
        zz[16] = Yq[row + 1][column + 4]; zz[17] = Yq[row + 2][column + 3];
        zz[18] = Yq[row + 3][column + 2]; zz[19] = Yq[row + 4][column + 1];
```

```
        zz[20] = Yq[row + 5][column]; zz[21] = Yq[row + 6][column];
        zz[22] = Yq[row + 5][column + 1]; zz[23] = Yq[row + 4][column + 2];
        zz[24] = Yq[row + 3][column + 3]; zz[25] = Yq[row + 2][column + 4];
        zz[26] = Yq[row + 1][column + 5]; zz[27] = Yq[row][column + 6];
        zz[28] = Yq[row][column + 7]; zz[29] = Yq[row + 1][column + 6];
        zz[30] = Yq[row + 2][column + 5]; zz[31] = Yq[row + 3][column + 4];
        zz[32] = Yq[row + 4][column + 3]; zz[33] = Yq[row + 5][column + 2];
        zz[34] = Yq[row + 6][column + 1]; zz[35] = Yq[row + 7][column];
        zz[36] = Yq[row + 7][column + 1]; zz[37] = Yq[row + 6][column + 2];
        zz[38] = Yq[row + 5][column + 3]; zz[39] = Yq[row + 4][column + 4];
        zz[40] = Yq[row + 3][column + 5]; zz[41] = Yq[row + 2][column + 6];
        zz[42] = Yq[row + 1][column + 7]; zz[43] = Yq[row + 2][column + 7];
        zz[44] = Yq[row + 3][column + 6]; zz[45] = Yq[row + 4][column + 5];
        zz[46] = Yq[row + 5][column + 4]; zz[47] = Yq[row + 6][column + 3];
        zz[48] = Yq[row + 7][column + 2]; zz[49] = Yq[row + 7][column + 3];
        zz[50] = Yq[row + 6][column + 4]; zz[51] = Yq[row + 5][column + 5];
        zz[52] = Yq[row + 4][column + 6]; zz[53] = Yq[row + 3][column + 7];
        zz[54] = Yq[row + 4][column + 7]; zz[55] = Yq[row + 5][column + 6];
        zz[56] = Yq[row + 6][column + 5]; zz[57] = Yq[row + 7][column + 4];
        zz[58] = Yq[row + 7][column + 5]; zz[59] = Yq[row + 6][column + 6];
        zz[60] = Yq[row + 5][column + 7]; zz[61] = Yq[row + 6][column + 7];
        zz[62] = Yq[row + 7][column + 6]; zz[63] = Yq[row + 7][column + 7];
        break;
    case 2 : // 4x4 blocks
    case 3 :
        zz[0] = Yq[row][column]; zz[1] = Yq[row][column + 1];
        zz[2] = Yq[row + 1][column]; zz[3] = Yq[row + 2][column];
        zz[4] = Yq[row + 1][column + 1]; zz[5] = Yq[row][column + 2];
        zz[6] = Yq[row][column + 3]; zz[7] = Yq[row + 1][column + 2];
        zz[8] = Yq[row + 2][column + 1]; zz[9] = Yq[row + 3][column];
        zz[10] = Yq[row + 3][column + 1]; zz[11] = Yq[row + 2][column + 2];
        zz[12] = Yq[row + 1][column + 3]; zz[13] = Yq[row + 2][column + 3];
        zz[14] = Yq[row + 3][column + 2]; zz[15] = Yq[row + 3][column + 3];
        break;
    case 4 : // 4x8 blocks
    case 5 :
        zz[0] = Yq[row][column]; zz[1] = Yq[row][column + 1];
        zz[2] = Yq[row + 1][column]; zz[3] = Yq[row + 2][column];
        zz[4] = Yq[row + 1][column + 1]; zz[5] = Yq[row][column + 2];
        zz[6] = Yq[row][column + 3]; zz[7] = Yq[row + 1][column + 2];
        zz[8] = Yq[row + 2][column + 1]; zz[9] = Yq[row + 3][column];
        zz[10] = Yq[row + 3][column + 1]; zz[11] = Yq[row + 2][column + 2];
        zz[12] = Yq[row + 1][column + 3]; zz[13] = Yq[row][column + 4];
        zz[14] = Yq[row][column + 5]; zz[15] = Yq[row + 1][column + 4];
        zz[16] = Yq[row + 2][column + 3]; zz[17] = Yq[row + 3][column + 2];
        zz[18] = Yq[row + 3][column + 3]; zz[19] = Yq[row + 2][column + 4];
        zz[20] = Yq[row + 1][column + 5]; zz[21] = Yq[row][column + 6];
        zz[22] = Yq[row][column + 7]; zz[23] = Yq[row + 1][column + 6];
        zz[24] = Yq[row + 2][column + 5]; zz[25] = Yq[row + 3][column + 4];
        zz[26] = Yq[row + 3][column + 5]; zz[27] = Yq[row + 2][column + 6];
        zz[28] = Yq[row + 1][column + 7]; zz[29] = Yq[row + 2][column + 7];
       zz[30] = Yq[row + 3][column + 6]; zz[31] = Yq[row + 3][column + 7];
    }
}
```

```
double d2b(int opt)
{
    int row, column, steps, start_row, stop_row, start_column, stop_column;
    int count, pos, max_pos, category, i;
    double bits, prev, ddc, bytes;

    switch (opt)
    {
    case 1 : // middle
        steps = 8; max_pos = 63; start_row = 4; stop_row = m - 4;
        start_column = 4; stop_column = n - 4;
        break;
    case 2 : // left
        steps = 4; max_pos = 15; start_row = 0; stop_row = m;
        start_column = 0; stop_column = 4;
        break;
    case 3 : // right
        steps = 4; max_pos = 15; start_row = 0; stop_row = m;
        start_column = n - 4; stop_column = n;
        break;
    case 4 : // top
        steps = 8; max_pos = 31; start_row = 0; stop_row = 4;
        start_column = 4; stop_column = n - 4;
        break;
    case 5 : // bottom
        steps = 8; max_pos = 31; start_row = m - 4; stop_row = m;
        start_column = 4; stop_column = n - 4;
    }

    bits = 0; prev = 0;

    for (row = start_row ; row < stop_row ; row = row + steps)
    {
        for (column = start_column ; column < stop_column ; column = column + steps)
        {
            zigzag(row, column, opt);
            // trailing zeros
            pos = max_pos;
            while ((pos != 0) && (zz[pos] == 0))
            {
                pos--;
            }
            // differential DC coding
            ddc = zz[0] - prev;
            category = int(ceil(log2(fabs(ddc) + 1)));
            bits = bits + hdc[category];
            bits = bits + category;
            prev = zz[0];
            if (pos == 0)
            {
                bits = bits + 4; // EOB 1010
            }
```

```
            else
            {
                // non-zero AC coefficients
                i = 1;
                count = 0;
                while (i != pos + 1)
                {
                    while (zz[i] == 0)
                    {
                        count++;
                        i++;
                        // more than 16 zeros
                        if (count == 16)
                        {
                            count = 0;
                            bits = bits + 11; // ZRL contributes 11 bits
                        }
                    }
                    category = int(ceil(log2(fabs(zz[i]) + 1)));
                    bits = bits + hac[count][category - 1];
                    bits = bits + category;
                    count = 0;
                    i++;
                }
                bits = bits + 4; // EOB 1010
            }
        }
    }
    bytes = ceil(bits/8);
    return bytes;
}


double dct2bytes()
{
    double bytes;

    bytes = d2b(1) + d2b(2) + d2b(3) + d2b(4) + d2b(5); // middle left right top bottom
    bytes = bytes + 354; // overhead
    return bytes;
}


void ga()
{
    // Genetic Algorithm

    double c = 35;        // penalty parameter
    double best = 0;      // best fitness in final population
    double bfc;           // best feasible cost
    double bic;           // best infeasible cost
    double B, E, dev, cost;
    double fitness[pop_size];
    double prob[pop_size];
```

```
double tot_fitness;
double r;
int iter, k, index, parent1, parent2;

for (iter = 1 ; iter <= total ; iter++)
{
    bfc = INFINITY;
    bic = INFINITY;
    tot_fitness = 0;

    // calculate cost and fitness
    for (k = 0 ; k < pop_size ; k++)
    {
        down_Q(old_pop[k]);
        qdq(old_pop[k]);
        E = calc_error();
        B = dct2bytes();

        // calculate deviation from constraint
        if (B > 1.001*target)
        {
            dev = 100*(B - 1.001*target)/(1.001*target);
        }
        else if (B < 0.999*target)
        {
            dev = 100*(0.999*target - B)/(0.999*target);
        }
        else
        {
            dev = 0;
        }

        cost = E + c*dev;
        fitness[k] = 1/cost;
        tot_fitness = tot_fitness + fitness[k];

        if (dev == 0)
        {
            if (cost < bfc)
            {
                bfc = cost;
                index = k;
            }
        }
        else if (cost < bic)
        {
            bic = cost;
        }
    }

    // update c
    c = c*bfc/bic;
    cout << "c = " << c << endl;
```

```
        // calculate probability interval
        prob[0] = fitness[0]/tot_fitness;
        for (k = 1 ; k < pop_size ; k++)
            {
                prob[k] = prob[k - 1] + fitness[k]/tot_fitness;
            }

        // generate new population
        for (k = 0 ; k < pop_size ; k = k + 2)
        {
            r = rand();
            r = r/RAND_MAX;
            parent1 = find_pos(prob, r);
            r = rand();
            r = r/RAND_MAX;
            parent2 = find_pos(prob, r);
            mate(parent1, parent2, k);
        }

        // retain best solution
        r = rand();
        r = r/RAND_MAX;
        r = round((pop_size - 1)*r);
        copy_table(old_pop[index], new_pop[int(r)]);
        cout << "best = " << bfc << endl;
        show_Q(old_pop[index]);
        update_pop();
    }

    // final population
    // calculate cost and fitness
    for (k = 0 ; k < pop_size ; k++)
    {
        down_Q(old_pop[k]);
        qdq(old_pop[k]);
        E = calc_error();
        B = dct2bytes();

        // calculate deviation from constraint
        if (B > 1.001*target)
        {
            dev = 100*(B - 1.001*target)/(1.001*target);
        }
        else if (B < 0.999*target)
        {
            dev = 100*(0.999*target - B)/(0.999*target);
        }
        else
        {
            dev = 0;
        }

        cost = E + c*dev;
        fitness[k] = 1/cost;
```

```
        if (fitness[k] > best)
        {
            best = fitness[k];
            index = k;
        }
    }
    copy_table(old_pop[index], Q);
}


void fill_Q(int q)
{
    // fills Q with a constant value

    int pos;

    for (pos = 0 ; pos < 64 ; pos++)
    {
        Q[pos] = q;
    }
}


void plane_Q()
{
    // evaluates plane function using values of kk0 and kk1 ; fills in Q

    int row, column;

    for (row = 0 ; row < 8 ; row++)
    {
        for (column = 0 ; column < 8 ; column++)
        {
            Q[8*row + column] = int(round(kk1*(row + column - 7))) + kk0;
        }
    }
}


int gr()
{
    // golden ratio search

    double r = 1 - (sqrt(5) - 1)/2;
    int w = 255;
    int L = 1; int R = 255;
    int a, b;
    double B, fL, fR, fa, fb, best;

    fill_Q(L);
    down_Q(Q);
    qdq(Q);
    B = dct2bytes();
    fL = fabs(B - target);
```

```
fill_Q(R);
down_Q(Q);
qdq(Q);
B = dct2bytes();
fR = fabs(B - target);
a = L + int(floor(r*w));
fill_Q(a);
down_Q(Q);
qdq(Q);
B = dct2bytes();
fa = fabs(B - target);
b = R - int(floor(r*w));
fill_Q(b);
down_Q(Q);
qdq(Q);
B = dct2bytes();
fb = fabs(B - target);

while (w > 3)
{
    if (fa < fb)
    {
        // discard RHS
        R = b; fR = fb;
        b = a; fb = fa;
        w = R - L + 1;
        a = L + int(floor(r*w));
        fill_Q(a);
        down_Q(Q);
        qdq(Q);
        B = dct2bytes();
        fa = fabs(B - target);
    }
    else
    {
        // discard LHS
        L = a; fL = fa;
        a = b; fa = fb;
        w = R - L + 1;
        b = R - int(floor(r*w));
        fill_Q(b);
        down_Q(Q);
        qdq(Q);
        B = dct2bytes();
        fb = fabs(B - target);
    }
}

best = fmin(fmin(fL, fR), fa);
if (fL == best)
{
    return L;
}
else if (fR == best)
```

```
    {
        return R;
    }
    else
    {
        return a;
    }
}


void get_gradient()
{
    // determines value of kk0 and kk1

    double B, dev, best_dev;
    int best_diag;
    int num, count;

    count = 1;
    num = k2diag[1][kk0 - 17]; // number of values to consider
    kk0 = k2diag[0][kk0 - 17]; // first new value of kk0
    cout << "testing " << kk0 << endl;
    kk1 = gradient[kk0 - 10];
    plane_Q();
    down_Q(Q);
    qdq(Q);
    B = dct2bytes();
    dev = fabs(B - target);
    best_dev = dev;
    best_diag = kk0;

    while (count < num)
    {
        kk0++; // try next value
        cout << "testing " << kk0 << endl;
        kk1 = gradient[kk0 - 10];
        plane_Q();
        down_Q(Q);
        qdq(Q);
        B = dct2bytes();
        dev = fabs(B - target);
        if (dev < best_dev)
        {
            best_dev = dev;
            best_diag = kk0;
        }
        count++;
    }

    kk0 = best_diag;
    kk1 = gradient[kk0 - 10];
}
```

```
void init_Q()
{
    // manually specify quantisation table

    Q[0] = 255; Q[1] = 255; Q[2] = 255; Q[3] = 255;
    Q[4] = 255; Q[5] = 255; Q[6] = 255; Q[7] = 255;
    Q[8] = 255; Q[9] = 255; Q[10] = 255; Q[11] = 255;
    Q[12] = 255; Q[13] = 255; Q[14] = 255; Q[15] = 255;
    Q[16] = 255; Q[17] = 255; Q[18] = 255; Q[19] = 255;
    Q[20] = 255; Q[21] = 255; Q[22] = 255; Q[23] = 255;
    Q[24] = 255; Q[25] = 255; Q[26] = 255; Q[27] = 255;
    Q[28] = 255; Q[29] = 255; Q[30] = 255; Q[31] = 255;
    Q[32] = 255; Q[33] = 255; Q[34] = 255; Q[35] = 255;
    Q[36] = 255; Q[37] = 255; Q[38] = 255; Q[39] = 255;
    Q[40] = 255; Q[41] = 255; Q[42] = 255; Q[43] = 255;
    Q[44] = 255; Q[45] = 255; Q[46] = 255; Q[47] = 255;
    Q[48] = 255; Q[49] = 255; Q[50] = 255; Q[51] = 255;
    Q[52] = 255; Q[53] = 255; Q[54] = 255; Q[55] = 255;
    Q[56] = 255; Q[57] = 255; Q[58] = 255; Q[59] = 255;
    Q[60] = 255; Q[61] = 255; Q[62] = 255; Q[63] = 255;
}


int main(int argc, char* argv[])
{
    double x, E, B, dev, nu_E, nu_B, lambda, best_lambda, best_E, best_B, Rmax, Rmin;
    int row, column, pos, q, qq, qqq, best_pos, best_q, k;

    if (argc != 3)
    {
        cout << "Must specify target file size and GA option" << endl;
        exit(1);
    }

// read in frequency components

    FILE* pic = fopen("lena_m2.mat", "r");
    fseek(pic, 184, SEEK_SET);
    for (column = 0 ; column < n ; column++)
    {
        for (row = 0 ; row < m ; row++)
        {
            fread(&x, 8, 1, pic);
            Y[row][column] = x;
        }
    }

// initialize random number generator and get target file size

    srand(time(NULL));
    target = atoi(argv[1]);

// enter indices in z
```

```
    z[0] = 0; z[1] = 1; z[2] = 8; z[3] = 16;
    z[4] = 9; z[5] = 2; z[6] = 3; z[7] = 10;
    z[8] = 17; z[9] = 24; z[10] = 32; z[11] = 25;
    z[12] = 18; z[13] = 11; z[14] = 4; z[15] = 5;
    z[16] = 12; z[17] = 19; z[18] = 26; z[19] = 33;
    z[20] = 40; z[21] = 48; z[22] = 41; z[23] = 34;
    z[24] = 27; z[25] = 20; z[26] = 13; z[27] = 6;
    z[28] = 7; z[29] = 14; z[30] = 21; z[31] = 28;
    z[32] = 35; z[33] = 42; z[34] = 49; z[35] = 56;
    z[36] = 57; z[37] = 50; z[38] = 43; z[39] = 36;
    z[40] = 29; z[41] = 22; z[42] = 15; z[43] = 23;
    z[44] = 30; z[45] = 37; z[46] = 44; z[47] = 51;
    z[48] = 58; z[49] = 59; z[50] = 52; z[51] = 45;
    z[52] = 38; z[53] = 31; z[54] = 39; z[55] = 46;
    z[56] = 53; z[57] = 60; z[58] = 61; z[59] = 54;
    z[60] = 47; z[61] = 55; z[62] = 62; z[63] = 63;

// fill in huffman tables

    hdc[0] = 2; hdc[1] = 3; hdc[2] = 3; hdc[3] = 3; hdc[4] = 3; hdc[5] = 3;
    hdc[6] = 4; hdc[7] = 5; hdc[8] = 6; hdc[9] = 7; hdc[10] = 8; hdc[11] = 9;

    hac[0][0] = 2; hac[0][1] = 2; hac[0][2] = 3; hac[0][3] = 4; hac[0][4] = 5;
    hac[0][5] = 7; hac[0][6] = 8; hac[0][7] = 10; hac[0][8] = 16; hac[0][9] = 16;
    hac[1][0] = 4; hac[1][1] = 5; hac[1][2] = 7; hac[1][3] = 9; hac[1][4] = 11;
    hac[1][5] = 16; hac[1][6] = 16; hac[1][7] = 16; hac[1][8] = 16; hac[1][9] = 16;
    hac[2][0] = 5; hac[2][1] = 8; hac[2][2] = 10; hac[2][3] = 12; hac[2][4] = 16;
    hac[2][5] = 16; hac[2][6] = 16; hac[2][7] = 16; hac[2][8] = 16; hac[2][9] = 16;
    hac[3][0] = 6; hac[3][1] = 9; hac[3][2] = 12; hac[3][3] = 16; hac[3][4] = 16;
    hac[3][5] = 16; hac[3][6] = 16; hac[3][7] = 16; hac[3][8] = 16; hac[3][9] = 16;
    hac[4][0] = 6; hac[4][1] = 10; hac[4][2] = 16; hac[4][3] = 16; hac[4][4] = 16;
    hac[4][5] = 16; hac[4][6] = 16; hac[4][7] = 16; hac[4][8] = 16; hac[4][9] = 16;
    hac[5][0] = 7; hac[5][1] = 11; hac[5][2] = 16; hac[5][3] = 16; hac[5][4] = 16;
    hac[5][5] = 16; hac[5][6] = 16; hac[5][7] = 16; hac[5][8] = 16; hac[5][9] = 16;
    hac[6][0] = 7; hac[6][1] = 12; hac[6][2] = 16; hac[6][3] = 16; hac[6][4] = 16;
    hac[6][5] = 16; hac[6][6] = 16; hac[6][7] = 16; hac[6][8] = 16; hac[6][9] = 16;
    hac[7][0] = 8; hac[7][1] = 12; hac[7][2] = 16; hac[7][3] = 16; hac[7][4] = 16;
    hac[7][5] = 16; hac[7][6] = 16; hac[7][7] = 16; hac[7][8] = 16; hac[7][9] = 16;
    hac[8][0] = 9; hac[8][1] = 15; hac[8][2] = 16; hac[8][3] = 16; hac[8][4] = 16;
    hac[8][5] = 16; hac[8][6] = 16; hac[8][7] = 16; hac[8][8] = 16; hac[8][9] = 16;
    hac[9][0] = 9; hac[9][1] = 16; hac[9][2] = 16; hac[9][3] = 16; hac[9][4] = 16;
    hac[9][5] = 16; hac[9][6] = 16; hac[9][7] = 16; hac[9][8] = 16; hac[9][9] = 16;
    hac[10][0] = 9; hac[10][1] = 16; hac[10][2] = 16; hac[10][3] = 16; hac[10][4] = 16;
    hac[10][5] = 16; hac[10][6] = 16; hac[10][7] = 16; hac[10][8] = 16; hac[10][9] = 16;
    hac[11][0] = 10; hac[11][1] = 16; hac[11][2] = 16; hac[11][3] = 16; hac[11][4] = 16;
    hac[11][5] = 16; hac[11][6] = 16; hac[11][7] = 16; hac[11][8] = 16; hac[11][9] = 16;
    hac[12][0] = 10; hac[12][1] = 16; hac[12][2] = 16; hac[12][3] = 16; hac[12][4] = 16;
    hac[12][5] = 16; hac[12][6] = 16; hac[12][7] = 16; hac[12][8] = 16; hac[12][9] = 16;
    hac[13][0] = 11; hac[13][1] = 16; hac[13][2] = 16; hac[13][3] = 16; hac[13][4] = 16;
    hac[13][5] = 16; hac[13][6] = 16; hac[13][7] = 16; hac[13][8] = 16; hac[13][9] = 16;
    hac[14][0] = 16; hac[14][1] = 16; hac[14][2] = 16; hac[14][3] = 16; hac[14][4] = 16;
    hac[14][5] = 16; hac[14][6] = 16; hac[14][7] = 16; hac[14][8] = 16; hac[14][9] = 16;
    hac[15][0] = 16; hac[15][1] = 16; hac[15][2] = 16; hac[15][3] = 16; hac[15][4] = 16;
    hac[15][5] = 16; hac[15][6] = 16; hac[15][7] = 16; hac[15][8] = 16; hac[15][9] = 16;
```

```
    if (atoi(argv[2]) == 2)
    {
        // go directly to main algorithm
        init_Q();
        goto L1;
    }

// fill in gradient values

    gradient[0] = 0.2969; gradient[1] = 0.3690;
    gradient[2] = 0.4405; gradient[3] = 0.4323;
    gradient[4] = 0.4658; gradient[5] = 0.4955;
    gradient[6] = 0.5841; gradient[7] = 0.6332;
    gradient[8] = 0.7217; gradient[9] = 0.7857;
    gradient[10] = 0.9003; gradient[11] = 0.9590;
    gradient[12] = 1.0350; gradient[13] = 1.2731;
    gradient[14] = 1.4672; gradient[15] = 1.7843;
    gradient[16] = 2.0640; gradient[17] = 2.2247;
    gradient[18] = 2.3512; gradient[19] = 2.3690;
    gradient[20] = 2.3110; gradient[21] = 2.4159;
    gradient[22] = 2.5685; gradient[23] = 2.5804;
    gradient[24] = 2.6354; gradient[25] = 2.6145;
    gradient[26] = 2.5789; gradient[27] = 2.9063;
    gradient[28] = 3.0104; gradient[29] = 3.1302;
    gradient[30] = 3.1518; gradient[31] = 3.2403;
    gradient[32] = 3.4650; gradient[33] = 3.6280;
    gradient[34] = 3.7902; gradient[35] = 3.9546;
    gradient[36] = 3.9851; gradient[37] = 3.9762;
    gradient[38] = 4.3593; gradient[39] = 4.3073;
    gradient[40] = 4.1711; gradient[41] = 4.1175;
    gradient[42] = 3.9196; gradient[43] = 3.7567;
    gradient[44] = 3.7827; gradient[45] = 4.3289;

// fill in k2diag values
// first value to consider

    k2diag[0][0] = 17; k2diag[0][1] = 18; k2diag[0][2] = 19; k2diag[0][3] = 20;
    k2diag[0][4] = 21; k2diag[0][5] = 22; k2diag[0][6] = 23; k2diag[0][7] = 24;
    k2diag[0][8] = 25; k2diag[0][9] = 26; k2diag[0][10] = 28; k2diag[0][11] = 29;
    k2diag[0][12] = 30; k2diag[0][13] = 32; k2diag[0][14] = 33; k2diag[0][15] = 34;
    k2diag[0][16] = 35; k2diag[0][17] = 36; k2diag[0][18] = 38; k2diag[0][19] = 39;
    k2diag[0][20] = 40; k2diag[0][21] = 41; k2diag[0][22] = 42; k2diag[0][23] = 44;
    k2diag[0][24] = 46; k2diag[0][25] = 47; k2diag[0][26] = 49; k2diag[0][27] = 49;
    k2diag[0][28] = 50; k2diag[0][29] = 51;

// number of values to consider

    k2diag[1][0] = 2; k2diag[1][1] = 3; k2diag[1][2] = 3; k2diag[1][3] = 3;
    k2diag[1][4] = 4; k2diag[1][5] = 5; k2diag[1][6] = 6; k2diag[1][7] = 6;
    k2diag[1][8] = 6; k2diag[1][9] = 6; k2diag[1][10] = 6; k2diag[1][11] = 6;
    k2diag[1][12] = 6; k2diag[1][13] = 6; k2diag[1][14] = 6; k2diag[1][15] = 6;
    k2diag[1][16] = 6; k2diag[1][17] = 7; k2diag[1][18] = 8; k2diag[1][19] = 8;
    k2diag[1][20] = 8; k2diag[1][21] = 9; k2diag[1][22] = 8; k2diag[1][23] = 7;
```

```
    k2diag[1][24] = 6; k2diag[1][25] = 6; k2diag[1][26] = 4; k2diag[1][27] = 4;
    k2diag[1][28] = 4; k2diag[1][29] = 5;


// get initial quantisation table

    kk0 = gr();
    cout << "kk0 = " << kk0 << endl;

    if (kk0 < 10)
    {
        cout << "Target file size too large" << endl;
        exit(1);
    }
    if (kk0 > 46)
    {
        cout << "Target file size too small" << endl;
        exit(1);
    }

    if (kk0 <= 16)
    {
        kk1 = gradient[kk0 - 10];
    }
    else
    {
        get_gradient();
    }

    cout << "kk0 = " << kk0 << endl;
    cout << "kk1 = " << kk1 << endl;
    plane_Q();
    down_Q(Q);
    qdq(Q);
    B = dct2bytes();
    dev = 100*fabs(B - target)/target;

    while (dev > 0.1)
    {
        cout << endl;
        cout << "Q = " << endl;
        show_Q(Q);
        cout << endl;
        cout << "Q is not yet feasible" << endl;
        cout << "bytes = " << B << endl;
        cout << "row = ";
        cin >> row;
        cout << "column = ";
        cin >> column;
        cout << "new entry = ";
        cin >> q;
        pos = 8*row + column;
        Q[pos] = q;
        down_Q(Q);
```

```
        qdq(Q);
        B = dct2bytes();
        dev = 100*fabs(B - target)/target;
    }

    cout << endl;
    cout << "Q is now feasible" << endl;

    if (atoi(argv[2]) == 1)
    {
        // feasible Q is first member of old_pop
        copy_table(Q, old_pop[0]);
        // fill in rest of old_pop
        for (k = 1 ; k < pop_size ; k++)
        {
            for (pos = 0 ; pos < 64 ; pos++)
            {
                x = rand();
                x = x/RAND_MAX;
                old_pop[k][pos] = Q[pos] + int(round(2*lower*x - lower));
                old_pop[k][pos] = int(fmax(old_pop[k][pos], 1));
                old_pop[k][pos] = int(fmin(old_pop[k][pos], 255));
            }
        }
        cout << "Q = " << endl;
        show_Q(Q);
        cout << endl;
        cout << "Running Genetic Algorithm" << endl;
        ga();
    }

L1:
    cout << "initial table = " << endl;
    show_Q(Q);

// quantise and dequantise Y

    down_Q(Q);
    qdq(Q);

// calculate error

    E = calc_error();
    cout << "Error = " << E << endl;

// calculate bytes

    B = dct2bytes();
    cout << "bytes = " << B << endl;

// main algorithm
    Rmax = INFINITY; Rmin = 0;

    while (Rmax > Rmin)
```

```
{
    if (B < target)
    {
        best_lambda = 0;
        for (pos = 0 ; pos < 28 ; pos++)
        {
            qq = Q[z[pos]];
            qqq = int(fmax(qq - lower, 1));
            for (q = qqq ; q < qq ; q++)
            {
                // replace current value with q
                Q[z[pos]] = q;
                down_Q(Q);
                // quantise and dequantise Y
                qdq(Q);
                // calculate best improvement
                nu_E = calc_error();
                nu_B = dct2bytes();
                lambda = (E - nu_E)/(nu_B - B);
                if (lambda == INFINITY)
                {
                    best_pos = pos;
                    best_q = q;
                    best_E = nu_E;
                    best_B = nu_B;
                    Rmax = lambda;
                    cout << "freebie found" << endl;
                    goto found;
                }
                if (isnan(lambda))
                {
                    break;
                }
                if (lambda > best_lambda)
                {
                    best_lambda = lambda;
                    best_pos = pos;
                    best_q = q;
                    best_E = nu_E;
                    best_B = nu_B;
                }
            }
            // revert back to original value
            Q[z[pos]] = qq;
            down_Q(Q);
        }
        for (pos = 28 ; pos < 64 ; pos++)
        {
            qq = Q[z[pos]];
            qqq = int(fmax(qq - upper, 1));
            for (q = qqq ; q < qq ; q++)
            {
                // replace current value with q
                Q[z[pos]] = q;
```

```
                down_Q(Q);
                // quantise and dequantise Y
                qdq(Q);
                // calculate best improvement
                nu_E = calc_error();
                nu_B = dct2bytes();
                lambda = (E - nu_E)/(nu_B - B);
                if (lambda == INFINITY)
                {
                    best_pos = pos;
                    best_q = q;
                    best_E = nu_E;
                    best_B = nu_B;
                    Rmax = lambda;
                    cout << "freebie found" << endl;
                    goto found;
                }
                if (isnan(lambda))
                {
                    break;
                }
                if (lambda > best_lambda)
                {
                    best_lambda = lambda;
                    best_pos = pos;
                    best_q = q;
                    best_E = nu_E;
                    best_B = nu_B;
                }
            }
            // revert back to original value
            Q[z[pos]] = qq;
            down_Q(Q);
        }
        Rmax = best_lambda;
    }
    else
    {
        best_lambda = INFINITY;
        for (pos = 0 ; pos < 28 ; pos++)
        {
            qq = Q[z[pos]];
            qqq = int(fmin(qq + lower, 255));
            for (q = qq + 1 ; q <= qqq ; q++)
            {
                // replace current value with q
                Q[z[pos]] = q;
                down_Q(Q);
                // quantise and dequantise Y
                qdq(Q);
                // calculate minimal degradation
                nu_E = calc_error();
                nu_B = dct2bytes();
                lambda = (nu_E - E)/(B - nu_B);
```

```
                    if (isnan(lambda))
                    {
                        break;
                    }
                    if ((lambda < best_lambda) && (lambda > 0))
                    {
                        best_lambda = lambda;
                        best_pos = pos;
                        best_q = q;
                        best_E = nu_E;
                        best_B = nu_B;
                    }
                }
                // revert back to original value
                Q[z[pos]] = qq;
                down_Q(Q);
            }
            for (pos = 28 ; pos < 64 ; pos++)
            {
                qq = Q[z[pos]];
                qqq = int(fmin(qq + upper, 255));
                for (q = qq + 1 ; q <= qqq ; q++)
                {
                    // replace current value with q
                    Q[z[pos]] = q;
                    down_Q(Q);
                    // quantise and dequantise Y
                    qdq(Q);
                    // calculate minimal degradation
                    nu_E = calc_error();
                    nu_B = dct2bytes();
                    lambda = (nu_E - E)/(B - nu_B);
                    if (isnan(lambda))
                    {
                        break;
                    }
                    if ((lambda < best_lambda) && (lambda > 0))
                    {
                        best_lambda = lambda;
                        best_pos = pos;
                        best_q = q;
                        best_E = nu_E;
                        best_B = nu_B;
                    }
                }
                // revert back to original value
                Q[z[pos]] = qq;
                down_Q(Q);
            }
            Rmin = best_lambda;
        }
        // update quantisation table
found:
        Q[z[best_pos]] = best_q;
```

```
        down_Q(Q);
        show_Q(Q);
        B = best_B;
        E = best_E;
        cout << "bytes = " << B << endl;
        cout << "Error = " << E << endl;
    }

    return 0;
}
```

Appendix C

Sensitivity Analysis

diag **T (bytes)**	**Widths** **B (bytes)** **PSNR**	**Widths** **B (bytes)** **PSNR**	**Widths** **B (bytes)** **PSNR**	**$lo = 1$, $hi = 1$** **B (bytes)** **PSNR**	**Initial QT** **B (bytes)** **PSNR**
10 14839	$lo = 1$, $hi = 2$ 14840 40.2454 dB			14840 40.2451 dB	14826 40.1679 dB
11 14057	$lo = 2$, $hi = 3$ 14058 39.7846 dB	$lo = 1$, $hi = 3$ 14057 39.7812 dB	$lo = 2$, $hi = 2$ 14059 39.7931 dB	14059 39.7708 dB	14064 39.7069 dB
12 13461	$lo = 2$, $hi = 4$ 13463 39.4207 dB	$lo = 1$, $hi = 4$ 13463 39.4162 dB	$lo = 2$, $hi = 3$ 13464 39.4151 dB	13461 39.4128 dB	13454 39.2889 dB
13 12664	$lo = 2$, $hi = 2$ 12664 38.8768 dB	$lo = 1$, $hi = 2$ 12665 38.8687 dB		12664 38.8626 dB	12659 38.7605 dB
14 11788	$lo = 1$, $hi = 2$ 11790 38.2526 dB			11791 38.2497 dB	11784 38.1301 dB
15 11403	$lo = 3$, $hi = 3$ 11401 37.9621 dB	$lo = 2$, $hi = 3$ 11401 37.9621 dB	$lo = 2$, $hi = 2$ 11403 37.9578 dB	11404 37.9418 dB	11408 37.8744 dB
16 10717	$lo = 3$, $hi = 4$ 10715 37.4314 dB	$lo = 2$, $hi = 4$ 10715 37.4341 dB	$lo = 3$, $hi = 3$ 10714 37.4365 dB	10718 37.4087 dB	10721 37.3230 dB
17 10468	$lo = 3$, $hi = 4$ 10466 37.2367 dB	$lo = 2$, $hi = 4$ 10469 37.2350 dB	$lo = 3$, $hi = 3$ 10468 37.2380 dB	10469 37.2205 dB	10474 37.1463 dB
18 10311	$lo = 4$, $hi = 4$ 10311 37.1028 dB	$lo = 3$, $hi = 4$ 10313 37.1095 dB	$lo = 3$, $hi = 3$ 10313 37.1097 dB	10313 37.0921 dB	10308 36.9705 dB
19 9897	$lo = 5$, $hi = 5$ 9903 36.7720 dB	$lo = 4$, $hi = 5$ 9900 36.7677 dB	$lo = 4$, $hi = 4$ 9897 36.7569 dB	9897 36.7353 dB	9904 36.6461 dB
20 9521	$lo = 4$, $hi = 5$ 9520 36.4327 dB	$lo = 3$, $hi = 5$ 9521 36.4289 dB	$lo = 4$, $hi = 4$ 9522 36.4350 dB	9521 36.4079 dB	9526 36.3228 dB

Table C.1: Results obtained for Lena (*continued on next page*)

diag **T (bytes)**	**Widths** **B (bytes)** **PSNR**	**Widths** **B (bytes)** **PSNR**	**Widths** **B (bytes)** **PSNR**	**$lo = 1$, $hi = 1$** **B (bytes)** **PSNR**	**Initial QT** **B (bytes)** **PSNR**
21	$lo = 3$, $hi = 10$	$lo = 2$, $hi = 10$	$lo = 3$, $hi = 5$		
9263	9265	9264	9261	9263	9257
	36.2086 dB	36.2050 dB	36.2039 dB	36.1861 dB	36.0683 dB
22	$lo = 2$, $hi = 15$	$lo = 1$, $hi = 15$	$lo = 2$, $hi = 10$		
9002	9000	9001	9000	9002	9009
	35.9704 dB	35.9726 dB	35.9702 dB	35.9611 dB	35.8581 dB
23	$lo = 5$, $hi = 15$	$lo = 4$, $hi = 15$	$lo = 5$, $hi = 10$		
8840	8839	8843	8842	8840	8844
	35.8244 dB	35.8212 dB	35.8289 dB	35.7931 dB	35.6769 dB
24	$lo = 5$, $hi = 30$	$lo = 4$, $hi = 30$	$lo = 5$, $hi = 25$		
8710	8711	8713	8713	8708	8709
	35.7054 dB	35.7042 dB	35.7073 dB	35.6584 dB	35.5261 dB
25	$lo = 5$, $hi = 30$	$lo = 4$, $hi = 30$	$lo = 5$, $hi = 25$		
8583	8584	8584	8584	8583	8580
	35.5964 dB	35.5929 dB	35.5905 dB	35.5376 dB	35.3902 dB
26	$lo = 4$, $hi = 20$	$lo = 3$, $hi = 20$	$lo = 4$, $hi = 15$		
8503	8506	8501	8504	8503	8498
	35.5232 dB	35.5117 dB	35.5183 dB	35.4373 dB	35.2797 dB
27	$lo = 4$, $hi = 20$	$lo = 3$, $hi = 20$	$lo = 4$, $hi = 15$		
8424	8423	8424	8424	8425	8418
	35.4522 dB	35.4519 dB	35.4576 dB	35.4077 dB	35.1557 dB
28	$lo = 4$, $hi = 20$	$lo = 3$, $hi = 20$	$lo = 4$, $hi = 15$		
8159	8160	8158	8158	8160	8154
	35.2206 dB	35.2185 dB	35.2127 dB	35.1350 dB	34.9519 dB
29	$lo = 4$, $hi = 20$	$lo = 3$, $hi = 20$	$lo = 4$, $hi = 15$		
7902	7904	7901	7899	7903	7905
	34.9658 dB	34.9628 dB	34.9638 dB	34.9135 dB	34.7320 dB
30	$lo = 8$, $hi = 20$	$lo = 7$, $hi = 20$	$lo = 8$, $hi = 15$		
7740	7738	7741	7739	7741	7736
	34.8057 dB	34.8108 dB	34.7969 dB	34.7678 dB	34.5607 dB
31	$lo = 7$, $hi = 20$	$lo = 6$, $hi = 20$	$lo = 7$, $hi = 15$		
7568	7571	7569	7572	7568	7564
	34.6355 dB	34.6400 dB	34.6391 dB	34.5272 dB	34.3963 dB
32	$lo = 7$, $hi = 25$	$lo = 6$, $hi = 25$	$lo = 7$, $hi = 20$		
7400	7403	7402	7398	7397	7402
	34.4670 dB	34.4693 dB	34.4625 dB	34.3778 dB	34.2391 dB
33	$lo = 6$, $hi = 20$	$lo = 5$, $hi = 20$	$lo = 6$, $hi = 15$		
7248	7248	7250	7250	7249	7255
	34.3136 dB	34.3089 dB	34.3163 dB	34.2457 dB	34.0867 dB
34	$lo = 6$, $hi = 20$	$lo = 5$, $hi = 20$	$lo = 6$, $hi = 15$		
7035	7036	7034	7035	7034	7035
	34.0926 dB	34.0807 dB	34.0824 dB	34.0224 dB	33.8926 dB
35	$lo = 8$, $hi = 25$	$lo = 7$, $hi = 25$	$lo = 8$, $hi = 20$		
6876	6876	6874	6874	6876	6879
	33.9161 dB	33.9154 dB	33.9154 dB	33.8301 dB	33.7172 dB
37	$lo = 6$, $hi = 15$	$lo = 5$, $hi = 15$	$lo = 6$, $hi = 10$		
6776	6774	6776	6776	6775	6782
	33.8064 dB	33.8077 dB	33.8082 dB	33.6966 dB	33.5456 dB

Table C.1: Results obtained for Lena (*continued on next page*)

diag **T (bytes)**	**Widths** **B (bytes)** **PSNR**	**Widths** **B (bytes)** **PSNR**	**Widths** **B (bytes)** **PSNR**	**$lo = 1$, $hi = 1$** **B (bytes)** **PSNR**	**Initial QT** **B (bytes)** **PSNR**
38	$lo = 7$, $hi = 35$	$lo = 6$, $hi = 35$	$lo = 7$, $hi = 30$		
6667	6667	6668	6668	6667	6662
	33.6782 dB	33.6745 dB	33.6755 dB	33.5571 dB	33.4058 dB
39	$lo = 7$, $hi = 35$	$lo = 6$, $hi = 35$	$lo = 7$, $hi = 30$		
6508	6508	6508	6510	6509	6503
	33.4900 dB	33.5007 dB	33.4824 dB	33.3657 dB	33.2580 dB
40	$lo = 7$, $hi = 35$	$lo = 6$, $hi = 35$	$lo = 7$, $hi = 30$		
6377	6377	6377	6375	6379	6373
	33.3299 dB	33.3370 dB	33.3337 dB	33.2355 dB	33.1112 dB
41	$lo = 11$, $hi = 35$	$lo = 10$, $hi = 35$	$lo = 11$, $hi = 30$		
6304	6306	6303	6306	6305	6305
	33.2503 dB	33.2484 dB	33.2545 dB	33.1244 dB	33.0098 dB
42	$lo = 6$, $hi = 35$	$lo = 5$, $hi = 35$	$lo = 6$, $hi = 30$		
6260	6260	6262	6262	6259	6262
	33.1920 dB	33.2034 dB	33.1994 dB	33.1037 dB	32.9432 dB
43	$lo = 7$, $hi = 35$	$lo = 6$, $hi = 35$	$lo = 7$, $hi = 30$		
6193	6193	6192	6193	6190	6190
	33.1211 dB	33.1201 dB	33.1204 dB	33.0059 dB	32.8594 dB
44	$lo = 6$, $hi = 35$	$lo = 5$, $hi = 35$	$lo = 6$, $hi = 30$		
6150	6151	6148	6153	6151	6147
	33.0743 dB	33.0624 dB	33.0722 dB	32.9700 dB	32.7913 dB
45	$lo = 12$, $hi = 35$	$lo = 11$, $hi = 35$	$lo = 12$, $hi = 30$		
6056	6056	6056	6058	6056	6052
	32.9580 dB	32.9569 dB	32.9617 dB	32.8752 dB	32.7030 dB
46	$lo = 9$, $hi = 35$	$lo = 8$, $hi = 35$	$lo = 9$, $hi = 30$		
5940	5939	5938	5942	5941	5940
	32.8278 dB	32.8259 dB	32.8251 dB	32.7364 dB	32.5864 dB
47	$lo = 9$, $hi = 35$	$lo = 8$, $hi = 35$	$lo = 9$, $hi = 30$		
5859	5862	5861	5860	5856	5863
	32.7413 dB	32.7271 dB	32.7282 dB	32.6394 dB	32.4889 dB
48	$lo = 14$, $hi = 35$	$lo = 13$, $hi = 35$	$lo = 14$, $hi = 30$		
5840	5842	5840	5839	5843	5842
	32.7077 dB	32.7082 dB	32.7071 dB	32.6174 dB	32.4459 dB
49	$lo = 8$, $hi = 35$	$lo = 7$, $hi = 35$	$lo = 8$, $hi = 30$		
5658	5657	5660	5658	5658	5656
	32.4900 dB	32.4927 dB	32.4906 dB	32.4151 dB	32.2707 dB
50	$lo = 9$, $hi = 35$	$lo = 8$, $hi = 35$	$lo = 9$, $hi = 30$		
5549	5549	5549	5548	5549	5546
	32.3637 dB	32.3641 dB	32.3640 dB	32.2455 dB	32.1367 dB
51	$lo = 10$, $hi = 35$	$lo = 9$, $hi = 35$	$lo = 10$, $hi = 30$		
5448	5447	5449	5449	5449	5446
	32.2268 dB	32.2376 dB	32.2345 dB	32.1325 dB	31.9864 dB
52	$lo = 8$, $hi = 35$	$lo = 7$, $hi = 35$	$lo = 8$, $hi = 30$		
5216	5218	5218	5216	5218	5220
	31.9223 dB	31.9299 dB	31.9215 dB	31.8341 dB	31.7472 dB
53	$lo = 9$, $hi = 35$	$lo = 8$, $hi = 35$	$lo = 9$, $hi = 30$		
5106	5108	5104	5108	5106	5106
	31.7650 dB	31.7678 dB	31.7792 dB	31.6692 dB	31.6148 dB

Table C.1: Results obtained for Lena (*continued on next page*)

diag **T (bytes)**	**Widths** **B (bytes)** **PSNR**	**Widths** **B (bytes)** **PSNR**	**Widths** **B (bytes)** **PSNR**	**$lo = 1$, $hi = 1$** **B (bytes)** **PSNR**	**Initial QT** **B (bytes)** **PSNR**
54	$lo = 9$, $hi = 35$	$lo = 8$, $hi = 35$	$lo = 9$, $hi = 30$		
4979	4981	4977	4977	4979	4976
	31.5955 dB	31.5888 dB	31.5892 dB	31.4953 dB	31.4324 dB

Table C.1: Results obtained for Lena (*continued*)

diag **T (bytes)**	**Widths** **B (bytes)** **PSNR**	**Widths** **B (bytes)** **PSNR**	**Widths** **B (bytes)** **PSNR**	**$lo = 1$, $hi = 1$** **B (bytes)** **PSNR**	**Initial QT** **B (bytes)** **PSNR**
10	$lo = 1$, $hi = 2$				
17157	17159			17162	17171
	40.0746 dB			40.0840 dB	40.0195 dB
11	$lo = 2$, $hi = 2$	$lo = 1$, $hi = 2$			
15904	15901	15909		15907	15919
	39.2636 dB	39.2660 dB		39.2652 dB	39.1971 dB
12	$lo = 1$, $hi = 2$				
15464	15466			15465	15465
	38.9686 dB			38.9785 dB	38.8582 dB
13	$lo = 2$, $hi = 3$	$lo = 1$, $hi = 3$	$lo = 2$, $hi = 2$		
14392	14389	14395	14394	14394	14387
	38.2095 dB	38.2098 dB	38.2111 dB	38.1959 dB	38.1417 dB
14	$lo = 3$, $hi = 3$	$lo = 2$, $hi = 3$	$lo = 2$, $hi = 2$		
14016	14018	14016	14016	14014	14021
	37.9440 dB	37.9377 dB	37.9377 dB	37.9255 dB	37.8460 dB
15	$lo = 3$, $hi = 4$	$lo = 2$, $hi = 4$	$lo = 3$, $hi = 3$		
13164	13164	13163	13163	13165	13161
	37.3267 dB	37.3288 dB	37.3303 dB	37.3128 dB	37.2064 dB
16	$lo = 3$, $hi = 5$	$lo = 2$, $hi = 5$	$lo = 3$, $hi = 4$		
12890	12892	12893	12893	12892	12881
	37.1232 dB	37.1231 dB	37.1213 dB	37.1094 dB	36.9651 dB
17	$lo = 3$, $hi = 10$	$lo = 2$, $hi = 10$	$lo = 3$, $hi = 5$		
12300	12300	12303	12298	12299	12307
	36.6536 dB	36.6485 dB	36.6465 dB	36.6302 dB	36.5301 dB
18	$lo = 3$, $hi = 5$	$lo = 2$, $hi = 5$	$lo = 3$, $hi = 4$		
11744	11744	11746	11745	11744	11744
	36.1948 dB	36.1825 dB	36.1908 dB	36.1807 dB	36.0884 dB
19	$lo = 4$, $hi = 4$	$lo = 3$, $hi = 4$	$lo = 3$, $hi = 3$		
11395	11395	11395	11395	11396	11404
	35.8913 dB	35.8913 dB	35.8913 dB	35.8732 dB	35.7922 dB
20	$lo = 4$, $hi = 4$	$lo = 3$, $hi = 4$	$lo = 3$, $hi = 3$		
11131	11134	11131	11129	11131	11134
	35.6635 dB	35.6561 dB	35.6497 dB	35.6293 dB	35.5265 dB
21	$lo = 4$, $hi = 5$	$lo = 3$, $hi = 5$	$lo = 4$, $hi = 4$		
10745	10746	10744	10746	10744	10742
	35.2977 dB	35.2886 dB	35.2974 dB	35.2720 dB	35.1813 dB

Table C.2: Results obtained for Plane (*continued on next page*)

diag **T (bytes)**	**Widths** **B (bytes)** **PSNR**	**Widths** **B (bytes)** **PSNR**	**Widths** **B (bytes)** **PSNR**	**$lo = 1$, $hi = 1$** **B (bytes)** **PSNR**	**Initial QT** **B (bytes)** **PSNR**
22	$lo = 4$, $hi = 10$	$lo = 3$, $hi = 10$	$lo = 4$, $hi = 5$		
10505	10506	10506	10505	10508	10506
	35.0820 dB	35.0807 dB	35.0850 dB	35.0322 dB	34.9395 dB
23	$lo = 4$, $hi = 10$	$lo = 3$, $hi = 10$	$lo = 4$, $hi = 5$		
10346	10343	10346	10346	10347	10350
	34.9386 dB	34.9291 dB	34.9325 dB	34.8856 dB	34.7462 dB
24	$lo = 5$, $hi = 5$	$lo = 4$, $hi = 5$	$lo = 4$, $hi = 4$		
10099	10098	10098	10102	10099	10098
	34.7350 dB	34.7299 dB	34.7307 dB	34.6676 dB	34.5145 dB
25	$lo = 4$, $hi = 5$	$lo = 3$, $hi = 5$	$lo = 4$, $hi = 4$		
9947	9947	9948	9949	9945	9945
	34.5924 dB	34.5860 dB	34.5912 dB	34.5316 dB	34.3365 dB
26	$lo = 5$, $hi = 15$	$lo = 4$, $hi = 15$	$lo = 5$, $hi = 10$		
9806	9807	9805	9805	9808	9799
	34.4666 dB	34.4600 dB	34.4628 dB	34.4012 dB	34.1586 dB
27	$lo = 7$, $hi = 10$	$lo = 6$, $hi = 10$	$lo = 5$, $hi = 5$		
9608	9609	9607	9606	9606	9607
	34.2916 dB	34.2796 dB	34.2818 dB	34.1863 dB	33.9619 dB
28	$lo = 7$, $hi = 10$	$lo = 6$, $hi = 10$	$lo = 5$, $hi = 5$		
9314	9313	9313	9315	9315	9308
	34.0187 dB	34.0200 dB	34.0161 dB	33.9351 dB	33.7317 dB
29	$lo = 5$, $hi = 20$	$lo = 4$, $hi = 20$	$lo = 5$, $hi = 15$		
9226	9225	9226	9224	9227	9225
	33.9416 dB	33.9459 dB	33.9399 dB	33.8426 dB	33.5783 dB
30	$lo = 7$, $hi = 30$	$lo = 6$, $hi = 30$	$lo = 7$, $hi = 25$		
8853	8853	8852	8855	8852	8853
	33.5802 dB	33.5748 dB	33.5832 dB	33.5133 dB	33.3150 dB
31	$lo = 6$, $hi = 25$	$lo = 5$, $hi = 25$	$lo = 6$, $hi = 20$		
8689	8688	8688	8692	8690	8694
	33.4168 dB	33.4131 dB	33.4153 dB	33.3391 dB	33.1584 dB
32	$lo = 5$, $hi = 15$	$lo = 4$, $hi = 15$	$lo = 5$, $hi = 10$		
8540	8540	8541	8539	8540	8543
	33.2718 dB	33.2580 dB	33.2618 dB	33.1482 dB	33.0094 dB
33	$lo = 6$, $hi = 15$	$lo = 5$, $hi = 15$	$lo = 6$, $hi = 10$		
8319	8320	8317	8321	8320	8325
	33.0640 dB	33.0551 dB	33.0612 dB	32.9461 dB	32.8107 dB
34	$lo = 7$, $hi = 30$	$lo = 6$, $hi = 30$	$lo = 7$, $hi = 25$		
8106	8106	8105	8104	8107	8112
	32.8597 dB	32.8596 dB	32.8561 dB	32.7579 dB	32.6145 dB
35	$lo = 4$, $hi = 20$	$lo = 3$, $hi = 20$	$lo = 4$, $hi = 15$		
7881	7879	7882	7882	7881	7879
	32.6401 dB	32.6295 dB	32.6374 dB	32.5312 dB	32.4026 dB
36	$lo = 5$, $hi = 25$	$lo = 4$, $hi = 25$	$lo = 5$, $hi = 20$		
7740	7741	7741	7741	7740	7742
	32.5103 dB	32.5097 dB	32.5112 dB	32.4058 dB	32.2680 dB
37	$lo = 6$, $hi = 20$	$lo = 5$, $hi = 20$	$lo = 6$, $hi = 15$		
7706	7704	7705	7707	7705	7707
	32.4714 dB	32.4776 dB	32.4722 dB	32.3725 dB	32.2147 dB

Table C.2: Results obtained for Plane (*continued on next page*)

diag **T (bytes)**	**Widths** **B (bytes)** **PSNR**	**Widths** **B (bytes)** **PSNR**	**Widths** **B (bytes)** **PSNR**	**$lo = 1$, $hi = 1$** **B (bytes)** **PSNR**	**Initial QT** **B (bytes)** **PSNR**
38	$lo = 8$, $hi = 20$	$lo = 7$, $hi = 20$	$lo = 8$, $hi = 15$		
7565	7567	7567	7564	7565	7566
	32.3397 dB	32.3316 dB	32.3365 dB	32.2226 dB	32.0789 dB
39	$lo = 9$, $hi = 20$	$lo = 8$, $hi = 20$	$lo = 9$, $hi = 15$		
7337	7336	7338	7337	7334	7338
	32.1127 dB	32.1063 dB	32.1158 dB	32.0184 dB	31.8930 dB
40	$lo = 9$, $hi = 20$	$lo = 8$, $hi = 20$	$lo = 9$, $hi = 15$		
7233	7235	7233	7234	7234	7232
	32.0258 dB	32.0254 dB	32.0107 dB	31.8999 dB	31.7739 dB
41	$lo = 9$, $hi = 20$	$lo = 8$, $hi = 20$	$lo = 9$, $hi = 15$		
7142	7142	7140	7144	7141	7140
	31.9298 dB	31.9233 dB	31.9257 dB	31.7743 dB	31.6551 dB
42	$lo = 9$, $hi = 25$	$lo = 8$, $hi = 25$	$lo = 9$, $hi = 20$		
7031	7032	7030	7030	7032	7032
	31.8140 dB	31.8154 dB	31.8124 dB	31.6391 dB	31.5497 dB
43	$lo = 9$, $hi = 25$	$lo = 8$, $hi = 25$	$lo = 9$, $hi = 20$		
6918	6919	6920	6919	6918	6920
	31.7029 dB	31.7013 dB	31.7009 dB	31.5870 dB	31.4594 dB
44	$lo = 9$, $hi = 30$	$lo = 8$, $hi = 30$	$lo = 9$, $hi = 25$		
6840	6839	6839	6840	6840	6836
	31.6230 dB	31.6141 dB	31.6195 dB	31.5051 dB	31.3690 dB
45	$lo = 9$, $hi = 20$	$lo = 8$, $hi = 20$	$lo = 9$, $hi = 15$		
6755	6755	6757	6757	6756	6757
	31.5233 dB	31.5334 dB	31.5281 dB	31.4201 dB	31.2799 dB
46	$lo = 9$, $hi = 25$	$lo = 8$, $hi = 25$	$lo = 9$, $hi = 20$		
6623	6623	6625	6622	6622	6628
	31.3844 dB	31.3824 dB	31.3840 dB	31.2923 dB	31.1486 dB
47	$lo = 9$, $hi = 25$	$lo = 8$, $hi = 25$	$lo = 9$, $hi = 20$		
6534	6535	6535	6534	6534	6538
	31.2896 dB	31.2919 dB	31.2894 dB	31.1657 dB	31.0355 dB
49	$lo = 8$, $hi = 25$	$lo = 7$, $hi = 25$	$lo = 8$, $hi = 20$		
6421	6420	6420	6423	6420	6417
	31.1682 dB	31.1694 dB	31.1682 dB	31.0396 dB	30.8816 dB
50	$lo = 8$, $hi = 25$	$lo = 7$, $hi = 25$	$lo = 8$, $hi = 20$		
6286	6286	6285	6289	6286	6281
	31.0317 dB	31.0273 dB	31.0265 dB	30.8961 dB	30.7621 dB
51	$lo = 9$, $hi = 25$	$lo = 8$, $hi = 25$	$lo = 9$, $hi = 20$		
6100	6101	6101	6099	6100	6103
	30.8228 dB	30.8262 dB	30.8209 dB	30.6801 dB	30.5947 dB
52	$lo = 12$, $hi = 30$	$lo = 11$, $hi = 30$	$lo = 12$, $hi = 25$		
5955	5957	5955	5955	5955	5955
	30.6633 dB	30.6668 dB	30.6610 dB	30.5373 dB	30.4477 dB
53	$lo = 14$, $hi = 30$	$lo = 13$, $hi = 30$	$lo = 14$, $hi = 25$		
5847	5846	5848	5848	5847	5844
	30.5416 dB	30.5395 dB	30.5353 dB	30.4061 dB	30.3323 dB

Table C.2: Results obtained for Plane (*continued*)

diag **T (bytes)**	**Widths** **B (bytes)** **PSNR**	**Widths** **B (bytes)** **PSNR**	**Widths** **B (bytes)** **PSNR**	**$lo = 1$, $hi = 1$** **B (bytes)** **PSNR**	**Initial QT** **B (bytes)** **PSNR**
10	$lo = 2$, $hi = 2$	$lo = 1$, $hi = 2$			
25200	25198	25203		25201	25220
	39.1426 dB	39.1328 dB		39.1437 dB	39.0200 dB
11	$lo = 2$, $hi = 2$	$lo = 1$, $hi = 2$			
23776	23775	23775		23775	23791
	38.1606 dB	38.1454 dB		38.1454 dB	38.0644 dB
12	$lo = 3$, $hi = 3$	$lo = 2$, $hi = 3$	$lo = 2$, $hi = 2$		
23200	23200	23202	23202	23197	23211
	37.7483 dB	37.7503 dB	37.7503 dB	37.7519 dB	37.6089 dB
13	$lo = 2$, $hi = 4$	$lo = 1$, $hi = 4$	$lo = 2$, $hi = 3$		
22080	22082	22075	22082	22084	22094
	36.9383 dB	36.9266 dB	36.9417 dB	36.9246 dB	36.8556 dB
14	$lo = 2$, $hi = 3$	$lo = 1$, $hi = 3$	$lo = 2$, $hi = 2$		
21416	21420	21420	21413	21420	21422
	36.4666 dB	36.4752 dB	36.4656 dB	36.4570 dB	36.3522 dB
15	$lo = 3$, $hi = 4$	$lo = 2$, $hi = 4$	$lo = 3$, $hi = 3$		
20633	20634	20637	20632	20628	20630
	35.9281 dB	35.9299 dB	35.9203 dB	35.9069 dB	35.8157 dB
16	$lo = 4$, $hi = 4$	$lo = 3$, $hi = 4$	$lo = 3$, $hi = 3$		
20070	20073	20076	20076	20076	20060
	35.5671 dB	35.5684 dB	35.5684 dB	35.5493 dB	35.3665 dB
17	$lo = 4$, $hi = 4$	$lo = 3$, $hi = 4$	$lo = 3$, $hi = 3$		
19426	19423	19425	19424	19427	19407
	35.1241 dB	35.1320 dB	35.1314 dB	35.1078 dB	34.9382 dB
18	$lo = 3$, $hi = 15$	$lo = 2$, $hi = 15$	$lo = 3$, $hi = 10$		
18533	18536	18530	18534	18535	18542
	34.5156 dB	34.5140 dB	34.5149 dB	34.5059 dB	34.4017 dB
19	$lo = 4$, $hi = 15$	$lo = 3$, $hi = 15$	$lo = 4$, $hi = 10$		
18029	18028	18032	18029	18028	18013
	34.1848 dB	34.1878 dB	34.1875 dB	34.1563 dB	34.0434 dB
20	$lo = 3$, $hi = 10$	$lo = 2$, $hi = 10$	$lo = 3$, $hi = 5$		
17416	17417	17419	17417	17414	17423
	33.7853 dB	33.7908 dB	33.7888 dB	33.7609 dB	33.6773 dB
21	$lo = 3$, $hi = 10$	$lo = 2$, $hi = 10$	$lo = 3$, $hi = 5$		
16824	16824	16824	16823	16822	16829
	33.4110 dB	33.4033 dB	33.4081 dB	33.3904 dB	33.3028 dB
22	$lo = 3$, $hi = 10$	$lo = 2$, $hi = 10$	$lo = 3$, $hi = 5$		
16328	16329	16327	16328	16328	16330
	33.0948 dB	33.0945 dB	33.0979 dB	33.0623 dB	32.9790 dB
23	$lo = 3$, $hi = 10$	$lo = 2$, $hi = 10$	$lo = 3$, $hi = 5$		
15951	15954	15952	15954	15952	15953
	32.8579 dB	32.8577 dB	32.8627 dB	32.8270 dB	32.7277 dB
24	$lo = 5$, $hi = 10$	$lo = 4$, $hi = 10$	$lo = 5$, $hi = 5$		
15688	15690	15691	15691	15690	15678
	32.6890 dB	32.6820 dB	32.6871 dB	32.6572 dB	32.4897 dB
25	$lo = 4$, $hi = 15$	$lo = 3$, $hi = 15$	$lo = 4$, $hi = 10$		
15358	15360	15360	15361	15358	15354
	32.4709 dB	32.4706 dB	32.4719 dB	32.4493 dB	32.2726 dB

Table C.3: Results obtained for Bridge (*continued on next page*)

diag **T (bytes)**	**Widths** **B (bytes)** **PSNR**	**Widths** **B (bytes)** **PSNR**	**Widths** **B (bytes)** **PSNR**	**$lo = 1$, $hi = 1$** **B (bytes)** **PSNR**	**Initial QT** **B (bytes)** **PSNR**
26	$lo = 5$, $hi = 10$	$lo = 4$, $hi = 10$	$lo = 5$, $hi = 5$		
14991	14990	14990	14991	14993	14986
	32.2428 dB	32.2420 dB	32.2418 dB	32.2285 dB	32.0404 dB
27	$lo = 5$, $hi = 10$	$lo = 4$, $hi = 10$	$lo = 5$, $hi = 5$		
14600	14598	14599	14597	14601	14599
	32.0002 dB	31.9979 dB	31.9956 dB	31.9744 dB	31.8195 dB
28	$lo = 4$, $hi = 10$	$lo = 3$, $hi = 10$	$lo = 4$, $hi = 5$		
14192	14191	14193	14190	14191	14191
	31.7487 dB	31.7511 dB	31.7442 dB	31.7050 dB	31.5712 dB
29	$lo = 6$, $hi = 10$	$lo = 5$, $hi = 10$	$lo = 5$, $hi = 5$		
13971	13973	13971	13971	13972	13968
	31.6133 dB	31.6120 dB	31.6024 dB	31.5727 dB	31.3894 dB
30	$lo = 6$, $hi = 10$	$lo = 5$, $hi = 10$	$lo = 5$, $hi = 5$		
13515	13516	13517	13514	13515	13515
	31.3203 dB	31.3249 dB	31.3108 dB	31.2743 dB	31.1450 dB
31	$lo = 6$, $hi = 10$	$lo = 5$, $hi = 10$	$lo = 5$, $hi = 5$		
13252	13250	13251	13251	13249	13251
	31.1517 dB	31.1521 dB	31.1523 dB	31.1172 dB	30.9512 dB
32	$lo = 5$, $hi = 10$	$lo = 4$, $hi = 10$	$lo = 5$, $hi = 5$		
12836	12836	12835	12836	12837	12838
	30.9172 dB	30.9113 dB	30.8992 dB	30.8491 dB	30.7461 dB
33	$lo = 6$, $hi = 10$	$lo = 5$, $hi = 10$	$lo = 5$, $hi = 5$		
12530	12530	12530	12529	12530	12533
	30.7309 dB	30.7259 dB	30.7089 dB	30.6710 dB	30.5557 dB
34	$lo = 6$, $hi = 25$	$lo = 5$, $hi = 25$	$lo = 6$, $hi = 20$		
12315	12316	12318	12312	12316	12321
	30.6110 dB	30.6126 dB	30.6098 dB	30.4998 dB	30.4091 dB
35	$lo = 9$, $hi = 20$	$lo = 8$, $hi = 20$	$lo = 9$, $hi = 15$		
11932	11935	11933	11935	11930	11928
	30.3820 dB	30.3813 dB	30.3835 dB	30.2781 dB	30.1846 dB
36	$lo = 6$, $hi = 15$	$lo = 5$, $hi = 15$	$lo = 6$, $hi = 10$		
11632	11634	11633	11632	11631	11635
	30.2028 dB	30.2019 dB	30.2018 dB	30.1077 dB	29.9998 dB
37	$lo = 5$, $hi = 20$	$lo = 4$, $hi = 20$	$lo = 5$, $hi = 15$		
11482	11484	11483	11480	11481	11484
	30.1227 dB	30.1050 dB	30.1222 dB	30.0434 dB	29.9193 dB
38	$lo = 7$, $hi = 15$	$lo = 6$, $hi = 15$	$lo = 7$, $hi = 10$		
11209	11205	11208	11212	11212	11212
	29.9593 dB	29.9608 dB	29.9568 dB	29.8811 dB	29.7610 dB
39	$lo = 7$, $hi = 15$	$lo = 6$, $hi = 15$	$lo = 7$, $hi = 10$		
11000	11002	11000	11001	11003	11002
	29.8518 dB	29.8456 dB	29.8316 dB	29.7500 dB	29.6408 dB
40	$lo = 6$, $hi = 30$	$lo = 5$, $hi = 30$	$lo = 6$, $hi = 25$		
10745	10745	10747	10747	10744	10751
	29.7046 dB	29.7000 dB	29.6943 dB	29.5746 dB	29.4891 dB
41	$lo = 6$, $hi = 30$	$lo = 5$, $hi = 30$	$lo = 6$, $hi = 25$		
10506	10508	10506	10506	10506	10505
	29.5610 dB	29.5608 dB	29.5605 dB	29.4155 dB	29.3434 dB

Table C.3: Results obtained for Bridge (*continued on next page*)

diag **T (bytes)**	**Widths** **B (bytes)** **PSNR**	**Widths** **B (bytes)** **PSNR**	**Widths** **B (bytes)** **PSNR**	**$lo = 1$, $hi = 1$** **B (bytes)** **PSNR**	**Initial QT** **B (bytes)** **PSNR**
42	$lo = 6$, $hi = 20$	$lo = 5$, $hi = 20$	$lo = 6$, $hi = 15$		
10358	10360	10361	10360	10357	10356
	29.4686 dB	29.4656 dB	29.4713 dB	29.3565 dB	29.2620 dB
43	$lo = 7$, $hi = 20$	$lo = 6$, $hi = 20$	$lo = 7$, $hi = 15$		
10207	10208	10207	10206	10209	10215
	29.3804 dB	29.3752 dB	29.3726 dB	29.2582 dB	29.1901 dB
44	$lo = 7$, $hi = 20$	$lo = 6$, $hi = 20$	$lo = 7$, $hi = 15$		
10069	10071	10070	10071	10069	10065
	29.2920 dB	29.2990 dB	29.3052 dB	29.1843 dB	29.0908 dB
45	$lo = 7$, $hi = 30$	$lo = 6$, $hi = 30$	$lo = 7$, $hi = 25$		
9909	9907	9910	9907	9910	9906
	29.2006 dB	29.2164 dB	29.2072 dB	29.0955 dB	29.0054 dB
46	$lo = 7$, $hi = 25$	$lo = 6$, $hi = 25$	$lo = 7$, $hi = 20$		
9740	9741	9738	9742	9741	9736
	29.1037 dB	29.1135 dB	29.1009 dB	29.0113 dB	28.8878 dB
47	$lo = 7$, $hi = 25$	$lo = 6$, $hi = 25$	$lo = 7$, $hi = 20$		
9550	9551	9551	9549	9550	9548
	28.9928 dB	28.9902 dB	28.9884 dB	28.8778 dB	28.7747 dB
48	$lo = 8$, $hi = 20$	$lo = 7$, $hi = 20$	$lo = 8$, $hi = 15$		
9472	9471	9471	9473	9472	9471
	28.9471 dB	28.9500 dB	28.9391 dB	28.8431 dB	28.7284 dB
49	$lo = 8$, $hi = 20$	$lo = 7$, $hi = 20$	$lo = 8$, $hi = 15$		
9150	9147	9152	9153	9148	9147
	28.7371 dB	28.7406 dB	28.7406 dB	28.6529 dB	28.5747 dB
50	$lo = 9$, $hi = 30$	$lo = 8$, $hi = 30$	$lo = 9$, $hi = 25$		
8987	8988	8986	8986	8988	8987
	28.6499 dB	28.6329 dB	28.6457 dB	28.5466 dB	28.4533 dB
51	$lo = 9$, $hi = 25$	$lo = 8$, $hi = 25$	$lo = 9$, $hi = 20$		
8672	8672	8674	8673	8673	8672
	28.4536 dB	28.4360 dB	28.4580 dB	28.3292 dB	28.2591 dB

Table C.3: Results obtained for Bridge (*continued*)

Bibliography

[1] Hei Tao Fung and Kevin J. Parker. Design of image-adaptive quantization tables for JPEG. *Journal of Electronic Imaging*, 4(2):144–150, 1995.

[2] Siu-Wai Wu and Allen Gersho. Rate-constrained picture-adaptive quantization for JPEG baseline coders. In *IEEE International Conference on Acoustics, Speech and Signal Processing*, volume 5, pages 365–368, 1993.

[3] Viresh Ratnakar and Miron Livny. RD-OPT: An efficient algorithm for optimizing DCT quantization tables. In *Data Compression Conference*, pages 332–341, 1995.

[4] Viresh Ratnakar and Miron Livny. RD-OPT: An efficient algorithm for optimizing DCT quantization. *IEEE Transactions on Image Processing*, 9(2):267–270, 2000.

[5] William B. Pennebaker and Joan L. Mitchell. *JPEG: Still Image Data Compression Standard*. Van Nostrand Reinhold, New York, 1993.

[6] Tinku Acharya and Ping-Sing Tsai. *JPEG2000: Standard for Image Compression*. Wiley-Interscience, New Jersey, 2005.

[7] Jerome M. Shapiro. Embedded image coding using zerotrees of wavelet coefficients. *IEEE Transactions on Signal Processing*, 41:3445–3459, 1993.

[8] Marina Bosi and Richard E. Goldberg. *Introduction to Digital Audio Coding and Standards*. Springer, New York, 2003.

[9] Ken C. Pohlmann. *Principles of Digital Audio*. McGraw-Hill, New York, 1995.

[10] John P. Princen and Alan Bernard Bradley. Analysis/synthesis filter bank design based on time domain aliasing cancellation. *IEEE Transactions on Accoustics, Speech, and Signal Processing*, ASSP-34(5):1153–1161, 1986.

[11] Chi-Min Liu and Wen-Chieh Lee. A unified fast algorithm for cosine modulated filter banks in current audio coding standards. *Journal of the Audio Engineering Society*, 47:1061–1075, 1999.

[12] International Telecommunications Union, Radiocommunications Sector, Geneva. *Methods for the Subjective Assessment of Small Impairments in Audio Systems Including Multichannel Sound Systems*, 1997. BS.1116 (rev. 1).

[13] Floris L. Van Nes and Maarten A. Bouman. Spatial modulation transfer in the human eye. *Journal of the Optical Society of America*, 57(3):401–406, 1967.

[14] Kathy T. Mullen. The contrast sensitivity of human colour vision to red–green and blue–yellow chromatic gratings. *Journal of Physiology*, 359:381–400, 1985.

[15] Albert J. Ahumada and Heidi A. Peterson. Luminance-model-based DCT quantization for color image compression. In *SPIE conference on Human Vision, Visual Processing, and Digital Display III*, volume 1666, pages 365–374, 1992.

[16] Albert J. Ahumada Heidi A. Peterson and Andrew B. Watson. An improved detection model for DCT coefficient quantization. In *SPIE conference on Human Vision, Visual Processing, and Digital Display IV*, volume 1913, pages 191–201, 1993.

[17] Andrew B. Watson. DCTune: A technique for visual optimization of DCT quantization matrices for individual images. *Society for Information Display Digest of Technical Papers*, XXIV:946–949, 1993.

[18] Andrew B. Watson. Visually optimal DCT quantization matrices for individual images. In *Data Compression Conference*, pages 178–187, 1993.

[19] Andrew B. Watson. DCT quantization matrices visually optimized for individual images. In *SPIE conference on Human Vision, Visual Processing, and Digital Display IV*, volume 1913, pages 202–216, 1993.

[20] Albert J. Ahumada Andrew B. Watson, Alan Gale and Joshua A. Solomon. DCT basis function visibility: Effects of viewing distance and contrast masking. In *SPIE conference on Human Vision, Visual Processing, and Digital Display IV*, pages 99–108, 1994.

[21] Andrew B. Watson Joshua A. Solomon and Albert J. Ahumada. Visibility of DCT basis functions: Effects of contrast masking. In *Data Compression Conference*, pages 361–370, 1994.

[22] Ingo Höntsch and Lina J. Karam. Adaptive image coding with perceptual distortion control. *IEEE Transactions on Image Processing*, 11(3):213–222, 2002.

[23] Trac Duy Tran and Robert Safranek. A locally adaptive perceptual masking threshold model for image coding. In *Proceedings of the IEEE International Conference on Acoustics, Speech and Signal Processing*, volume 4, pages 1882–1885, 1996.

[24] Trac Duy Tran. A locally adaptive perceptual masking threshold model for image coding. Master's thesis, Massachusetts Institute of Technology, 1994.

[25] S. J. P. Westen, R. L. Lagendijk, and J. Biemond. Optimization of JPEG color image coding using a human visual system model. In *SPIE conference on Human Vision and Electronic Imaging*, volume 2657, pages 370–381, 1996.

[26] Melanie Mitchell. *An Introduction to Genetic Algorithms*. The MIT Press, Massachusetts, 1996.

[27] M. H. Afshar and M. A. Mariño. A parameter-free self-adapting boundary genetic search for pipe network optimization. *Computational Optimization and Applications*, 37:83–102, 2007.

[28] C. T. Kelly. *Iterative Methods for Optimization*. Society for Industrial and Applied Mathematics, Philadelphia, 1999.

[29] Matthew Crouse and Kannan Ramchandran. Joint thresholding and quantizer selection for transform image coding: entropy-constrained analysis and applications to baseline JPEG. *IEEE Transactions on Image Processing*, 6(2):285–297, 1997.